UNIVERSITÉ DE GENÈVE
FACULTÉ DE MÉDECINE

Clinical Medicine Section
Department of Radiology and
Medical Informatics

Combining Medical Imaging and Motion Capture for the Dynamic Analysis of Personalized Osteoarticular Structures

Thesis submitted to the Faculty of Medicine of
the University of Geneva

for the degree of Privat-Docent

by

Caecilia CHARBONNIER

Geneva

2017

Acknowledgments

My first thanks and gratitude go to Sylvain Chagué, my partner both in my personal and professional life for his invaluable support over the years and his close collaboration on any project I have undertaken.

I would like to express my gratitude to the Prof. Christoph Becker from the Department of Radiology of the University Hospitals of Geneva and Prof. Antoine Geissbühler from the Department of Radiology and Medical Informatics of the University of Geneva who have supported my candidature and given me their trust. Many thanks to the experts for accepting to review the manuscript.

I would like to thank everyone who works or have worked directly in my team: Bart Kevelham, Marcelo Elias de Oliveira, Henrique Galvan Debarba, Jacky C.K. Chow, and all the persons who collaborate or have collaborated with my team: Jérôme Schmid and Christophe Chênes from the Geneva School of Health (HEdS).

My work would not have been possible without a very active participation from the clinical side: so, many thanks to Dr. Alexandre Lädermann and Dr. Panayiotis Christofilopoulos from La Tour Hospital, Dr. Frank Kolo from the Rive Droite Radiology Center, Prof. Jacques Ménétrey, Dr. Victoria Duthon and Dr. Jean-Luc Ziltener from the Clinic Hirslanden La Colline, Prof. Pierre Hoffmeyer from the Clinique des Grangettes, Dr. Gregory Cunningham and Dr. Nicolas Holzer from the University Hospitals of Geneva for their enthusiasm and availability.

I am also grateful to all volunteers and patients for having accepted to take part in the different studies.

Finally, last but not least, I would like to thank my personal relatives, family and friends who have supported me in my endeavors.

Abstract

Musculoskeletal disorders affect all joints of the body and can result in chronic pain and long-term physical disability. Through research, we have the possibility to improve prevention and treatment thanks to a better understanding of the musculoskeletal system and its disorders. In this context, 3D anatomical models obtained from medical image segmentation and 4D kinematic models obtained from motion capture provide more insight than standard radiological and clinical examination (image stacks, palpation, assessment of passive range of motion). Indeed, 3D reconstruction provides additional information to better understand the complexity of the anatomy, whereas the study of joint kinematics is instrumental to diagnose abnormalities and to understand the joint physiology, since most of the pathological cases are related to the functional level. The work presented in this dissertation aims at improving the diagnosis, therapy planning and prevention of musculoskeletal disorders by providing orthopedic surgeons and sports medicine doctors with a novel paradigm to analyze patient's anatomy in 3D and in motion. The originality of our research lies in the ability to fuse patient-specific 3D anatomical models and computer-assisted techniques to track and simulate moving joint structures.

The first part of this thesis presents our interdisciplinary approach and the methodology implemented in this research, as well as the objectives and challenges to be addressed in order to combine medical imaging and motion capture to study and dynamically analyze personalized osteoarticular structures. The second part presents a selection of our most significant work in the field that illustrates concretely how this methodology was implemented to answer clinical questions in the framework of diagnosis, treatment and surgical planning of orthopedic disorders. This work is organized around the 3D modeling and simulation of three particular joints: 1) the hip, 2) the shoulder complex and 3) the knee. This thesis includes scientific and clinical studies focusing on the biomechanical modeling of human joints and on the exploration of several motion-related disorders, such as femoroacetabular impingement in the prosthetic hip, knee ligaments biomechanics, glenohumeral instability and impingement, rotator cuff hyperelongation, hip and shoulder implants design, etc. A summary of our contributions and future improvements of our work are presented in the third part of this thesis with a discussion on the research perspectives offered by virtual and augmented reality.

Contents

Chapter 1

Introduction

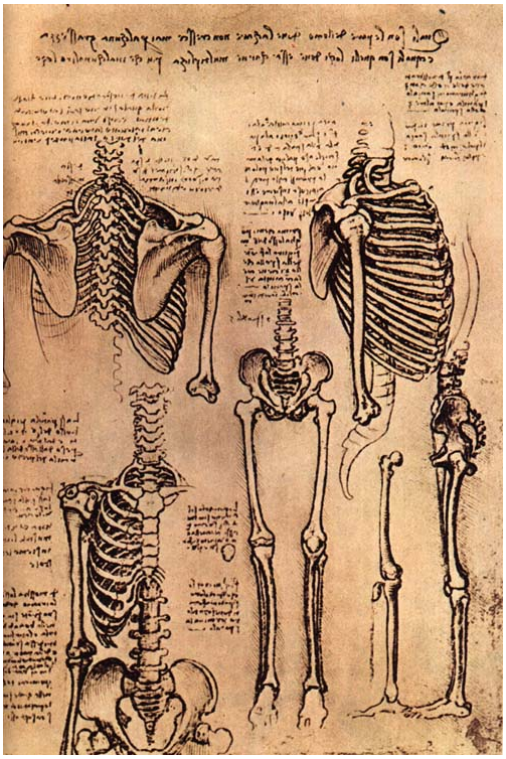

[1]Leonardo da Vinci, date unknown. Drawing of the torso and the arms, Biblioteca Ambrosiana, Milan.

1.1 Research context

Musculoskeletal disorders are common causes of long-term pain and physical disability[2]. They affect all joints of the body and result mostly from gradual or chronic development (e.g., osteoarthritis, back pain) or from an acute event (e.g., fall, sport injury). Overall, the number of people suffering from musculoskeletal disorders has increased by 25% over the last decade and is expected to increase with the aging population. Through research, we have the possibility to improve prevention and treatment thanks to a better understanding of the musculoskeletal system and its disorders.

When a patient consults an orthopedic surgeon or sports medicine doctor, the clinician establishes his/her diagnosis on the clinical examination that usually includes palpation, assessment of the passive range of motion (ROM) of the joint under investigation and specific tests (e.g., impingement test). A radiological analysis can also complement the clinical examination to confirm the suspicion of bone or soft tissue lesions. Two limitations can be evidenced with this approach:

- The clinician relies on *2D information only*, he/she has no direct 3D visualization of the joint structures. Although medical imaging provides three-dimensional volumes, the clinician must mentally represent himself/herself the articulation in 3D from the image stacks. In fact, the only time the clinician has a three-dimensional but limited view of the joint is when the patient is asleep on the operating table during surgery, so well after the diagnostic assessment.
- When relying on passive ROM which are *simple non-active motions*, the clinician cannot always reproduce the movements that elicit the pain or cannot apprehend specific non-physiologic joint behavior during complex movements (e.g., sport activities).

In this context, 3D anatomical models (e.g., shape, surface, volume) obtained from medical image segmentation and 4D kinematic models (e.g., joint angles and stability) provide more insight than image stacks and assessment of passive ROM. Indeed, reading medical images is a difficult task which is not always sufficient to deduct all the features necessary for diagnosis. 3D reconstruction provides additional information to better understand the complexity of the anatomy. However, static 3D anatomical models are not enough to diagnose certain abnormalities and to fully understand the joint physiology, since most of the pathological cases are linked to the joint kinematics – thus at the functional level. The development of 4D kinematic models, that include both patient-specific anatomy and kinematics information, are hence essential to allow the establishment of a better diagnosis and therapy planning. Moreover, besides diagnosis, they can be used for prediction through computer simulations (e.g., a dynamic analysis of a prosthesis to detect early wear), which offers unique opportunities for the prevention of musculoskeletal disorders.

The work presented in this dissertation was conducted over the last six years at Artanim Foundation[3], a private not-for-profit research center located in Geneva, Switzerland. The laboratory has specialized in motion capture technologies in different fields: orthopedics, sports medicine, 3D animation, virtual and augmented reality. Our contributions within this research context are: 1) the development of biomechanical joint models, in particular the 3D anatomical modeling and motion analysis of the hip, knee and shoulder complex; and 2) the 3D simulation and computer-assisted surgical planning of native and prosthetic joints.

[2]The Bone and Joint Decade, `http://www.boneandjointdecade.org`, accessed October 2016

[3]Artanim, `http://www.artanim.ch`, accessed October 2016

1.2 Medical pipeline

To fulfill the aforementioned contributions, we need to adopt an interdisciplinary approach at the crossroads of the following disciplines: radiology, orthopedics, biomechanics and computer graphics. Concretely, our research focus is to combine medical imaging and motion capture to study and dynamically analyze personalized osteoarticular structures. To this aim, we rely on a dedicated methodology, as illustrated in Figure 1.1.

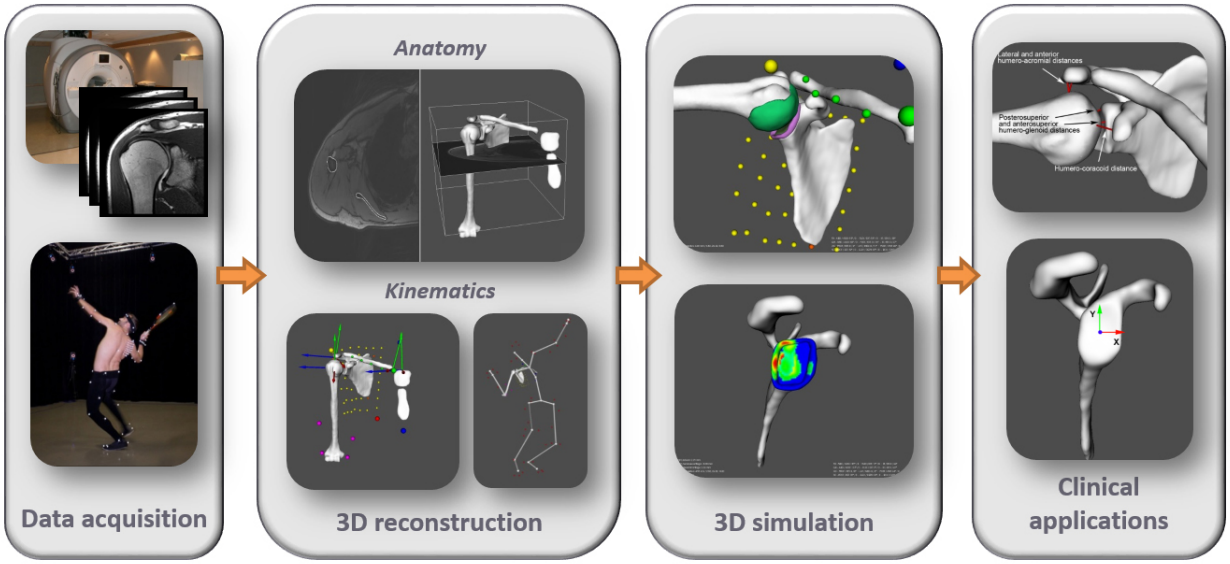

Figure 1.1: Methodology implemented in the framework of this research.

First, patients or volunteers undergo two types of *data acquisition*: we use Magnetic Resonance Imaging (MRI) or Computed Tomography (CT) to image anatomical structures in 3D and optical motion capture (or stereophotogrammetry) – a system based on infrared cameras and skin markers – to record subject's movements. Compared to dynamic imaging techniques (see Section 1.3.2) and other devices for 3D motion recording (see Section 1.4.1), optical motion capture systems are not invasive and allow the recording of larger ROM, but are subject to soft tissue artifact (STA) causing marker movement with respect to the underlying bone, which affects the estimation of the skeletal system kinematics [LCCC05, Cro06] (see Section 1.4.2).

Second, a *3D reconstruction* is performed. Patient-specific 3D bone and/or soft tissue models are extracted from the segmented images. Biomechanical parameters are also defined (e.g., joint center, standard anatomical axes [WSA$^+$02, WvdHV$^+$05]) and the joint kinematics is computed from the markers trajectories. Here, we make advantage of having 3D reconstructed models: anatomical landmarks (ALs) necessary to define these biomechanical parameters can be precisely determined on the 3D surface of the bones (i.e., by virtual palpation) to cope with the inaccuracies of determining ALs location based on external palpation – the standard procedure used in human motion analysis [CCCL95, CCK99, CLCC05]. Moreover, knowing the bones geometry can help devise correction algorithms taking into account specific joint constraints (e.g., Multi-Body Optimization (MBO) [LO99, DCD10, GSJ$^+$15, CDHdG15, RLL$^+$16, CDHdG17, RCD17]) for minimizing STA in the computation of joint kinematics.

Third and last, a *3D simulation* of the joint under investigation can be performed, once its motion is accurately estimated. Several simulation techniques (see Section 1.5) can be developed to answer specific questions depending on the *clinical applications*, such as the evaluation of joint impingements [CMTB+10, CKD+11, CCKL15] to detect early osteoarthritis (OA), the assessment of joint instability [LCKC16, LDT+16], the evaluation of prosthesis mobility and design to improve surgical planning [CCP+14, SCC+15, CCS+15, LC18] or the analysis of muscles-tendons elongation to better define the rehabilitation protocol [CLK+18].

In the next sections, we provide more details about this methodology with a focus on the objectives and challenges to be addressed. Relevant state of art is also presented and discussed.

1.3 Medical imaging

The use of medical imaging in our research context is twofold: first, it provides high resolution static images necessary for the anatomical modeling of patient-specific structures. Second, dynamic imaging techniques are used to evaluate anatomical structures during motion. These latter techniques are however difficult to implement clinically, because they are limited to the acquisition of low amplitude movements due to the confined area of measurement (i.e., small field of view) or they are invasive (e.g., fluoroscopy). Their clinical use hence remains limited and they mainly serve as gold standard to validate the development of biomechanical joint models based on skin-mounted markers and stereophotogrammetry (e.g., see [YCGMMT04, SFCL05, SMC+06, CAVMT09, SFC09, TLKL11, CCK+14, LLL+16, RLL+16, RCD17]).

1.3.1 Anatomical modeling

The acquisition of 3D medical images is the beginning of any clinical study. Two types of images are privileged, namely MRI and CT images, because they offer three-dimensional volumes with sufficient spatial resolution and contrast to allow proper tissues differentiation for segmentation. The choice between these two types of images is generally motivated by the nature of the study. For example, if we seek to reconstruct bones, CT is the modality of choice. On the contrary, if we seek to reconstruct soft tissues, MRI is preferred because this modality is appropriate for both soft and hard tissues examination. Both modalities can be combined with contrast agent injected inside the joint to improve the visualization of the joint tissues (i.e., MR or CT arthrography). However, the degree of invasiveness is another key point to consider. Indeed, CT is an invasive modality whereas it is admitted that MRI does not create any harmful ionizing radiation [MTCS08, SC04]. The injection of contrast agent also includes risks of infection. Therefore, CT or arthrography should be avoided in studies involving young patients or professional athletes.

Image protocols are defined in close collaboration with musculoskeletal radiologists. Compared to CT which allows to acquire large image volumes with a minimum of acquisition time, MRI protocols are subject to the ubiquitous image quality-speed trade-off [MTCS08, Gil07]. Since we want to fully cover the joint and the bones of interest, specific protocols must be developed by combining several overlapping datasets of different slice thickness (could be from 0.8 mm to 10 mm according to the region of interest) that are registered together (Figure 1.2). This allows to acquire the whole area in a clinically reasonable time.

Once the image volumes are acquired, a segmentation can be performed. This process consists in extracting structures of interest from the images stack. Unfortunately, no automatic tools exist that are

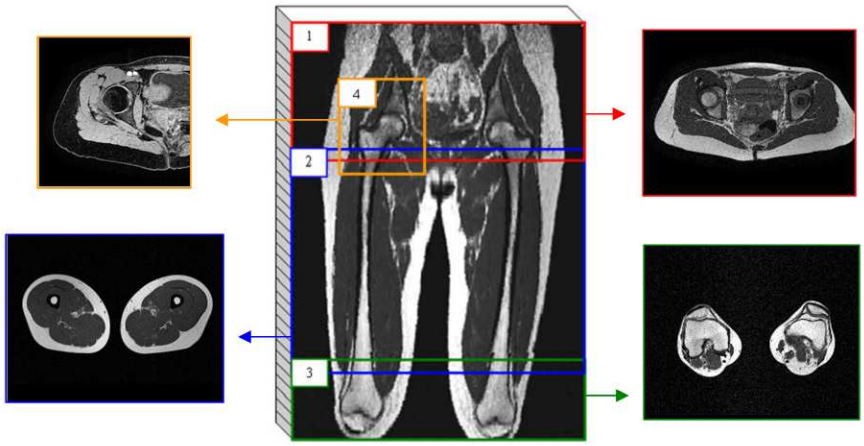

Figure 1.2: Static MRI protocol for the hip: • Axial 2D T1 Turbo Spin Echo, TR/TE= 578/18 ms, FOV/Matrix= 40 cm/512 × 512, thickness= 2 (hip (1)), 4 (knees (3)) or 10 mm (thigh (2)), gap/FA= 0 mm/90 deg, resolution= 0.78 × 0.78 mm. • Axial 3D T1 Gradient-Echo, TR/TE= 20/7 ms, FOV/Matrix= 20 cm/256 × 256, thickness= 2 mm (4), gap/FA= 0 mm/50 deg, NSA/resolution= 2/0.78 × 0.78 mm. Image from [Gil07] used with permission.

capable of recognizing any referenced structure on sectional images of any modality. Indeed, segmentation approaches tend to be sensitive to the type of modality, the inherent artifacts (e.g., noise, lack of contrast) and the intra- and inter-subject variability [SKMT11]. Image segmentation has been an intensive research topic for many years. Different methodologies were proposed, such as direct approaches – usually combining pre-processing algorithms (e.g., anisotopic filtering) to reduce image noise, region detection (e.g., Laplacian, Sobel filters) and classification (e.g., thresholding, morphological operators) – deformable models (e.g., active contours or snakes [MDA01], simplex meshes [GMMT06]), or statistical shape models [HM09, Sch11]. Here, our research focus is not the development of new segmentation techniques. We rather make use of commercial software, such as Materialise Mimics®(Materialise NV, Leuven, Belgium[4]) enabling accurate segmentation and reconstruction of 3D models of the patient's anatomy (Figure 1.3) from different imaging modalities. The solution provides semi-automatic segmentation tools, but the process remains time consuming. Typically, about 15 minutes are required to reconstruct the bones of a shoulder or hip joint.

The access to 3D reconstructed models offers many advantages. Within this research context, there are useful for the following aspects:

- First, standardized biomechanical parameters can be more precisely computed. To report joint motion in an intra- and inter-subject repeatable way, local bone coordinates systems or anatomical frames (AFs) must be defined for each bone segment. According to classical mechanics, the relative movement of a distal segment with respect to the proximal segment can be described by the relative movement of two local frames fixed to each bone segment (or rigid bodies). The International Society of Biomechanics (ISB) provides standard definitions and construction rules to determine relevant AFs for each joint [GS83, WSA$^+$02, WvdHV$^+$05] (Figure 1.4A). Moreover, their planes approximate the frontal, transverse and sagittal anatomical planes, allowing a motion description in clinically relevant terms (i.e., flexion/extension, abduction/adduction, internal/external rotation). These AFs are constructed

[4]Materialise Mimics, `http://biomedical.materialise.com/mimics`, accessed November 2016

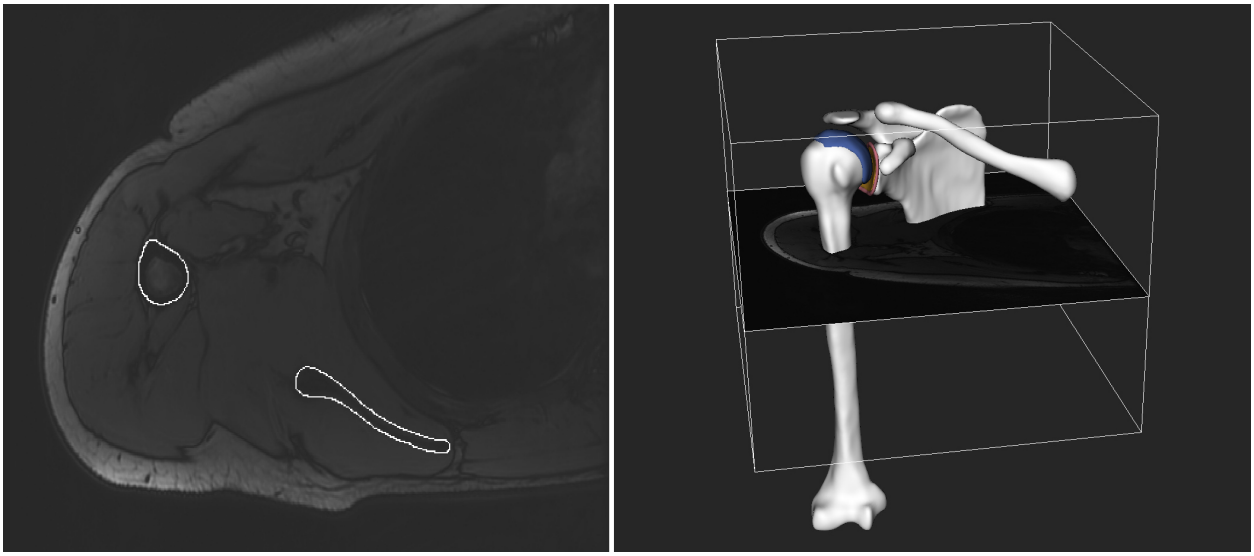

Figure 1.3: 3D reconstruction of the shoulder from MRI showing the bones, labrum, glenoid and humeral cartilages.

using selected ALs defined on the bone segments (e.g., anterior and posterior superior iliac spines for the pelvis, lateral and medial femoral epicondyles for the femur). In human movement analysis using skin markers-based measurements, ALs are located by external palpation and their position recorded by placing markers on them – a technique referred to as the CAST protocol [CCCL95]. Unfortunately, this technique lacks accuracy due to the overlying soft tissues or to AL misplacement (e.g., errors can be up to 20 mm [CCK99]). Using virtual palpation, ALs locations can be precisely determined on the 3D reconstructed bone models. Moreover, the estimation of spherical joint centers, such as the hip or glenohumeral joint, can be improved using sphere fitting methods [SE03, CCK$^+$14] (Figure 1.4B) or functional approaches [KSMMT03, GKMT$^+$09].

- Second, as mentioned previously, knowing the bones geometry can help develop personalized kinematic models to effectively reduce STA in the computation of joint kinematics. This topic is further discussed in Section 1.4.2.

- Lastly, 3D measurement tools can be implemented to quantify morphological features, improving the (subjective) reading of medical images. Indeed, measuring in the 3D space, that is independently from the patient positioning in the scanner, has the advantage to provide more accurate, reader-independent, reproducible and repeatable results. For instance, we developed in previous studies [KCP$^+$13, CCP$^+$18, LCP$^+$18] specific tools to assess the normality of the hip joint (e.g., computation of the acetabular version [RLK99], femoral α angle [PMD$^+$06]) or glenohumeral joint (e.g., computation of the critical shoulder angle (CSA) [MBR$^+$13] as shown in Figure 1.4C, β angle [MFP$^+$12]).

1.3.2 Dynamic imaging

Fluoroscopy-based measurements provide a direct access to the bones and sufficient accuracy for the analysis of dynamic human motion, but use ionizing radiation. 3D positions and orientations of the bones are

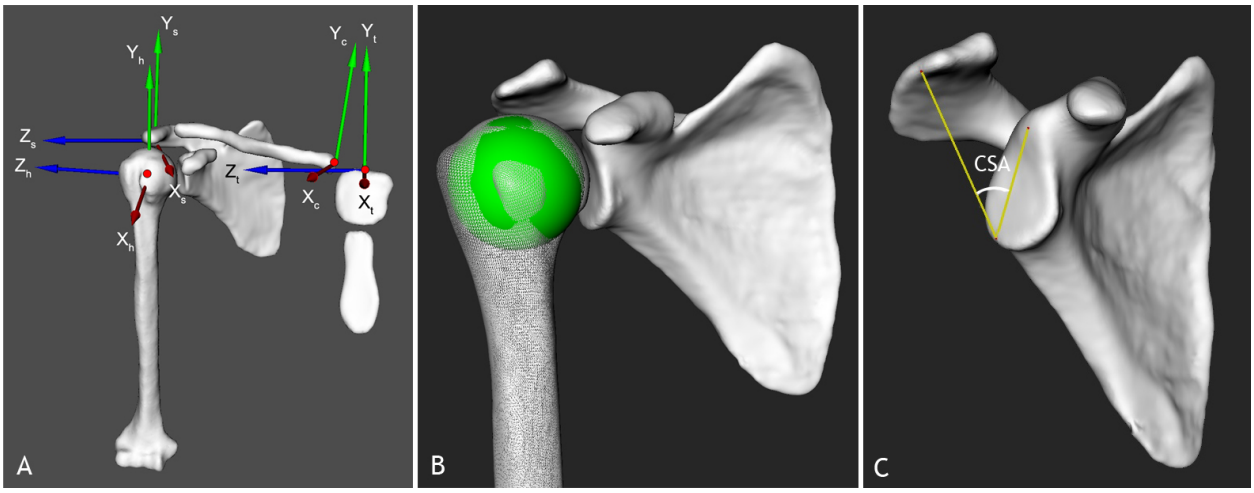

Figure 1.4: A) Bone coordinate systems for the thorax ($X_t\ Y_t\ Z_t$), clavicle ($X_c\ Y_c\ Z_c$), scapula ($X_s\ Y_s\ Z_s$) and humerus ($X_h\ Y_h\ Z_h$). Image from [CCK+14] used with permission. B) Glenohumeral center computation by fitting a sphere (in green) on the humeral head model. C) CSA measurement.

computed with 3D-to-2D shape matching techniques [FRB05, OHM+07, TLC+10, ZMW+12] (Figure 1.5A). These techniques involve the reconstruction of 3D surface models of the bones from MRI or CT which are then projected and iteratively matched to 2D fluoroscopic images. Different studies were carried out based on single-plane or biplane fluoroscopy to study subtle glenohumeral movements or instability [NTM+08, MBP+12, MMY+12], total knee arthroplasty kinematics [ZGS+06] or natural knee kinematics [LTK+08]. Whereas biplane fluoroscopy provides smaller measurement errors (typically, 1.0° for rotations and 0.5 mm for translations) compared to single-plane fluoroscopy, in particular with respect to out-of-plane translation, the subject is however exposed to twice more radiation.

Another interesting modality to study skeletal movement is MRI. This modality is not invasive, but like fluoroscopy-based measurements, the confined area and restricted field of view limit the movement possibilities of the subject. Moreover, a trade-off must be found between the image quality and acquisition time. Real time MR imaging of the joint structures is challenging and the number of studies achieving this result remains sparse in the literature (e.g., shoulder translations [HBT+11], hip kinematics [GMT05]). Quasi-static or sequential MR imaging has been hence performed in order to obtain image volumes of better quality but at the detriment of speed. Knee kinematics [PHR+04, SMC+06] or shoulder kinematics [PLCS+14] were thus studied.

Compared to stereophotogrammetry based on skin-mounted markers, dynamic imaging techniques are more reliable and accurate (i.e., STA-free), but their use is limited because they are invasive or restricted to single joint analysis at low ROM. However, they are useful as gold standard to assess STA [SFCL05, YCMT06, SMC+06, TLKL11, BJTA15] or to validate the development of biomechanical joint models [YCGMMT04, CAVMT09, SFC09, CCK+14, LLL+16, RLL+16, RCD17]. In fact, this is where our research interest lies in. For instance, we used dynamic MRI to validate the hip kinematics derived from skin markers [CAVMT09], we performed simultaneous fluoroscopic and motion capture measurements to model the kinematics of the shoulder [CCK+14] (Figure 1.5B), and we used MRI to analyze the knee joint at various flexion angles [CCK+17].

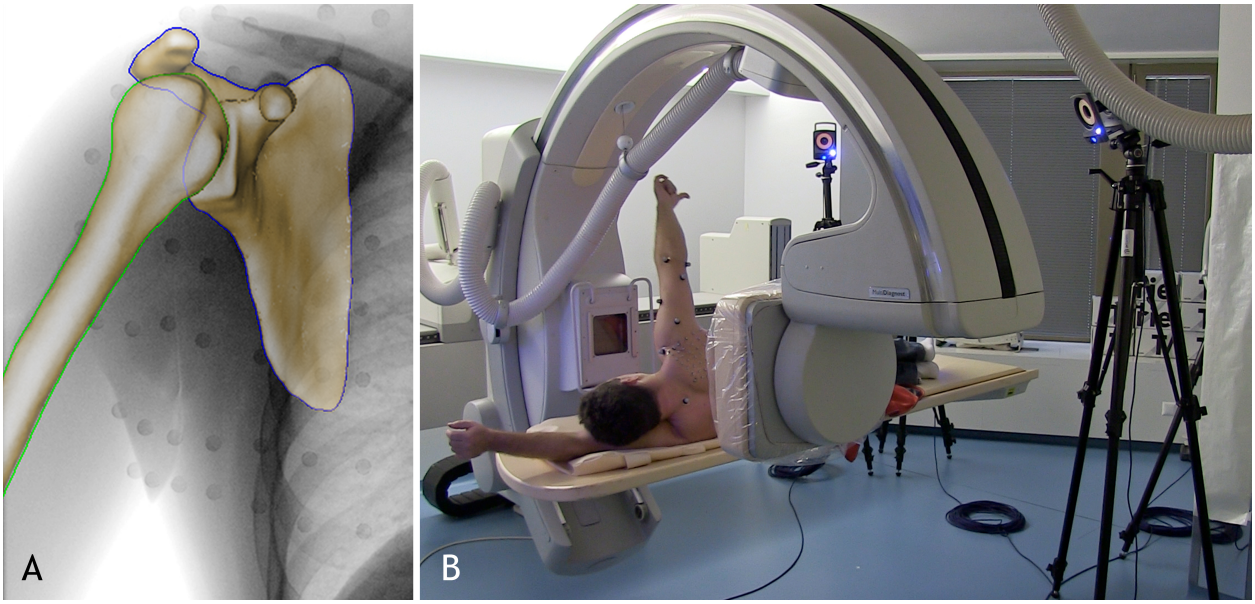

Figure 1.5: A) 3D-to-2D shape matching technique. Image from [CCK+14] used with permission. B) Simultaneous motion capture and X-ray fluoroscopy of the shoulder joint.

1.4 Motion capture

Besides dynamic imaging techniques, the use of reflective markers and stereophotogrammetry are the most common and widely recognized techniques to analyze human movement. However, when the markers are fixed on the skin, such technique is subject to STA due to muscle contractions and skin sliding, causing the markers to move with respect to the underlying bone [LCCC05, Cro06]. This phenomenon was studied in vivo and many researchers tried to devise methods or algorithms to minimize this parasitic effect.

In this section, we provide an overview of the techniques based on the use of reflective markers and stereophotogrammetry, and we briefly discuss the inherent issues related to STA, as well as our researches in this field.

1.4.1 Devices for 3D motion recording

Stereophotogrammetry involves the tracking of reflective spherical markers (usually, between 6 mm and 14 mm of diameter) with infrared cameras (sampling rate ranges from 30 Hz to 1000 Hz) and with great accuracy (markers reconstruction error ≈ 0.5 mm). Several joints can be recorded at the same time and the 3D poses (position and orientation) of the bone segments can be then evaluated from the markers trajectories. Two main categories of techniques can be distinguished:

- *Bone-based techniques* – these techniques require the implantation of pins or metallic rods directly into the bone under surgical guidance and instrumented with cluster of markers to derive true bone movements. Numerous studies were conducted with intra-cortical pins (Figure 1.6A) to quantify joint kinematics and STA during various activities [LCS+94, RvdBL+97, KMMS01, HYC04, BRL+06, NJL+07, WLJ+08]. Another set of studies was carried out with patients treated for a bone fracture with external fixators [ACCL92, ACCL93, CCL+96]. Percutaneous trackers were also proposed as an alternative to

investigate STA [HOS+97, MMS+00, MMR+02]. Despite their advantage of being STA-free, the common issue with these devices is associated with their evident invasiveness and encumbrance. Moreover, they do not reflect the natural motion patterns of the subject (i.e., motion restrictions due to pain, subjects recovering from a fracture). Their use has been hence limited for routine analysis and for ethical reasons.

- *Skin-based techniques* – these techniques have been favored as they require the fixation of markers directly onto the skin using double-sided adhesive tape (Figure 1.6B). However, STA must be effectively addressed, as discussed in the next section. Clinically, these techniques are routinely used for gait analysis [DBD+04, SAL+13], rehabilitation [SdQD+07] and the evaluation of neuromuscular disorders [YOES08, BMSL+13] when combined with electromyography (EMG) and force plates to infer musculoskeletal dynamics.

The interested reader can refer to my PhD thesis [Cha10] for more details related to the different instrumentation devices for 3D motion recording, as well as for information about other skin-based techniques, such as video systems or inertial sensors (accelerometers and gyroscopes) which are two other techniques commonly used in gait labs.

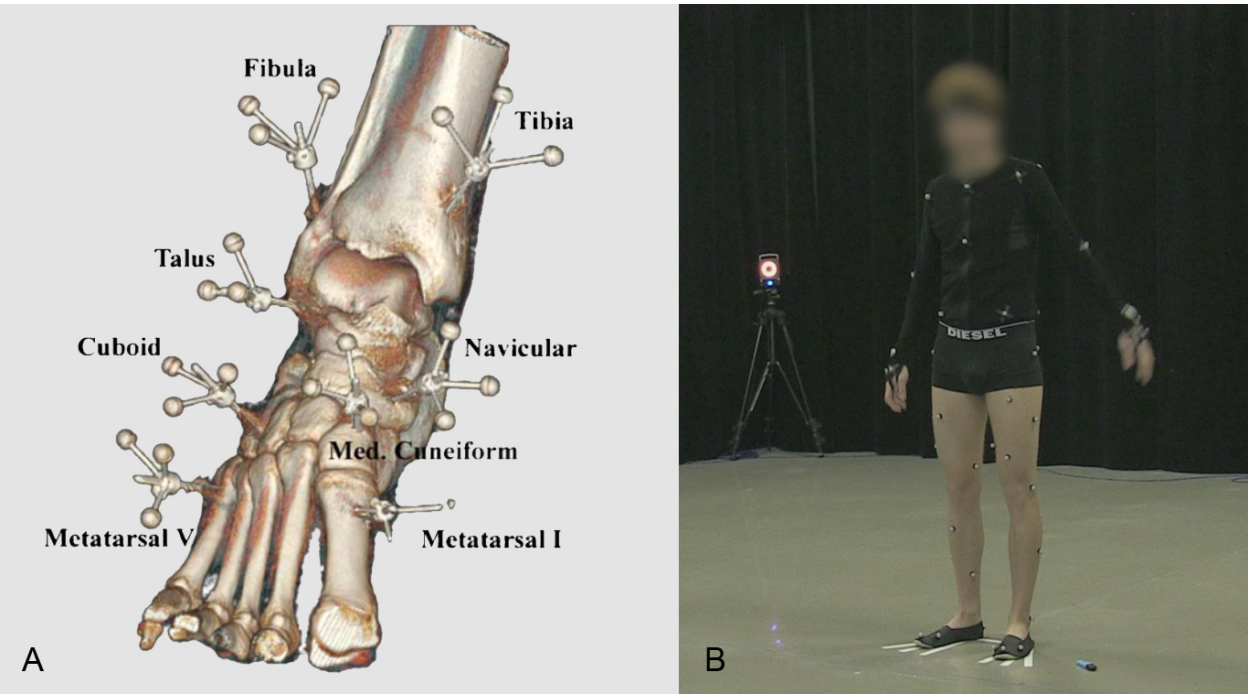

Figure 1.6: A) CT image of bone pins inserted into the foot. Image from [LNL+08] used with permission. B) Full body motion capture with a focus here on the lower extremities (markers are placed directly on the skin).

1.4.2 Soft tissue artifact

STA was intensively studied by the research community, in particular at the lower extremities. Despite some discrepancies between the different works – mainly due to the variability in the protocols and techniques

used, the number of tested subjects and the locations of skin markers – interesting conclusions could be evidenced on the magnitude and patterns of STA [Cha10]: the pattern of the STA is task and subject dependent, STA is reproducible within subjects but not among, its magnitude is bigger in areas closer to the joints, it introduces random and systematic errors, it depends on the markers placement and non redundant markers increase its effect, it is greater at the thigh and scapula with respect to any other bone segment at the lower and upper extremities, respectively.

These conclusions are useful because they provide information that can help determine correction/compensation methods to solve the issue of STA. A first step in this direction is to adequately define optimized markers protocols to account for STA. Some authors proposed the utilization of rigid supports [HOS+97, BCL+98, LCC+99, LBC+99, MMS+00, YHC+00, HYC04] to reduce the internal deformation of the markers cluster (i.e., inter-marker distance changes). However, this method is not sufficient because it is unable to discard the second effect of STA, that is the rigid displacement of the markers cluster (i.e., the cluster moves rigidly with respect to the bone due to muscle contraction). For an effective STA minimization, these two different aspects must be addressed. In terms of markers placement, our strategy is to use redundant markers distributed all over the segment surfaces and located far from the joint line (if possible). We have thus developed specific markers configurations [CCK+14, CCS+15, CCK+17] for the following joints:

- For the hips, we use two clusters of 7 markers (⊘ 14 mm) placed on the lateral and frontal parts of both thighs and 6 markers (⊘ 14 mm) on the pelvis (four fixed on the anterior and posterior superior iliac spines and two on each pelvic side), as shown in Figure 1.7A.
- To capture the knee kinematics, we use the same two clusters of 7 markers on the thighs and two clusters of 5 markers (⊘ 14 mm) distributed on the shank segments (Figure 1.7A).
- For the shoulder complex, we use 4 markers (⊘ 14 mm) placed on anatomical landmarks of the thorax (sternal notch, xyphoid process, C7 and T8 vertebra), 4 markers (⊘ 6.5 mm) on the clavicle, 4 markers (⊘ 14 mm) on the upper arm (two placed on the lateral and medial epicondyles and two as far as possible from the deltoid), and 57 markers on the scapula (1x ⊘ 14 mm on the acromion and a 7x8 grid of ⊘ 6.5 mm), as depicted in Figure 1.7B.

The next step is to deduct the joint kinematics from the markers trajectories by effectively minimizing STA. Several techniques were proposed, such as:

- *Mathematical approaches* – these approaches solve the STA problem by finding the least perturbed triangle of markers over the entire ROM (i.e., Solidification model [CFD95]) or by considering redundant markers where the mass of each marker is adjusted at each step to minimize changes of eigenvalues (i.e, Point cluster technique [AA01, ABA03]). However, these approaches do not perform better than traditional bone pose estimators (e.g., Single Value Decomposition algorithm [SW93]).
- *Methods based on calibration data* – these methods acquire two or multiple calibration poses at specific ROM of the activity considered to compute a linear model of soft tissue deformation used to compensate STA (e.g., Multiple anatomical landmark calibration [CCCL97, CSFL05], Dynamic calibration [LCCC98]). However, these methods are based on invalid assumptions (e.g., skin motion during a static posture $\neq$ dynamic activities) and the major drawback is the increased number of data acquisitions required.

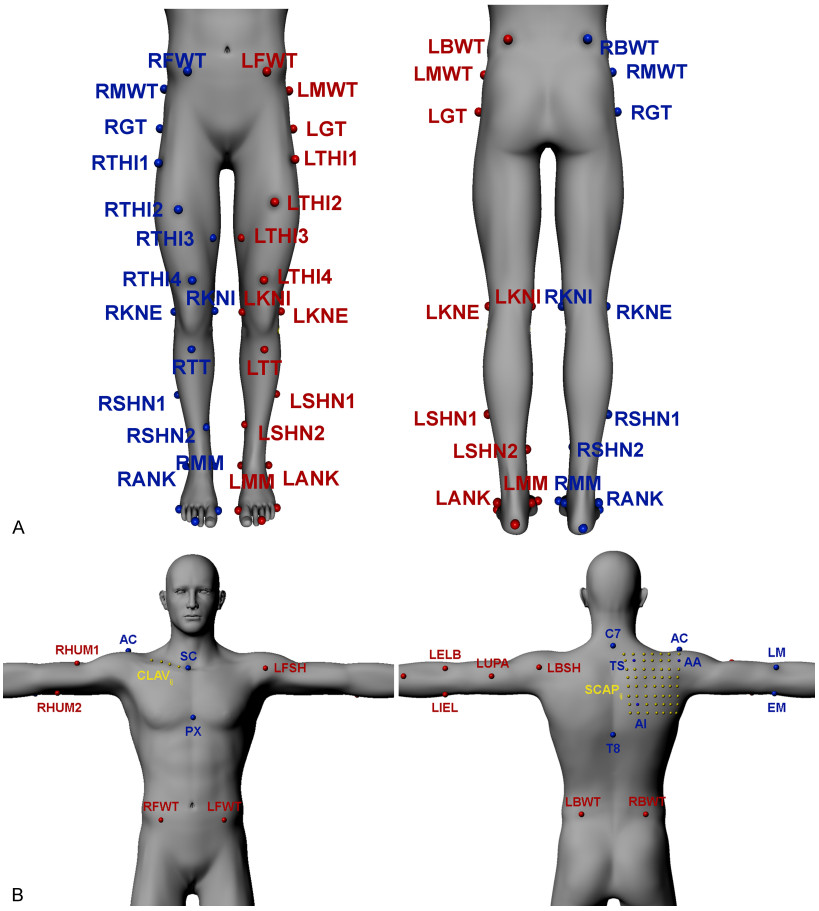

Figure 1.7: A) Markers configuration for lower body motion capture. B) Markers configuration for shoulder motion capture (here the right shoulder). Image from [CCKL15] used with permission.

- *Techniques based on global optimization* – these techniques aim at optimally estimating the location of bone segments as a whole (and not each segment separately like the previous techniques) by minimizing the distances between the model-determined and the measured marker trajectories (i.e., MBO [LO99, DCD10, GSJ+15, CDHdG15, RLL+16, RCD17, CDHdG17, LBN+17]). These techniques rely on a predefined kinematic model with several joint constraints: spherical or hinge joints, more complex anatomical constraints (e.g., for the knee, a parallel mechanism composed of two sphere-on-plane contacts and four ligaments lengths constraints). They hence offer promising results as joint models with subject-specific constraints can be introduced to reproduce specific bone geometry and behavior.

This latter type of techniques has been the focus of our researches, as they provide the possibility to account for 3D anatomical models and flexibility in terms of joint degrees of freedom (DoF). Therefore, we developed different strategies to model the actual biomechanical behavior of the hip, knee and shoulder complex. In all cases, we start by considering a subject-specific kinematic chain using the 3D anatomical models of the segments under evaluation (for the hip, the pelvis and femur; for the knee, the femur and tibia; for the shoulder complex, the thorax, clavicle, scapula and humerus), so that we can minimize the overall STA error through the entire kinematic chain. Then, specific joint constraints are introduced in the global optimization problem:

- For the hip joint, we first model it as a spherical joint or ball-and-socket joint (i.e., 3 DoFs, no joint translation) since this articulation is considered as very stable (maximum joint translation in non-pathological subjects ≈ 0.5 mm [GKMT$^+$09]). We then use a collision detection algorithm to correct the position of the femur in case an abnormal contact with the acetabulum occurs (this is especially the case during extreme motion), allowing the hip joint center to slightly shift during movement [CAVMT09, Cha10].

- For the knee, the joint is modeled as a parallel mechanism (6 DoFs) with four ligaments (anterior cruciate ligament (ACL), posterior cruciate ligament (PCL), medial collateral ligament (MCL) and lateral collateral ligament (LCL)) and two surface-on-plane contacts that force the lateral and medial femoral condyles surfaces to maintain contact with the tibial plateaus, modeled as a 3D plane [CCK$^+$17].

- Eventually, for the shoulder complex, the sternoclavicular (SC), acromioclavicular (AC) and glenohumeral (GH) joints are each defined as ball-and-socket joint, but with loose constraints on translation implemented as a penalty-based method [CCK$^+$14]. Joint translations are thus permitted but limited, which allows to model the large ROM of the shoulder in particular at the GH joint.

The accuracy of the models developed ranges from 0.24 to 3.7 mm in translations and from 0.55° to 6° in rotations, which is acceptable for clinical use in the study of joint pathology. Best accuracy is obtained for the hip joint. As a result, the 3D anatomical joint models of the subjects can be visualized in motion. Figure 1.8 shows examples of computed postures.

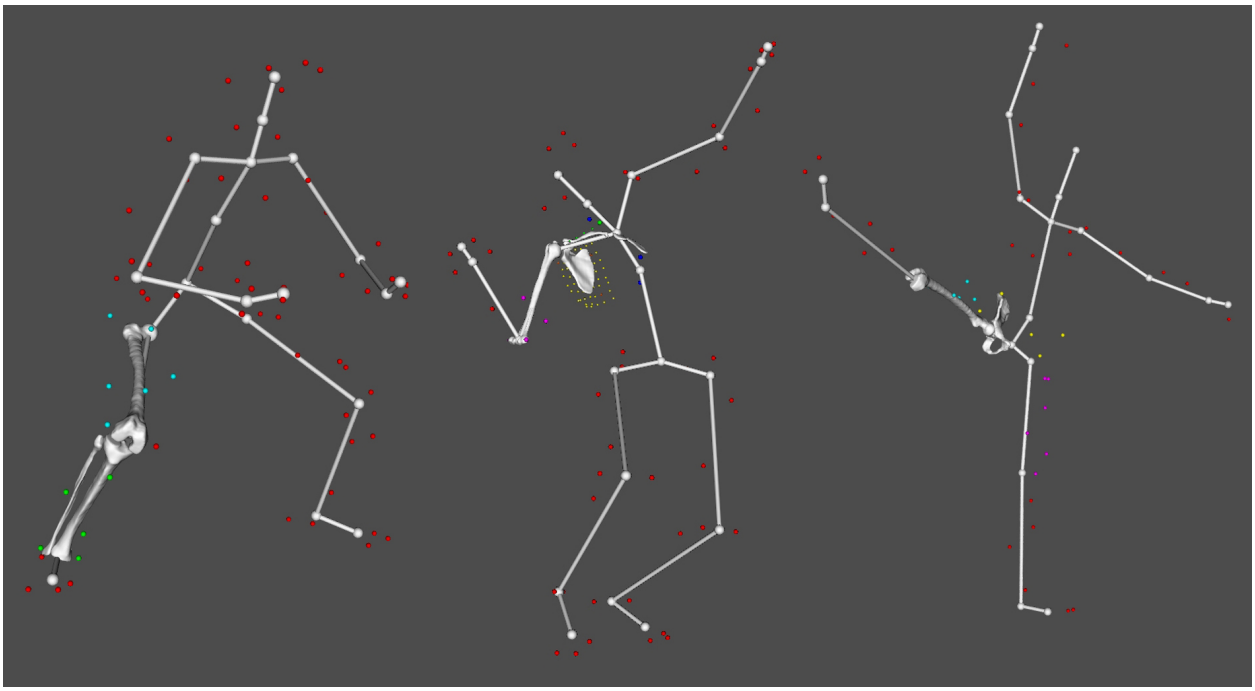

Figure 1.8: Computed postures for the knee, shoulder complex and hip obtained with the developed kinematic models: side step (left), tennis serve (middle) and dancing movement (right). Additional markers placed on the rest of the body and a virtual skeleton are also used to visualize the motion as a whole.

1.5 3D simulation and surgical planning

3D simulation and surgical planning can be undertaken once the kinematic behavior of the joint is accurately estimated. Several simulation techniques can be developed to answer specific clinical questions in the framework of diagnosis, treatment or surgical planning. The clinical studies that we undertook the last few years are discussed in the next chapter of this manuscript. However, we would like to briefly summarize below the type of developments we have carried out in terms of simulation in the native and prosthetic joint.

1.5.1 Native joint

In the native joint, dedicated simulation and motion analysis techniques were developed to study the functional behavior of the hip, knee and shoulder complex during daily living activities, sport activities or rehabilitation exercises, and before/after specific treatments. Independently of the clinical goals, they can be classified as follows:

- *Motion analysis techniques* – this class of techniques allows the description at each time instant of the ROM of the joint in clinical terms (i.e., flexion/extension, abduction/adduction, internal/external rotation) [GS83, WSA$^+$02, WvdHV$^+$05], as well as the assessment of the joint congruency and instability. These techniques are based on biomechanical calculations using the relevant bone AFs and centers of rotation. They are at the basis of any kinematic study and were used for instance to analyze the hip joint congruency and ROM necessary for the practice of dancing [CKD$^+$11], to evaluate the accuracy of the hip clinical examination [CCS$^+$15], to determine shoulder joint instability in tennis players [LCKC16] and in patients before and after glenohumeral stabilization [LDT$^+$16].

- *Contact and conflict analysis techniques* – this class of techniques is dedicated to the analysis of conflicts between the joint structures, such as bone-to-bone contact or cartilages compression. Simple simulations allow the computation of minimal distance thresholds between the bone structures (Figure 1.9A). More advanced simulations include the use of collision detection algorithms and penetration depth methods to virtually locate abnormal contacts and to compute the topographic extent of tissue compression (Figure 1.9B). These techniques were useful in the assessment of femoroacetabular impingements in the dancer's hip [CMTB$^+$10, CKD$^+$11], in the analysis of glenohumeral external and internal impingements during tennis movements [CCKL15] and rehabilitation exercises [CLK$^+$18], as well as for the planning of arthroscopic acromioplasty surgery [CCK$^+$16, CCP$^+$18, LCP$^+$18].

- *Elongation analysis techniques* – this class of techniques allows the simulation of deformation of simplified soft tissues models (e.g., ligament, muscle-tendon) during motion and the measurement of their length variation (i.e., elongation/compression). The soft tissues are modeled as 3D splines discretized into a set of connected particles and their deformations are obtained using a position-based dynamics approach [MHHR07] (Figure 1.9C) that offers the advantage to derive position updates from the particles positions itself using constraints – instead of relying on the calculation of forces to determine accelerations, velocities and ultimately particle positions using numerical integration methods. For example, we used such techniques to simulate the rotator cuff muscles during shoulder strength training exercises [CLK$^+$18] and more recently to simulate the knee ligaments during dynamic activities.

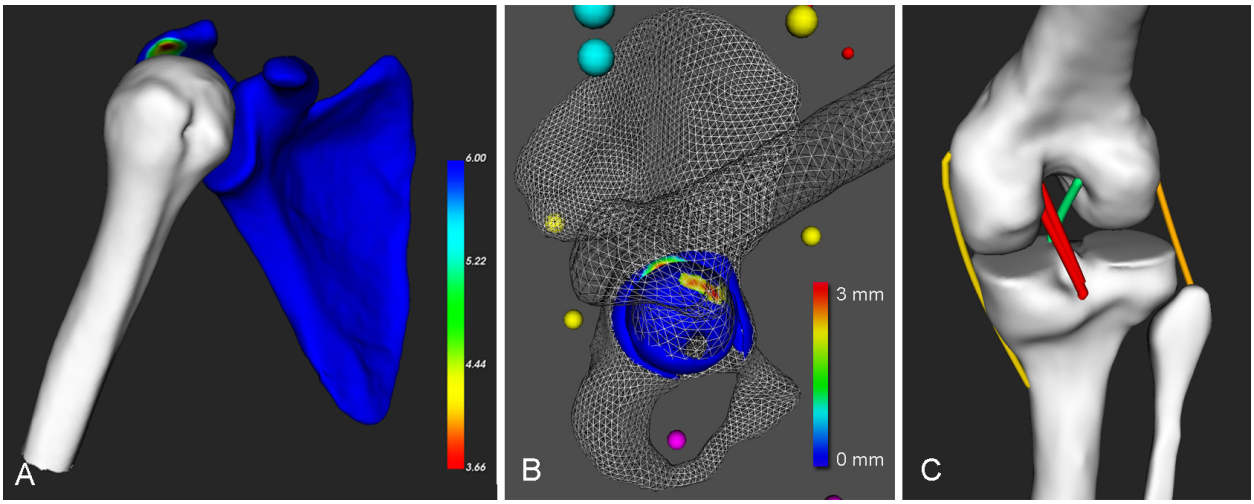

Figure 1.9: A) Variation of minimal distances between the humeral head and inferior acromion for the evaluation of subacromial impingement (colors other than blue are distances of less than 6 mm, meaning that impingement may occur [CD12, MRS06]). B) Penetration depth distribution on the hip cartilages and labrum for the evaluation of femoroacetabular impingement (blue color = no collision, other colors show the compression zones in millimeters). C) Simulation of the knee ligaments with colors representing length variations with respect to the neutral knee pose (warms colors = elongation, cold colors = compression).

Nowadays, a strong focus is being made on physically-based simulations (e.g., finite element models [RTTS05, RSGP06, CBF09, FSH+12, WBD14], mass-spring models [SMBT05, ACS+09, CAVMT09]) which are more advanced and realistic methods accounting for the dynamics and physical properties of the joint tissues. However, current physically-based methods are difficult to set up and are limited to simple ROM simulation where loads can be estimated [BD05]. Moreover, they require accurate tissue segmentation on medical images, which remains a complicated task with respect to muscles and ligaments. Although the aforementioned techniques are simplified non-physical approaches, they provide valuable clinical data and are generalizable to different joints. In particular, the techniques developed are based on subject-specific bone-soft tissue representation enabling stable and real time simulation of osteoarticular structures during complex motion.

1.5.2 Prosthetic joint

In the prosthetic joint, our work has been focused on the total hip arthroplasty (THA) and shoulder reverse arthroplasty (RSA). The developed simulation and motion analysis techniques were hence adapted to sustain these particular scenarios. The same motion analysis techniques were used to study the hip ROM during daily living activities in patients after THA [SCC+15]. We however extended the contact analysis techniques to account for collision detection between the bones and the prosthesis components (cup, liner, glenosphere, stem) which are typical impingements occurring after RSA or THA (Figure 1.10). By combining these two categories of techniques, subluxation due to impingements can also be assessed and quantified during motion. Therefore, we tested in previous studies the kinematics of different implant configurations to improve surgical planning [CCP+14, CCS+15, LC18] and assessed impingements and subluxations in patients after THA during ROM of everyday life [SCC+15].

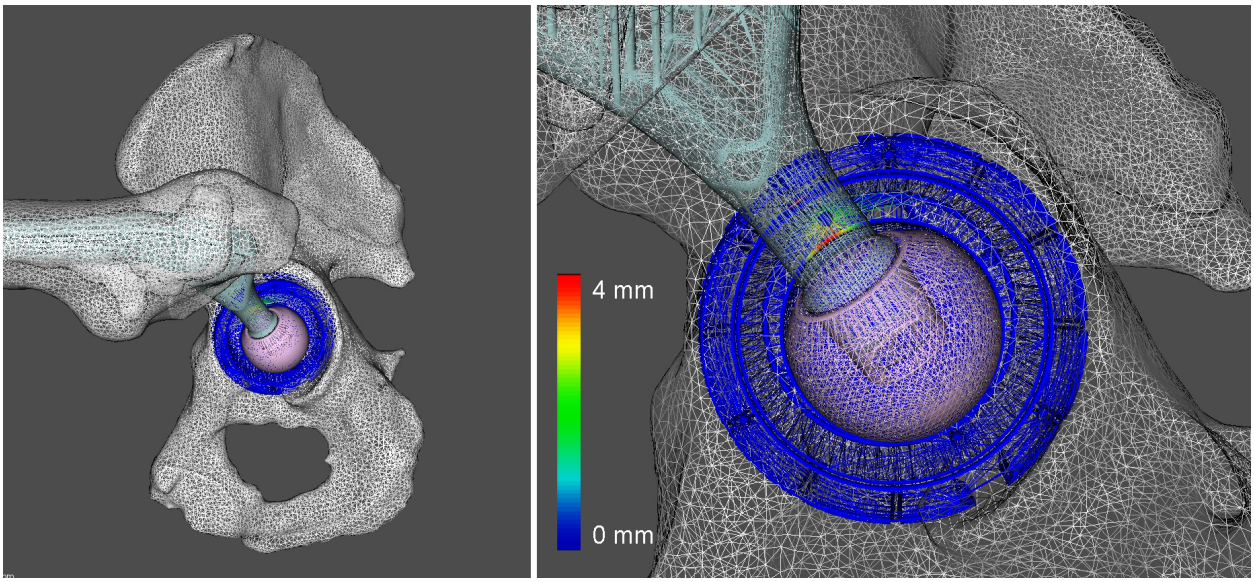

Figure 1.10: Collision detection between the prosthetic components of the hip. The color represents the impingement zone (blue = no collision, other colors = collisions).

1.6 Outline

This first chapter highlights our methodology to combine medical imaging and motion capture to study and dynamically analyze personalized osteoarticular structures, as well as the line of research developed over the past six years. This work has required an interdisciplinary approach and scientific knowledge at the crossroads of radiology, orthopedics, biomechanics and computer graphics. More specifically, this work has involved expertise in the segmentation and 3D reconstruction of hard and soft tissues from medical images, the development of specific registration algorithms based on different modalities (optical motion capture, dynamic imaging techniques), and the development of simulation tools for the evaluation of joint tissues or implants during motion.

The remaining of the manuscript is organized as follows: Chapter 2 presents a selection of our most significant work in the field that illustrates concretely how this methodology was implemented to answer scientific and clinical questions. We finally conclude with our achievements and perspectives in Chapter 3, followed by Annexes.

Chapter 2

Selection of work

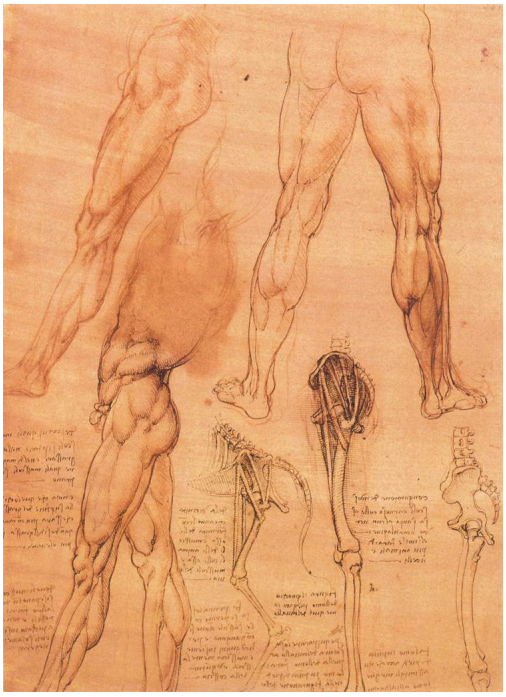

[5]Leonardo da Vinci, 1506-1507. Studies of legs of man and the leg of a horse, Royal Library, Windsor.

2.1 Introduction

Over the past six years, we devoted significant research to the biomechanical modeling of human joints and to the exploration of several motion-related disorders. This work was primarily focused on the 3D modeling and simulation of three particular joints: 1) the hip, 2) the shoulder complex and 3) the knee. This chapter provides an overview of the scientific and clinical studies carried out in this field which can be organized as follows:

- We developed personalized biomechanical models for the shoulder [CCK$^+$14] and the knee [CCK$^+$17] to estimate joint kinematics from motion capture data. As explained in Section 1.4.2, our kinematic models are based on MBO including specific joint constraints.
- We improved the THA planning by developing simulation software tools taking into account both the morphology and the kinematics of the joint [SCC$^+$15]. We also assessed the kinematics of different implant configurations and the necessary hip joint mobility for everyday tasks [CCP$^+$14, CCS$^+$15] to improve surgical undertaking.
- We evaluated the GH joint during sport and more specifically in tennis players [CCKL15, LCKC16], a population subject to shoulder impingements and instability due to the repetitive overhead arm movements performed during this activity, in particular during tennis serve.
- We assessed shoulder treatment outcomes and rehabilitation, such as the impact of shoulder strength training exercises on the GH joint [CLK$^+$18], the validity of the pendular Codman's exercises [CCL$^+$18] – pillars of the shoulder rehabilitation program – and the effect of GH surgical stabilization in patients suffering from anterior instability [LDT$^+$16].
- We developed surgical planning tools for acromioplasty [CCP$^+$18, LCP$^+$18] and extended our work to the analysis of RSA [LC18] where our interest was to better apprehend the impact of the prosthesis design on the mobility of the joint.
- Finally, we recently studied the functional behavior of the knee ligaments through an MRI study conducted at different degrees of knee flexions and during sports movements recorded by motion capture.

The remaining of this chapter briefly summarizes five peer-reviewed journal articles selected among this work. To our opinion, they represent nicely the interdisciplinary of our research. The full articles can also be found at the end of this chapter.

2.2 Analyzing hip range of motion in everyday life

***Charbonnier C**, Chagué S, Schmid J, Kolo FC, Bernardoni M and Christofilopoulos P. Analysis of hip range of motion in everyday life: A pilot study. Hip Int, 25(1):82-90, 2015.*

To date, there is no clear consensus as to the amplitude of the "normal hip" in everyday life. Knowing the necessary joint mobility for everyday life is important to better plan the THA surgery, particularly when dealing with young active patients since they have a higher demand concerning hip ROM. The aim

of this study was twofold: first, routine activities were acquired with young volunteers to determine the hip ROM necessary for everyday tasks. The idea was also to use the motion data in computer simulations of prosthetic hip joint 3D models to evaluate relative risk of impingement and loss of joint congruence during their practice. The second objective was to assess the accuracy of passive hip ROM measurements during clinical examination. Indeed, patient care starts with correct physical examination and determining the patient's passive hip ROM is one of its key points. Unfortunately, this process may lack precision because of movement of other joints around the pelvis (i.e., no direct access to the joint).

Young healthy volunteers participated to the study. They were MRI scanned and their hips were reconstructed in 3D from the medical images [Sch11]. For the first motion experiment, data from the participants were acquired during five activities known to be painful in case of hip disorders or prone to implant impingement and dislocation: stand-to-sit, lie down on the floor, lace the shoes while seated and pick an object on the floor while sitting or standing. The hip kinematics was computed from the markers trajectories [CAVMT09, CKD$^+$11] and the ROM was quantified for each subject and all activities. For all movements, a minimum of 95° hip flexion was required (mean range 95°-107°), lacing the shoes and lying down being the more demanding. Abduction/adduction and IR/ER remained low ($\pm$ 20°) and variable across subjects. The next step was to apply the recorded motion data to prosthetic hip joint 3D models. Nine implant configurations, with variations of acetabular cup's inclination (40°, 45°, 60°) and anteversion (0°, 15°, 30°) parameters, were tested. During the simulations, impingements were detected and femoral head translations (subluxation) were computed to evaluate the joint congruence [CCP$^+$14]. Results showed that impingements and subluxations occurred at maximal ROM in the anterosuperior area of the acetabulum. The frequency of impingements varied according to the cup orientation (see article for details).

During the second motion experiment, a hip clinical exam was performed successively by two orthopedists with respectively two and twelve years' experience, while the motion of the subjects was simultaneously recorded using motion capture. Hip angles measured by the clinicians with the hand held goniometer were compared with the kinematic data computed from motion capture. The error made by the clinicians during physical examination varied in the range of $\pm$10°, except for flexion and abduction where the error was higher (flexion: mean 9.5°, range -7°-22°; abduction: mean 19.5°, range 8-32°). No significant differences between the errors made by the two examiners were noted.

This study concluded that the clinical exam was an accurate method for determining hip passive motion, if extra care was taken to stabilize the pelvis during flexion and abduction to prevent overestimation of the ROM. Moreover, we showed that daily activities involved important hip flexion that could expose the prosthetic hip to impingement and subluxation.

2.3 Improving surgical planning for THA

Schmid J, Chênes C, Chagué S, Hoffmeyer P, Christofilopoulos P, Bernardoni M and ***Charbonnier C****. MyHip: supporting planning and surgical guidance for a better total hip arthroplasty: A pilot study. Int J CARS, 10(10):1547-1556, 2015.*

The THA planning and its execution during surgery rely on the experience of the surgeon. This process could be greatly improved by considering pre-operatively the morphology and ROM of the patient's hip

to optimally select and position the implant, and consequently avoid undesirable functional mechanisms following this type of surgery such as impingements or dislocations [MMD07, PLSH11]. Moreover, the use of intra-operative patient-specific surgical guides can help the surgeon to accurately execute the planning. This article summarizes the "MyHip" computer-assisted framework[6] designed to support the preparation and execution of the THA planning and developed in collaboration with the Geneva School of Health (HEdS), the University Hospitals of Geneva (HUG) and Medacta International SA.

Pre-operative planning: Based on CT images, we reconstruct patient-specific hip bone models. Anatomical and functional landmarks are also defined from the reconstructed models to determine key parameters of the surgical planning (e.g., implant orientation) and the kinematics (e.g., AFs, hip joint center). To account for the patient's posture and to correct the cup anteversion accordingly, the pelvic tilt [BPT+09] is measured from lateral radiographs since the patient can be acquired in weight-bearing position. A dedicated protocol was developed allowing computation of the relevant pelvic descriptors (pelvic tilt, sacral slope angle) with great accuracy. Based on the reconstructed models and pelvic tilt information, a first virtual planning is performed and the implants that best fit the morphology of the patient are selected. This initial planning is subsequently refined by performing a dynamic simulation of the prosthetic 3D models driven by a motion database of daily activities (e.g., walk, stand-to-sit, lace the shoes). This database was created from motion capture of healthy volunteers [CCS+15]. The goal of this simulation is to detect potential risk of impingement and joint instability during everyday activities. The pre-computed hip ROM stored in the database are applied to the virtual prosthetic hip and collision detections [CCP+14] are performed to locate abnormal contacts between both prosthetic and bony components. Based on the simulation's results, the surgeon adapts and refines the initial implant configuration and selects the optimal planning for the surgery.

Intra-operative guidance: Surgical guides – which are placed intra-operatively on bones – are produced by rapid prototyping, matching accurately the patient anatomy to ensure a good anchoring during surgery. Their aim is to support the bone resection process. In this framework, we devised a computer-assisted process for the automatic creation of these guides based on the 3D meshes of the patient and information of the surgical planning.

Pre-operative and post-operative experiments: For validation purposes, we ran a pre-operative experiment to investigate the impact of pelvic tilt on THA planning and two post-operative experiments with operated patients. To quantitatively assess the impact of significant pelvic tilts in the dynamic planning, two sets of prosthetic 3D models were produced whether or not the pelvic tilt was accounted for in the planning. Dynamic simulations were then performed with the two sets of models in order to compare the incidence of impingements during motion. Post-operatively, the first experiment studied the efficiency of the intra-operative guidance with respect to surgical outcomes by registering the pre-operative bone and implant models of the patients with their respective post-operative CT images and by comparing the differences of implants orientation and position. The aim of the second post-operative experiment was to perform a dynamic analysis of the reconstructed post-operative patient's hips based on kinematics acquired from post-operative motion capture sessions or extracted from our motion database.

Results showed that if the pelvic tilt was ignored in the planning, there was an increased risk of

[6]MyHip: Patient-Specific Pre-operative Planning and Intra-operative Surgical Guidance for Total Hip Arthroplasty, CTI project n°13573.1 PFFLE-LS

significant subluxation and impingement in the prosthetic hip. Regarding the use of intra-operative guidance, we measured small differences in the position and orientation of the virtual and effective cutting planes of femurs, highlighting the surgeon's capability to correctly replicate the planned bone cutting by using the femoral guide. However, the surgeon did not fully respect the suggested placement of the femoral component as we measured an average error of 4.4 mm between planned and executed positions of the stem head. For the acetabular guide, we unfortunately did not perform a similar post-operative analysis, because the guide was not available at the time of experiment. Finally, the second post-operative experiment revealed that the patient's motion was free of impingements, but not when testing with ROM of healthy subjects (i.e, ROM from the motion database). Moreover, patients adopted less hip flexion with more abduction, which seems to be a motion adaption and a good strategy to avoid impingement.

In conclusion, we presented in this paper a computer-assisted framework to better plan and execute THA. By taking into account both morphology and dynamic information (posture, kinematics) of the patient, traditional planning can be improved and possible causes of implant failures can be early detected. Surgical guides can be designed with computer assistance and effectively assisted surgeons to execute the planning – yielding a more cost-effective surgery. This framework is today routinely used by Medacta International SA in their"MyHip" surgeries.

2.4 Modeling the kinematics of the glenohumeral joint

***Charbonnier C**, Chagué S, Kolo FC, Chow JCK and Lädermann A. A patient-specific measurement technique to model the kinematics of the glenohumeral joint. Orthop & Traumatol: Surg & Res, 100(7):715-719, 2014.*

Measuring dynamic in vivo shoulder kinematics is crucial to better understanding numerous pathologies and sport injuries, but remains a challenging problem due to the complicated anatomy and large ROM. Unfortunately, the motion of the shoulder joints cannot be explored with standard MRI or CT because these modalities are limited to static measurement and might therefore miss some specificities of dynamic motion. Fluoroscopy-based measurement provides sufficient accuracy for dynamic shoulder analysis [ZMW$^+$12], but uses ionizing radiation. Motion capture systems using skin-mounted markers are good solutions to determine shoulder kinematics non-invasively during dynamic movement [JMTB12, KKB$^+$12], but are subject to STA. Moreover, none of the current motion capture techniques have been used to study translation values at the joint, which is crucial to assess shoulder instability. The aim of the present study was to develop a dedicated patient-specific measurement technique based on motion capture and MRI to determine shoulder kinematics accurately, and to assess the effectiveness of the proposed technique by comparing the resulting 3D kinematics with that obtained by simultaneous X-ray fluoroscopy during functional activity.

Six healthy volunteers were recruited for this study. They were MRI scanned and their shoulder bones (scapula, humerus, clavicle and sternum) were reconstructed in 3D from the medical images. Local coordinate systems [WvdHV$^+$05] were then established for each bone using ALs identified on the reconstructed bone models and MR images. The volunteers participated to a simultaneous X-ray fluoroscopy and motion capture acquisition. Kinematics was acquired during three consecutive flexions of the arm from neutral to maximum flexion, and three consecutive empty-can abductions of the arm from neutral to maximum abduction in

the scapular plane. During testing, participants were equipped with a dedicated shoulder markers protocol (see Section 1.4.2), including 69 spherical reflective markers placed directly onto the skin using double sided adhesive tape.

Shoulder kinematics was computed from the recorded markers trajectories. We developed a patient-specific kinematic chain comprising four rigid bodies (thorax, clavicle, scapula and humerus) using the individual subject's 3D MRI-based models. The position and orientation of the thorax relative to the global coordinate system was determined with 6 DoF, and the SC, AC and GH joints were each defined as ball-and-socket joint (3 DoF) with loose constraints on translation. Joint translation was thus permitted but limited. The optimal pose of the kinematic chain was obtained by MBO using a non-linear sequential quadratic programming algorithm [LT01]. Reference shoulder kinematics was computed from the fluoroscopic measurements where the 3D poses of the scapula and humerus were obtained using a 3D-to-2D shape matching technique [MMY$^+$12]. Humeral motion with respect to the scapula was finally determined for both measurement methods and the results compared.

Root mean square errors (RMSE) for shoulder orientation were within 4° (mean range: 2.0° to 3.4°) for each anatomical axis and each motion. For glenohumeral translations, RMSE were between 2.2 mm and 3.7 mm (mean range: 1.9 to 3.3 mm). Although the translation errors were significant, the computed patterns of humeral translation showed good agreement with related works [MBP$^+$12, MMY$^+$12]. For example, the data computed from the skin markers showed that the humeral head translated superiorly during the early phase of arm elevation and inferiorly toward maximum elevation.

In this paper, we presented a patient-specific measurement technique based on the fusion of motion capture and MRI data. We demonstrated that a first estimation of joint translation at the shoulder joint was feasible based on skin-mounted markers. This original technique may open new horizons leading to improved understanding of shoulder pathologies and new possibilities of analyzing large ranges of shoulder motion, for instance during sport movements.

2.5 Evaluating the glenohumeral joint during sport

***Charbonnier C**, Chagué S, Kolo FC and Lädermann A. Shoulder motion during tennis serve: dynamic and radiological evaluation based on motion capture and magnetic resonance imaging. Int J CARS, 10(8):1289-1297, 2015.*

During tennis serve, several impingements could occur in the shoulder of the tennis players, such as postero-superior internal impingement [WBND92] or subacromial impingement [Nee72, NWS$^+$06]. These impingements result in joint damages of the glenoid labrum and rotator cuff tendons. The concurrence of the actual impingement zone and resulting joint damage in the same patient has not yet been confirmed. Moreover, there is a lack of validated non-invasive methods to ascertain impingement during motion. The goal of this study was to perform functional simulations of patient-specific shoulder joints during tennis serve and to detect potential impingement during their practice. This study also aimed at evaluating the prevalence of shoulder lesions in this group of tennis players based on MRI and at determining their relevance with the simulation findings.

Ten intermediate or ex-professional tennis players volunteered for the study. They underwent MR

shoulder arthrography. Two musculoskeletal radiologists assessed all MRI arthrograms for shoulder pathology (rotator cuff abnormalities [SPP+91], labral lesions [WBI+05] and bony changes [MAB+99]). For each tennis player, patient-specific 3D models of the shoulder bones, cartilage surfaces and labrum were obtained from MRI and AFs were determined according to ISB [WvdHV+05]. The volunteers participated to a motion capture session and performed three trials of the following variants of tennis serve: flat serve, when the ball is hit down and through with little to no spin; and kick serve, when the ball is hit with an upward motion, imparting top-spin on the ball.

Shoulder kinematics was obtained from motion capture using our kinematic model [CCK+14]. During motion simulation, internal and subacromial impingements were evaluated at the critical position: the late cocking stage of the serve. For internal impingement, a penetration depth method [CAVMT09, CKD+11] was used to virtually locate abnormal contacts and to compute the topographic extent of tissue compression. For subacromial impingement, the minimum humero-acromial distance that is typically used for the evaluation of such impingement was measured [CD12, GHER+05, TLAB+13].

Internal impingement was observed in 76% and 75% of the tennis players' shoulders during flat serve and kick serve, respectively. The computed zones of internal impingement were mainly located in the posterosuperior or superior region of the glenoid. Subacromial impingement was detected during flat serve for 29% of the tennis players' shoulders and was slightly more frequent during kick serve (38%). These findings were relevant with respect to radiologically diagnosed damaged zones in the rotator cuff and glenoid labrum.

In this paper, we dynamically evaluated shoulder impingement during tennis serve based on a methodology using motion capture and computer-assisted techniques. From our data, we concluded that tennis players presented frequent radiographic signs of structural lesions which seem to be mainly related to posterosuperior internal impingement due to repetitive abnormal motion contacts. Recurrent posterosuperior internal impingement could lead with time to cartilage/tendon hyper compression, which could be damageable for the GH joint.

2.6 Modeling the kinematics of the knee joint

***Charbonnier C**, Chagué S, Kolo FC, Duthon VB, Menetrey J. Multi-body optimization with subject-specific knee models: performance at high knee flexion angles. Comput Meth Biomech Biomed Eng, 20(14):1571-1579, 2017.*

When estimating knee kinematics from skin markers and stereophotogrammetry, MBO has provided promising results for reducing STA, but can still be improved. Moreover, the validation of the method remains limited. In particular, MBO methods rely on the determination of a predefined kinematic model with specific joint constraints. Simple kinematic constraints (spherical or hinge joints) were introduced, but showed limitations in reducing STA [SFC09, ABD+10, CDHdG17, RCD17], especially its effect on joint translations. Recently, anatomical constraints were proposed taking into account the articular surfaces and the ligaments [DCD10, BPH+11, GDJ13, GSJ+15, CDHdG17]. However, to our knowledge, only one work [CDHdG15] evaluated the performance of knee joint models with subject-specific kinematic constraints, showing MBO improvements. Another aspect common to all previous studies is that the knee ROM of the activities

considered in the in vivo experiments were limited to small flexion angles (usually between 40-65°). The performance of MBO at higher knee flexion angles should be hence verified. The goal of this study was thus to assess the performance of MBO with subject-specific knee models at high knee flexion angles (up to 110°) against knee joint kinematics measured by MRI.

Eight subjects were recruited for the study. They were MRI scanned at several unloaded knee flexions: 0°, 45°, 90° and 110°. The subjects were equipped with external MRI-compatible markers set (i.e., spherical capsules of Burgenstein Vitamin E) placed directly onto the skin using adhesive tape. Bone geometry was obtained from 3D reconstruction based on the 3D images in neutral knee flexion. Parallel mechanism was modeled with four ligaments (ACL, PCL, MCL, LCL) with prescribed ligament length variations as a function of knee flexion angle and two surface-on-plane contacts, providing more accurate constraints than the standard sphere-on-plane contacts. Moreover, the ligaments attachment sites were defined with reference to MRI. Three different kinematic models were considered in the MBO problem: no kinematic constraints (N), a spherical joint constraint (S) and parallel mechanism constraints (P) implemented as a penalty-based method [GDJ13].

In order to assess the performance of the three models used in MBO to compensate for STA at several knee flexions, model-based knee kinematics derived from the skin markers was compared to the knee kinematics derived from the MRI scans. To this end, the MR series were processed, the bones segmented and the reference bone positions and orientations were calculated by registering the subject-specific knee bone models to each MRI pose. After MBO, the RMSE between the model-based and the reference kinematics were computed for each method, each flexion angle and for the overall ROM.

The ranges of RMSE for knee rotations / displacements were 3.0°-9.2° / 1.3-3.5 mm for subject-specific knee models, 6.8°-8.7° / 6.0-12.4 mm without kinematic constraint and 7.1°-9.8° / 4.9-12.5 mm for spherical constraints. Overall, the lowest RMSE in all anatomical planes were obtained with the parallel mechanism constraints. Compared to constraints N and S, the model P was particularly good in minimizing displacements errors. RMSEs for flexion/extension and abduction/adduction obtained with model P were also smaller (5.8° and 3.0°, respectively), but were comparable for internal/external rotation compared to the other models (9.2°). For constraints N and S, the RMSE among the joint angles showed comparable results (difference of 1°). RMSE for flexion/extension increased for constraints N and S with higher knee flexion angles, whereas RMSE were in the similar range over all flexion angles for model P. For the other anatomical planes, as well as for displacements, parallel mechanism constraints had more stable errors across the whole ROM and less inter-subject variability.

In this study, we compared three MBO methods with different joint constraints against in vivo knee joint kinematics measured by MRI at high knee flexion angles, up to 110°. Moreover, we introduced anatomical constraints based on subject-specific knee joint models, taking into account personalized ligaments attachment sites and knee bone geometry. The results of this study indicate that MBO with subject-specific knee models was more effective in compensating STA compared to no kinematic and spherical constraints, in particular for joint displacements. Moreover, it seems to be more reliable over large ranges of knee flexion angle, since it models more precisely the physiological behavior of the knee joint (i.e., knee rollback), as previously evidenced [DCD10, LBN$^+$17].

HIP
ISSN 1120-7000

Hip Int 2015; 00 (00): 000-000
DOI: 10.5301/hipint.5000192

ORIGINAL ARTICLE

Analysis of hip range of motion in everyday life: a pilot study

Caecilia Charbonnier[1], Sylvain Chagué[1], Jérôme Schmid[2], Frank C. Kolo[3], Massimiliano Bernardoni[4], Panayiotis Christofilopoulos[5]

[1] Artanim Foundation, Medical Research Department, Geneva - Switzerland
[2] Geneva Health School (HEdS), HES-SO, Geneva - Switzerland
[3] Rive Droite Radiology Center, Geneva - Switzerland
[4] Medacta International SA, Castel San Pietro - Switzerland
[5] Department of Surgery, Orthopedics and Trauma Service, University Hospitals of Geneva, Geneva - Switzerland

ABSTRACT

Patients undergoing total hip arthroplasty are increasingly younger and have a higher demand concerning hip range of motion. To date, there is no clear consensus as to the amplitude of the "normal hip" in everyday life. It is also unknown if the physical examination is an accurate test for setting the values of true hip motion. The purpose of this study was: 1) to precisely determine the necessary hip joint mobility for everyday tasks in young active subjects to be used in computer simulations of prosthetic models in order to evaluate impingement and instability during their practice; 2) to assess the accuracy of passive hip range of motion measurements during clinical examination. A total of 4 healthy volunteers underwent Magnetic Resonance Imaging and 2 motion capture experiments. During experiment 1, routine activities were recorded and applied to prosthetic hip 3D models including nine cup configurations. During experiment 2, a clinical examination was performed, while the motion of the subjects was simultaneously captured. Important hip flexion (mean range 95°-107°) was measured during daily activities that could expose the prosthetic hip to impingement and instability. The error made by the clinicians during physical examination varied in the range of ±10°, except for flexion and abduction where the error was higher. This study provides useful information for the surgical planning to help restore hip mobility and stability, when dealing with young active patients. The physical examination seems to be a precise method for determining passive hip motion, if care is taken to stabilise the pelvis during hip flexion and abduction.

Keywords: Total hip arthroplasty, Range of motion, Impingement, Joint instability, Daily activities, Physical examination

Introduction

Total Hip Arthroplasty (THA) aims to restore patient mobility by providing a pain-free and stable joint. An increasing number of younger and more active patients undergo THA for early onset arthritis (1, 2). Good function and longevity of a prosthetic hip depend on many inter-related factors. Suboptimal geometry, spatial positioning and orientation of implant components may contribute to early failures (3-5). Hip kinematics is also an important factor, since routine movements can cause impingements within the joint between both bony and prosthetic components, reducing the range of motion (ROM) and causing dislocations (6, 7).

The effects of prosthetic components positioning in resultant hip ROM, impingements and dislocation mechanisms have been previously documented (8-11). These studies were generally based on *in vitro* simulations of prosthetic models using simple, idealised kinematic sequences presumed to be representative of activities prone to implant failures. Unlike the works of Nadzadi et al (6) or Pedersen et al (7), too few studies have considered the use of more realistic subject's kinematic data as input for the simulation. Moreover, there exist no motion data matching the hip ROM of young patients in daily tasks, since previous simulation studies have focused on the prosthetic mobility of elderly patients. Nowadays, candidates for a THA are increasingly younger and more demanding on hip ROM, collecting data concerning this group is hence relevant for better surgical undertaking.

Another aspect that has caught our attention in this study is that patient care starts with correct physical examination and determining the patient's passive hip ROM is one of its key points. Usually, measurements of passive hip ROM are

Accepted: August 4, 2014
Published online: November 6, 2014

Corresponding author:
Caecilia Charbonnier
Artanim Foundation
41b, Route des Jeunes
1227 Carouge
Geneva, Switzerland
caecilia.charbonnier@artanim.ch

performed by clinicians using standard goniometers or inclinometers whose reliability has been well studied (12-15). Unfortunately, this process may lack precision because of movement of other joints around the pelvis (i.e., no direct access to the joint). It is also unknown whether the examiner's clinical experience plays a role in obtaining correct results. To our knowledge, assessing the accuracy of the physical examination as a method for determining the true passive hip ROM is little investigated. Some authors compared hip ROM measurements obtained with goniometer and electromagnetic tracking system (14) or optical motion capture (13), but these studies were affected by skin movement artifacts that could hinder accurate kinematic estimation with electromagnetic or optical motion capture systems (16). Therefore, research is still needed in order to attest the validity of the physical examination.

The purpose of this study was hence twofold: 1) to define in a precise way the necessary hip joint mobility for everyday tasks in young active subjects. These data would be then used in computer simulations of prosthetic hip joint 3D models to evaluate relative risk of impingement and loss of joint congruence during their practice; 2) to assess the accuracy of the passive hip ROM clinical examination as a method for setting the values of true hip motion.

In order to obtain accurate hip joint kinematic data, we performed a pilot study using a validated patient-specific technique coupling optical motion capture to magnetic resonance imaging (MRI) where skin movement artifacts are effectively tackled.

Materials and Methods

The present study included an MRI study and two different motion capture experiments. Experiment 1 - aimed at determining the hip ROM in everyday activities to be used in computer simulations of prosthetic hip models, while experiment 2 - intended to assess the accuracy of passive hip ROM measurements during clinical examination.

A total of 4 healthy young active participants (1 female, 3 males – 8 hips) were recruited from staff of the investigators' research teams. Subject demographics are shown in Table I. Exclusion criteria were previous hip injuries, any kind of groin pain, hip surgery or contraindications for MRI. Institutional ethical approval and informed consent were obtained prior to data collection.

MR Imaging and bone model reconstruction

The 4 volunteers were MRI scanned with a 1.5 T HDxT system (General Electric Healthcare, Milwaukee, WI, USA). A flexible surface coil was used and the images were acquired in the supine position. The imaging protocol was issued from a previous study (17) that allowed for the acquisition of images suitable for both radiologic analysis and bone model reconstruction. The region of interest of MRI datasets extended from the L4 vertebra to the knee. DICOM files of the scans were transferred to a personal computer and virtual 3D models of the hip joint were reconstructed thanks to custom-made segmentation software (18). MRI was privileged over Computed Tomography (CT) imaging, because it was not invasive and the software used has proven to be very accurate for the reconstruction of hip 3D bone models from MRI data (mean ± standard deviation error: 1.25 ± 1.0 mm) (18). As a result, patient-specific 3D models of the pelvis and femur were reconstructed for each volunteer.

A musculoskeletal radiology specialist evaluated all images to assess any bony abnormalities, such as hip dysplasia or cam/pincer morphology. The morphological analysis included the following radiographic criteria: acetabular depth (19), acetabular version (17), lateral center edge (CE) angle (20), anterior CE angle (20), femoral head-neck alpha angle (21), neck-shaft angle (22) and femoral neck anteversion (22). Measurements were performed on the MRI scans in accordance with the methods cited in the mentioned references. Thus, the acetabular depth and version were considered as normal when the value was positive. For the angles, they were considered as normal when included in the following ranges: lateral CE angle within [25°, 39°]; anterior CE angle within [25°, 39°]; alpha angle <55°; neck-shaft angle within [120°, 140°]; femoral neck anteversion <15°.

Motion capture experiment 1

To record the hip ROM in everyday life, the 4 participants were equipped with spherical retroreflective markers (Ø14 mm) placed directly onto the skin using double sided adhesive tape. A total of 2 clusters of 6 markers were placed on the lateral and frontal parts of both thighs; 6 markers were also stuck on pelvic anatomical landmarks (e.g., anterior superior iliac spines). Additional markers were distributed over the body (trunk, upper limbs, legs and feet) to confer a more complete visualisation from general to detailed.

Motion capture data from the participants were acquired during 5 activities: stand-to-sit, lie down on the floor, lace the shoes while seated and pick an object on the floor while sitting or standing. These movements were chosen, because they are known to be painful in case of hip disorders or prone to hip implants related complications (e.g., dislocation, impingements) (6, 7). Marker data were captured within a 108 m^3 measurement volume (6 x 6 x 3 m) using 24 infrared cameras (Vicon

TABLE I - Subject demographics

Subjects #	Gender	Race	Age	Weight (kg)	Height (cm)	BMI (kg/m²)
1	Male	Caucasian	33	78	182	23.55
2	Male	Caucasian	24	70	184	20.68
3	Male	Caucasian	25	80	180	24.69
4	Female	Caucasian	30	69	180	21.30

MXT40S, Oxford Metrics, UK), sampling at 120 Hz. Participants were asked to perform each activity 3 times. For the activities requiring a chair, a standard 45 cm height stool was used to ensure that all pelvic markers were visible to motion capture cameras.

Motion capture experiment 2

In order to assess the accuracy of passive hip ROM measurement by physical examination, 2 orthopaedic surgeons with different levels of experience were involved in this experiment. Surgeon 1 (junior) had 2 years of clinical experience. Surgeon 2 (senior) had 12 years of clinical experience. Each examiner performed successively and in turn a measurement of hip ROM of the participants' hips, while the motion of the subjects was simultaneously recorded using motion capture. Marker data were collected with the same motion capture system and the same markers set-up as those used for experiment 1.

Measurement of passive hip ROM was acquired according to the following sequences: 1) supine: maximal flexion, maximal internal/external rotation with hip flexed 90°, maximal abduction; 2) seated: maximal internal/external rotation with hip and knee flexed 90°. For all measurements, a hand held goniometer was used by the examiner to measure hip angles in those different positions according to the neutral zero method (23). Care was taken to stabilise the pelvis during passive motion to prevent overestimation of the motion values obtained. For both sequences, a standard hard table was utilised as an examination table in order to avoid movement artefacts occurring because of a mattress. The values obtained by the examiners were noted down to be later compared with the kinematic data computed from simultaneous motion capture.

Kinematic analysis

Marker data from motion capture experiments 1 and 2 were used to compute the 3D kinematics of the hip joint. The major drawback with optical motion capture systems is that markers are placed on the skin surface and move relatively to the underlying bone during activities with the deformation of the soft tissues. This represents an artefact and is usually referred to as soft tissue artefact (STA). STA has been proved to be the major source of errors in skin marker-based joint motion analysis (16). To solve this issue, we used a validated optimised fitting algorithm which accounted for STA and patient-specific anatomical constraints (24, 25). Indeed, computed motion was applied to the subject's hip joint 3D models reconstructed from their MRI data, which allowed accounting for the subject's anatomy and kinematic parameters (e.g., hip joint centre). The accuracy of this algorithm was 0.4, 0.59, 0.24 mm for medio-lateral, antero-posterior and proximo-distal translations, and 0.55°, 2.86°, 1.71° for flexion/extension, abduction/adduction and internal/external rotation, respectively. This provided sufficient accuracy for clinical use in the study of hip pathology and kinematics.

To permit motion description of the hip joint, local coordinate systems (Fig. 1) were established based on the definitions

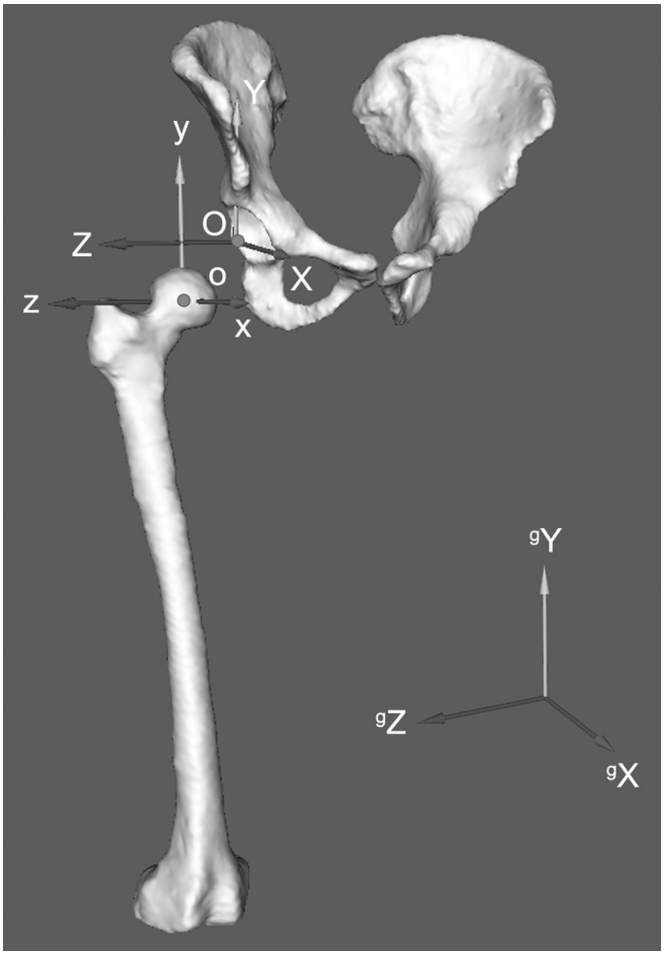

Fig. 1 - Reconstructed pelvis and femur bone models with pelvic (XYZ) and femoral (xyz) coordinate systems in relation to the global coordinate system (^{g}X ^{g}Y ^{g}Z). By computing the relative orientation of the femoral frame to the pelvic frame, the relative orientation between the pelvis and femur can be determined and decomposed into three successive rotations (flex/ext, abd/add and IR/ER).

suggested by the International Society of Biomechanics (26) to represent the pelvic and femoral segments using anatomical landmarks identified on the subject's bony 3D models. The hip joint center was calculated using a functional method (27). For the motion capture experiment 1, the hip ROM was quantified for each participant and for all recorded daily activities. This was obtained given the computed bones poses from motion capture data by calculating the relative orientation between the pelvic and femoral coordinate systems at each point of the movement (25). This was finally expressed in clinically recognisable terms (flex/ext, abd/add and IR/ER) by decomposing the relative orientation into three successive rotations (28). It is important to note that the computations were performed independently of the major anatomical planes (i.e., sagittal, transverse, frontal planes). For the motion capture experiment 2, passive hip ROM recorded during clinical examination were quantified with the same method. Relevant angles were computed when the examiners were holding position of the lower limb in order to be compared with their measurements.

Simulation of prosthetic hips

Movements recorded in the motion capture experiment 1 were applied to prosthetic hip models, in order to evaluate relative the risk of impingement and joint instability during everyday activities. To this aim, a 3D hip model with a prosthesis constituted by an acetabular cup of 48 mm and a femoral head of 28 mm diameter was created. Bone geometry was obtained from a 3D reconstruction of a pelvic CT in a young patient undergoing hip arthroplasty. Acetabular and femoral implants were modeled according to a standard commercial design (Medacta International, Castel San Pietro, Switzerland). The femoral component was implanted respecting the natural anteversion of the femur being parallel to the posterior cortex of the femoral neck. To explore the effect of acetabular component positioning, nine acetabular cup positions (combinations of 40°, 45° and 60° of inclination with 0°, 15° and 30° of anteversion) were chosen, including and extending beyond the conventional "safe zone" of 30°-50° of inclination and 5-25° of anteversion (29). Coordinate systems were established for the pelvis and femur based upon anatomical landmarks and definitions of the International Society of Biomechanics (26).

Simulation was executed with custom-made software that allows testing of the prosthetic hip model with real-time evaluation of impingement and joint instability (30). Hip angles (3 rotations) computed from motion capture data were first applied at each time step to the prosthetic model in its anatomical frame. Then, a collision detection algorithm (24, 25) was used to virtually locate any prosthetic or bony impingements. The impingement zone was denoted using a color scale (Fig. 2) of increasing contact (e.g., blue = no contact, red = highest contact) and its location documented based on a reference system dividing the acetabulum into 8 sectors (position 1, anterior; position 2, anterosuperior; position 3, superior; position 4, posterosuperior; position 5, posterior; position 6, posteroinferior; position 7, inferior; position 8, anteroinferior). When impingement occurred, the hip ROM was noted down. Moreover, femoral head translations were computed to evaluate the joint congruence. Since no loads were applied to the joint, the computed translations should therefore be viewed as only representative of joint instability or subluxation rather than dislocation. The reader can refer to the reference (30) for a more comprehensive description of the simulation technique. The 5 different daily activities (3 trials for each subject) were examined, thus a total of 60 simulations were performed for each cup position.

Statistical analysis

We analysed all subject's hips according to the radiographic criteria. Maximum hip ROM from the 3 trials recorded in experiment 1 was determined for all participants and for all daily activities. For the simulations, we calculated the frequency of prosthetic and bony impingement and the distribution of the zone of impingement. We also computed the hip ROM and the amount and direction of subluxation when impingement occurred. We computed the errors made by the 2 examiners during the clinical exams recorded in experiment 2. The 2 different tests for measuring hip internal/external rotation (supine or seated) were also compared. For the comparisons between the goniometer and the motion capture measurements, Kolmogorov-Smirnov tests were first used to test for a normal distribution. Then, two-tailed Wilcoxon Signed-Rank tests were performed. A significance level was chosen at $p<0.05$. Descriptive statistics are presented as mean, range and standard deviations (SD) for each figure. The statistical software package R, version 3.1.1 was employed.

Results

Imaging data

According to the morphological analysis, the hips of the 4 volunteers did not present any cam or pincer morphology. No dysplastic hips, acetabular retroversion, femoral neck retroversion, deep acetabulum or abnormal offset of the femoral head-neck junction was noted. It was concluded that based on the radiologic criteria all 8 measured hips were morphologically normal. Table II summarises the results of our morphological analysis. For the femoral head-neck alpha angles, only the measurements in anterior and anterosuperior positions are reported, since they are the more significant.

Motion data

As shown in Table III, daily activities involve intensive hip flexion. For all movements, a minimum of 95° hip flexion was required. Globally, the angles showed low standard deviations (range 3.6 to 12.2), suggesting that movements were performed similarly across subjects.

Regarding the clinical examination, the errors made by the examiners varied in the range of ± 10°, except for the flexion and abduction where the errors were more significant (Table IV, flexion: mean 9.5°, range -7° to 22°, $p = 0.058$; abduction: mean 19.5°, range 8° to 32°, $p = 0.014$). No substantial differences between the errors made by the 2 examiners were noted (average error for each examiner: 7.4° vs. 8.4°). In Table IV, it is also interesting to note that examiners tended to overestimate flexion, abduction and internal rotation in supine position (positive mean values), while internal and external rotation tended to be slightly underestimated (negative mean values) in sitting position. For the differences between the hip internal/external rotations when measured in supine or sitting position, the results issued from both orthopaedists and motion capture measurements showed that the 2 tests did not yield similar results. Particularly, internal rotation was lower in supine than sitting for all measurements. Similarly, external rotation was always higher in supine than sitting.

Simulation data

Simulations showed collisions occurring at maximal ranges of motion in all cup positions (Tab. V). For all activities, cups with more inclination and anteversion encountered less impingement. ROM in flexion increased with increasing cup anteversion (e.g., 99° at 45°/0°, 101° at 45°/15°and 103° at 45°/30° in average during pick an object on the floor while

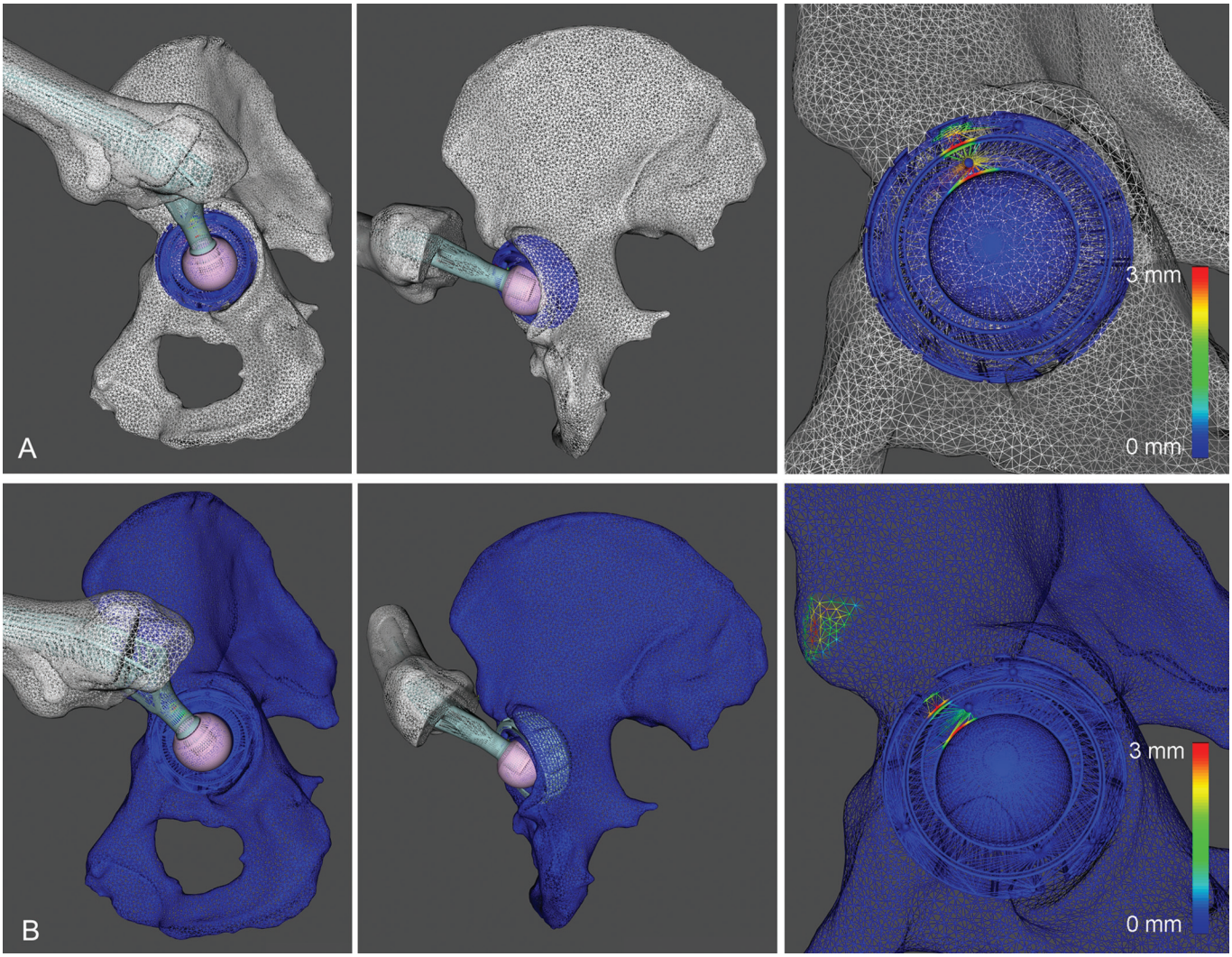

Fig. 2 - Visualisation of the impingement region during simulation (lateral and posterior views). The colours represent the area of increased contact (blue = no contact, red = highest contact). **A**) Prosthetic impingement between the stem and the cup/liner (cup at 40°/0°, lace the shoes). **B**) Prosthetic impingement between the stem and cup/liner including bony impingement between the medial corner of the femoral osteotomy and the anterior inferior iliac spine (cup at 45°/15°, lie down).

TABLE II - Morphological analysis (n = 8)*

Measures	Mean	SD	Min	Max
Acetabular depth (mm)	10.8	2.4	7.7	13.6
Acetabular version (°)	4.5	2.0	1.3	6.6
Lateral CE angle (°)	27.3	2.0	25.4	31.6
Anterior CE angle (°)	35.7	2.7	31.0	38.7
Femoral head-neck alpha angle - anterior (°)	39.5	3.7	34.7	47.3
Femoral head-neck alpha angle - anterosuperior (°)	40.9	6.3	33.8	51.0
Neck-shaft angle (°)	131.2	4.3	126.4	137.9
Femoral neck anteversion (°)	7.6	3.8	3.1	13.4

*Data are the number of hips.

TABLE III - Maximum hip ROM (°) during everyday activities (n = 24)*

Movements	Mean	SD	Range
Stand-to-sit			
Flex	96.5	11.7	80-115
Abd/Add	7.4/0	6.1	2 (add)-19 (abd)
IR/ER	0/2.3	4.7	9 (IR)-14 (ER)
Lie down on the floor			
Flex	107.1	12.1	85-130
Abd/Add	6.2/0	8.4	5 (add)-25 (abd)
IR/ER	1.9/0	7.1	11 (IR)-21 (ER)
Lace the shoes (seated)			
Flex	107.8	10.5	92-121
Abd/Add	3.8/0	6.3	7 (add)-14 (abd)
IR/ER	0.3/0	3.6	5 (ER)-10 (IR)
Pick an object on the floor (seated)			
Flex	94.8	8.8	74-110
Abd/Add	13.4/0	4.3	5-21 (abd)
IR/ER	7.3/0	4.1	1-13 (IR)
Pick an object on the floor (standing)			
Flex	102.1	5.7	92-109
Abd/Add	11.2/0	5.7	3-20 (abd)
IR/ER	8.5/0	12.2	3 (ER)-32 (IR)

*Data are reported for the four participants (8 hips) performing three trials for each activity.

TABLE IV - Errors (°) made by the examiners and comparison between goniometer vs. motion capture measurements during clinical examination

Motion	Mean (abs)*	Mean**	SD	Min	Max	*P* Value†
Supine						
Flex	9.5	7.7	6.7	-7	22	0.058
IR	3.5	2.2	2.8	-2	8	0.259
ER	5.7	-3.5	4	-11	6	0.207
Abd	19.5	19.5	8.1	8	32	0.014
Seated						
IR	3.6	-0.6	3.2	-9	6	0.916
ER	5.7	-1.5	2.9	-9	9	0.574

*Mean calculated from absolute errors.
**A negative value means that the examiners tended to underestimate the angle, otherwise they tended to overestimate it.
† *P* values obtained with use of Wilcoxon Signed-Rank test.

seated). Regardless of the cup positions, most impingements were observed during lie down (83/108 trials, 77%) and lace the shoes (63/108 trials, 58%) which were the movements requiring the highest hip flexion. Both prosthetic and bony impingements were observed (Fig. 2), but prosthetic impingements were the most frequent (251 prosthetic impingements vs. 117 bony impingements out of 540 trials tested). Bony impingements between the medial corner of the femoral osteotomy and the anterior inferior iliac spine (subspine impingement) occurred during lie down (50%), lace the shoes (33%), pick an object on the floor while standing (25%), and their frequency was indifferent of the cup positioning. Concerning the location of impingements, they were located in either the anterosuperior or anterosuperior/superior area of the acetabulum (position 2 and 2/3 according to our documentation).

TABLE V - Impingement's location and occurrence, subluxation (mm) and hip ROM (°) when impingement occurred during daily activities. For each activity, the 3 trials of the 4 subjects were tested (n = 12)

	0° anteversion						15° anteversion						30° anteversion					
	Loc*	Count	Subluxation†	Flex†	Abd†	IR/ER†	Loc*	Count	Subluxation†	Flex†	Abd†	IR/ER†	Loc*	Count	Subluxation†	Flex†	Abd†	IR/ER†
Stand-to-sit																		
40° inclination	2	9	2.1 ± 1.4	102 ± 11	8 ± 4	0/3 ± 9	2	5	0.9 ± 1.2	103 ± 14	10 ± 2	3 ± 8/0	2	3	0.5 ± 1.0	104 ± 15	10 ± 2	0/0 ± 8
45° inclination	2	7	1.2 ± 1.1	98 ± 12	7 ± 4	0/1 ± 9	-	0	-	-	-	-	-	0	-	-	-	-
60° inclination	-	0	-	-	-	-	-	0	-	-	-	-	-	0	-	-	-	-
Lie down																		
40° inclination	2/3	12	5.1 ± 1.2	108 ± 8	7 ± 8	2 ± 4/0	2/3	12	4.1 ± 1.1	109 ± 9	7 ± 9	2 ± 4/0	2/3	10	3.3 ± 1.8	113 ± 9	8 ± 11	2 ± 4/0
45° inclination	2/3	12	3.9 ± 1.5	108 ± 8	6 ± 8	2 ± 4/0	2/3	10	2.5 ± 1.4	110 ± 7	6 ± 8	2 ± 5/0	2/3	9	2.0 ± 1.5	113 ± 9	9 ± 11	2 ± 5/0
60° inclination	2	6	0.5 ± 0.8	109 ± 2	3 ± 6	1 ± 5/0	2	6	0.3 ± 0.4	111 ± 2	4 ± 7	1 ± 5/0	2	6	0.3 ± 0.5	111 ± 2	4 ± 7	1 ± 5/0
Lace the shoes																		
40° inclination	2	12	4.6 ± 1.9	111 ± 10	5 ± 7	1 ± 2/0	2	10	3.2 ± 2.0	112 ± 9	4 ± 7	1 ± 1/0	2	6	2.1 ± 2.2	118 ± 4	5 ± 7	2 ± 1/0
45° inclination	2	11	3.2 ± 2.0	112 ± 9	5 ± 7	1 ± 1/0	2	6	1.6 ± 1.8	116 ± 3	2 ± 7	2 ± 1/0	2	6	1.4 ± 1.5	117 ± 4	3 ± 7	2 ± 1/0
60° inclination	2	4	0.5 ± 0.9	115 ± 3	0 ± 4	2 ± 1/0	2	4	0.5 ± 1.0	116 ± 6	1 ± 7	2 ± 2/0	2	4	0.5 ± 1.2	116 ± 6	1 ± 7	2 ± 2/0
Pick object (seated)																		
40° inclination	2	12	3.8 ± 1.0	96 ± 10	15 ± 2	10 ± 2/0	2	10	2.8 ± 1.6	99 ± 9	14 ± 1	9 ± 2/0	2	10	2.5 ± 1.3	99 ± 9	14 ± 1	9 ± 2/0
45° inclination	2	10	2.5 ± 1.3	99 ± 9	14 ± 1	9 ± 2/0	2	7	1.5 ± 1.3	101 ± 7	15 ± 2	9 ± 2/0	2	6	1.1 ± 1.2	103 ± 7	15 ± 1	9 ± 3/0
60° inclination	-	0	-	-	-	-	-	0	-	-	-	-	-	0	-	-	-	-
Pick object (standing)																		
40° inclination	2	12	4.3 ± 2.3	101 ± 4	12 ± 3	13 ± 9/0	2	10	3.3 ± 2.6	101 ± 4	12 ± 3	15 ± 8/0	2	9	2.7 ± 2.5	102 ± 3	12 ± 3	16 ± 7/0
45° inclination	2	9	2.7 ± 2.7	102 ± 3	11 ± 3	17 ± 7/0	2	7	2.0 ± 2.5	102 ± 2	10 ± 1	19 ± 5/0	2	9	1.6 ± 2.4	102 ± 2	10 ± 1	21 ± 1/0
60° inclination	2	6	0.9 ± 1.3	102 ± 2	10 ± 1	21 ± 1/0	2	6	0.3 ± 0.4	103 ± 1	10 ± 1	21 ± 1/0	2	6	0.3 ± 0.4	103 ± 1	10 ± 1	21 ± 1/0

*Location of the impingement zone around the acetabulum according to our documentation (2 = anterosuperior, 2/3 = anterosuperior/superior).
†Mean ± SD.

Subluxations followed the same trend and were less important in cups with more inclination and anteversion (e.g., 5.1 mm at 40°/0°, 2.5 mm at 45°/15°and 0.3 mm at 60°/30° in average during lie down). For all cup positions and all activities, subluxations occurred in a posterior direction as a consequence of impingements.

Discussion

To date, there is no clear consensus as to the amplitude of the "normal hip". Moreover, young patients are increasingly receiving surgical treatment for early onset hip disease. Current research related to THA generally focuses on the analysis of typical patients undergoing THA. Unlike previous works, we have presented an *in-vivo* study based on motion capture and MRI to accurately determine the ROM of the hip joint in young active subjects during daily activities. With the use of captured motion, computer simulations of prosthetic hip joint 3D models were performed to evaluate impingement and related joint instability during their practice. As far as we know, this is the first study that aims to objectively assess the accuracy of passive hip ROM measurements during physical examination.

Daily activities of a "normal hip" involve intensive hip flexion. For all movements, a minimum of 95° hip flexion was required, lacing the shoes and lying down being the more demanding. Abduction/adduction and internal/external rotation remained low and variable across subjects. As expected, the necessary hip joint mobility for everyday tasks in young active subjects was significant, which could explain why such motion can yield hip pain or possible early implant failure.

Regarding this latter aspect, simulations showed frequent impingements during movements occurring at maximal ranges of motion. No cup position was spared, but the ones with more inclination and anteversion encountered less impingement for all activities. This could be explained by the type of movements tested requiring a high degree of flexion, which renders the cups with less inclination and anteversion more favorable to abutment during such motion. We did not perform testing of movements of daily living requiring extension such as pivoting in a standing position or rolling over in bed, which could have yielded different results. It is also important to note that cups with more inclination or anteversion are often subject to greater stress concentrations and wear (7, 31). In terms of mobility, our data showed that the ROM in flexion increased with increasing cup anteversion, as previously noted (9, 10). Moreover, leaning over from a seated position to tie a shoe or lying down on the floor proved to be the most impingement-prone challenges. Concerning the location of impingement, they were mainly located in the anterosuperior area of the acetabulum leading to posterior subluxation. These instability patterns were consistent with previous works (7, 10). Eventually, both prosthetic and bony impingements were observed. The frequency of bony impingements was indifferent of the cup positioning. This may be due to the geometry of the bones used in the simulation with the high amplitude of movements tested which render the conflict inevitable whatever the position of the cup.

Concerning physical examination, the results showed that the errors made by the 2 examiners were acceptable for internal/external rotation, but were quite significant when evaluating passive flexion and abduction. For these last 2 measurements, virtual simulations of the process revealed interesting motion trends of the pelvis during the exams. During flexion, a posterior rotation of the pelvis in the sagittal anatomical plane was observed. This movement was accompanied by a slight flexion of the hip joint that hence followed the alignment of the acetabulum. During abduction, a medial rotation of the pelvis in the frontal anatomical plane was observed. These motion patterns could explain why examiners overestimated the values of these 2 measurements by ignoring subtle motion of the pelvis. Regarding the differences between the 2 tests for measuring hip internal/external rotation, internal rotation was lower in supine than sitting, while external rotation was higher in supine than sitting. The errors made by the examiners were equivalent in both tests. Therefore, both tests should be performed when examining the hip joint since the results observed express different values of pelvic position variation. The examiner's experience was also not found to be a determining factor.

Several study limitations need to be stated: firstly, the collection of motion data was based on a small number of participants. This work is part of a larger research project that aims to improve the pre-operative planning for THA by including a dynamic simulation of the prosthesis using motion data in everyday life of representative subjects. Our goal was to perform a pilot study to attest the validity of the methods developed before performing clinical studies with patients undergoing THA. Secondly, potential sources of errors should be mentioned such as the 3D bone reconstruction from MRI data (error ≈ 1.25 mm) and the kinematics computation from motion capture data (translational error ≈ 0.5 mm, rotational error <3°). Thirdly, our prosthetic joint simulation ignores the contributions of loads and soft tissue structures around the joint that could play a role in the impingement and dislocation mechanisms. Finally, the radiological analysis for hip abnormalities was based on native hip MRI (reliability of the findings estimated at 65%) and not MR arthrography that may offer better definition of intra-articular pathology.

Daily activities involve important hip flexion that could expose the prosthetic hip to impingement and subluxation. This information should be considered in the surgical planning and prosthesis design when restoring hip mobility and stability, particularly when dealing with young active patients. The clinical examination seems to be a precise method for determining passive hip motion, if extra care is taken to stabilise the pelvis during flexion and abduction to prevent overestimation of the range of motion. Further studies are required before attesting to the accuracy of this test.

Acknowledgments

We would like to thank Dr. Placido Bartolone for his participation in the motion capture experiment #2 and Matteo Ponzoni for his help in the preparation of the different implant configurations.

Disclosures

Financial support: This research work was supported by the "MyHip: Patient-Specific Pre-operative Planning and Intra-operative Surgical Guidance for Total Hip Arthroplasty" project funded by the Swiss Commission for Technology and Innovation (CTI n° 13573.1 PFFLE-LS).
Conflict of interest: None.

References

1. Kurtz SM, Lau E, Ong K, Zhao K, Kelly M, Bozic KJ. Future young patient demand for primary and revision joint replacement: National projections from 2010 to 2030. Clin Orthop Relat Res. 2009;467(10):2606-2612.
2. Nemes S, Gordon M, Rogmark C, Rolfson O. Projections of total hip replacement in Sweden from 2013 to 2030. Acta Orthop. 2014;85(3):238-243.
3. Barrack RL. Dislocation after total hip arthroplasty: implant design and orientation. J Am Acad Orthop Surg. 2003;11(2):89-99.
4. Malik A, Maheshwari A, Dorr LD. Impingement with total hip replacement. J Bone Joint Surg Am. 2007;89(8):1832-1842.
5. Peter R, Lübbeke A, Stern R, Hoffmeyer P. Cup size and risk of dislocation after primary total hip arthroplasty. J Arthroplasty. 2011;26(8):1305-1309.
6. Nadzadi ME, Pedersen DR, Yack HJ, Callaghan JJ, Brown TD. Kinematics, kinetics, and finite element analysis of commonplace maneuvers at risk for total hip dislocation. J Biomech. 2003;36(4):577-591.
7. Pedersen DR, Callaghan JJ, Brown TD. Activity-dependence of the "safe zone" for impingement versus dislocation avoidance. Med Eng Phys. 2005;27(4):323-328.
8. D'Lima DD, Urquhart AG, Buehler KO, Walker RH, Colwell CW Jr. The effect of the orientation of the acetabular and femoral components on the range of motion of the hip at different head-neck ratios. J Bone Joint Surg Am. 2000;82(3):315-321.
9. Higa M, Tanino H, Abo M, Kakunai S, Banks SA. Effect of acetabular component anteversion on dislocation mechanisms in total hip arthroplasty. J Biomech. 2011;44(9):1810-1813.
10. Patel AB, Wagle RR, Usrey MM, Thompson MT, Incavo SJ, Noble PC. Guidelines for implant placement to minimize impingement during activities of daily living after total hip arthroplasty. J Arthroplasty. 2010;25(8):1275-1281, e1.
11. Widmer KH, Zurfluh B. Compliant positioning of total hip components for optimal range of motion. J Orthop Res. 2004;22(4):815-821.
12. Clapis PA, Davis SM, Davis RO. Reliability of inclinometer and goniometric measurements of hip extension flexibility using the modified Thomas test. Physiother Theory Pract. 2008;24(2):135-141.
13. Moreside JM, McGill SM. Quantifying normal 3D hip ROM in healthy young adult males with clinical and laboratory tools: hip mobility restrictions appear to be plane-specific. Clin Biomech (Bristol, Avon). 2011;26(8):824-829.
14. Nussbaumer S, Leunig M, Glatthorn JF, Stauffacher S, Gerber H, Maffiuletti NA. Validity and test-retest reliability of manual goniometers for measuring passive hip range of motion in femoroacetabular impingement patients. BMC Musculoskelet Disord. 2010;11(1):194.
15. Roach S, San Juan JG, Suprak DN, Lyda M. Concurrent validity of digital inclinometer and universal goniometer in assessing passive hip mobility in healthy subjects. Int J Sports Phys Ther. 2013;8(5):680-688.
16. Leardini A, Chiari L, Della Croce U, Cappozzo A. Human movement analysis using stereophotogrammetry. Part 3. Soft tissue artifact assessment and compensation. Gait Posture. 2005;21(2):212-225.
17. Kolo FC, Charbonnier C, Pfirrmann CWA, et al. Extreme Hip Motion in Professional Ballet Dancers: Dynamic and Morphologic Evaluation Based on MRI. Skeletal Radiol. 2013;42:689-698.
18. Schmid J, Kim J, Magnenat-Thalmann N. Robust statistical shape models for MRI bone segmentation in presence of small field of view. Med Image Anal. 2011;15(1):155-168.
19. Pfirrmann CWA, Mengiardi B, Dora C, Kalberer F, Zanetti M, Hodler J. Cam and pincer femoroacetabular impingement: characteristic MR arthrographic findings in 50 patients. Radiology. 2006;240(3):778-785.
20. Stelzeneder D, Hingsammer A, Bixby SD, Kim Y-J. Can radiographic morphometric parameters for the hip be assessed on MRI? Clin Orthop Relat Res. 2013;471(3):989-999.
21. Nötzli HP, Wyss TF, Stoecklin CH, Schmid MR, Treiber K, Hodler J. The contour of the femoral head-neck junction as a predictor for the risk of anterior impingement. J Bone Joint Surg Br. 2002;84(4):556-560.
22. Duthon VB, Charbonnier C, Kolo FC, et al. Correlation of Clinical and MRI Findings in Hips of Elite Female Ballet Dancers. Arthroscopy. 2013;29:411-419.
23. Cave EF, Roberts SM. A method of measuring and recording joint function. J Bone Joint Surg. 1936;18:455-466.
24. Charbonnier C, Assassi L, Volino P, Magnenat-Thalmann N. Motion Study of the Hip Joint in Extreme Postures. Vis Comput. 2009;25(9):873-882.
25. Charbonnier C, Kolo FC, Duthon VB, et al. Assessment of congruence and impingement of the hip joint in professional ballet dancers: a motion capture study. Am J Sports Med. 2011;39(3):557-566.
26. Wu G, Siegler S, Allard P, et al; Standardization and Terminology Committee of the International Society of Biomechanics; International Society of Biomechanics. ISB recommendation on definitions of joint coordinate system of various joints for the reporting of human joint motion—part I: ankle, hip, and spine. J Biomech. 2002;35(4):543-548.
27. Gilles B, Christophe FK, Magnenat-Thalmann N, et al. MRI-based assessment of hip joint translations. J Biomech. 2009;42(9):1201-1205.
28. Grood ES, Suntay WJ. A joint coordinate system for the clinical description of three-dimensional motions: application to the knee. J Biomech Eng. 1983;105(2):136-144.
29. Lewinnek GE, Lewis JL, Tarr R, Compere CL, Zimmerman JR. Dislocations after total hip-replacement arthroplasties. J Bone Joint Surg Am. 1978;60(2):217-220.
30. Charbonnier C, Chagué S, Ponzoni M, Bernardoni M, Hoffmeyer P, Christofilopoulos P. Sexual activity after total hip arthroplasty: a motion capture study. J Arthroplasty. 2014;29(3):640-647.
31. D'Lima DD, Chen PC, Colwell CW Jr. Optimizing acetabular component position to minimize impingement and reduce contact stress. J Bone Joint Surg Am. 2001;83(Suppl 2 Pt 2):87-91.

Int J CARS
DOI 10.1007/s11548-015-1177-2

ORIGINAL ARTICLE

MyHip: supporting planning and surgical guidance for a better total hip arthroplasty

A pilot study

Jérôme Schmid[1] · Christophe Chênes[1] · Sylvain Chagué[2] · Pierre Hoffmeyer[3] · Panayiotis Christofilopoulos[3] · Massimiliano Bernardoni[4] · Caecilia Charbonnier[2]

Received: 15 November 2014 / Accepted: 13 March 2015

Abstract
Purpose Total hip arthroplasty (THA) aims to restore patient mobility by providing a pain-free and stable artificial joint. A successful THA depends on the planning and its execution during surgery. Both tasks rely on the experience of the surgeon to understand the complex biomechanical behavior of the hip. We investigate the hypothesis that a computer-assisted solution for THA effectively supports the preparation and execution of the planning.
Methods We devised *MyHip* as a computer-assisted framework for THA. The framework provides pre-operative planning based on medical imaging and optical motion capture to optimally select and position the implant. The planning considers the morphology and range of motion of the patient's hip to reduce the risk of impingements and joint instability. The framework also provides intra-operative support based on patient-specific surgical guides. We performed a post-operative analysis on three patients who underwent THA. Based on post-operative radiological images, we reconstructed a patient-specific model of the prosthetic hip to compare planned and effective positioning of the implants.
Results When the guides were used, we measured non-significant variations of planned executions such as bone cutting. Moreover, patients' hip motions were acquired and used in a dynamic simulation of the prosthetic hip. Conflicts prone to implant failure, such as impingements or subluxations, were not detected.
Conclusions The results show that *MyHip* provides a promising computer assistance for THA. The results of the dynamic simulation highlighted the quality of the surgery and especially of its planning. The planning was properly executed since non-significant variations were detected during the radiological analysis.

Keywords Total hip arthroplasty · Pre-operative planning · Guiding blocks · Medical imaging · Joint kinematics · Impingements and joint instability

✉ Jérôme Schmid
jerome.schmid@hesge.ch

1 Geneva School of Health (HEdS), University of Applied Sciences of Western Switzerland (HES-SO), Av. de Champel 47, 1206 Geneva, Switzerland

2 Medical Research Department, Artanim Foundation, Geneva, Switzerland

3 Orthopedics and Trauma Service, University Hospitals of Geneva, Geneva, Switzerland

4 Medacta International SA, Lugano, Switzerland

Introduction

Total hip arthroplasty (THA) aims to restore patient mobility by providing a pain-free and stable joint. A successful THA is mainly characterized by the efficiency of the prosthetic hip in terms of biomechanics and fulfillment of patient expectations [31]. Another success criterion is the cost-effectiveness of the surgery—which includes economic aspects such as the surgical time and reduction in implant revisions (up to 150 % of the cost of a primary hip arthroplasty [50]).

THA is constantly evolving to reduce possible complications such as implant fracture or dislocation—despite it presents a very good survivorship (e.g., 80 % at 25 years of post-operative follow-up [31]). Complications are particularly related to the selection and positioning of the implants. These factors are also critical to ensure patients' comfort and satisfactory hip range of motion (ROM).

Conventional planning mostly relies on antero-posterior radiographs to image the patient's anatomy. Such procedure is subjective and lacks accuracy in assessing the correct posi-

Published online: 01 April 2015

tioning of implants from 2D projected images [3]. To improve the planning accuracy, some authors devised computer-assisted solutions to select and fit the implants [25,28,43,52].

Despite these improvements, the planning adopts a "static" approach that ignores dynamic aspects such as joint kinematics and postural variations (i.e., pelvic tilt [29]). Kinematics play an important role since some movements may yield excessive wear [5,37] and create impingements resulting in reduced ROM [54], dislocations [40,45] and implant loosening [34]. The influence of kinematics has been studied in relation with kinetics (load, stress) in computer simulations [1,21,45,53]—but these works did not focus on planning strategies to provide computer-assisted support to THA.

While the THA success is undoubtedly dependent on the planning quality [16,18], the surgeon's ability to exactly reproduce the planning is also critical [38]. Without intra-operative assistance, surgeons usually refine their choice of resected areas and of the type and positioning of implants during surgery, which is time-consuming and may result in a loss of accuracy [47]. For instance, Callanan et al. [9] reported a 50 % of malpositioned cups in non-assisted THA and hip resurfacing surgeries.

Computer-assisted surgical systems have often been reported with an increase in accuracy in implant positioning [2,57]—but with some possible lengthening of surgical time [36]. An adequate intra-operative assistance should help to reproduce the planning while being cost-effective and respectful to patients (e.g., reasonable blood loss and short recovery time).

In this paper, our research hypothesis is that the consideration of patient morphology and dynamics during the pre- and intra-operative phases are expected to improve the quality and success of THA, as suggested by Wixson et al. [56]. To test it, we developed and present here our computer-assisted framework "*MyHip*" for THA that considers the anatomy and kinematics of the prosthetic hip during planning. The planning relies on morphology and ROM of the patient's hip to optimally position the implant, and reduce the risk of impingements and joint instability. The framework also facilitates the automatic creation of patient-specific surgical guides for intra-operative assistance—a technology successfully used in total knee arthoplasties (TKA) [14,15].

Materials and methods

Pre-operative planning

The goal of pre-operative planning is to assess the surgical parameters regarding acetabular and femoral positioning of implants—including size of implant components, cup orientation and stem anteversion, femoral neck cut height and angle, and differences in leg length and lateralization. Cup orientation is controlled by inclination and anteversion angles [39]. The positioning and the size of implants are known to be correlated with implant failures such as dislocations [26,46], impingements [26], reduced ROM [7], excessive wear [8] and leg length discrepancy [27].

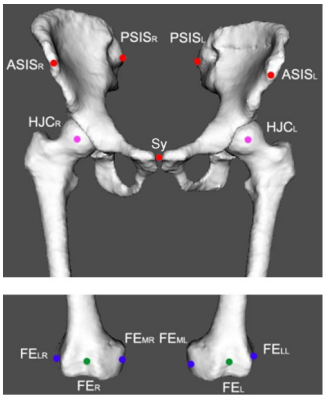

ASIS: *anterior superior iliac spine*
PSIS: *posterior superior iliac spine*
HJC: *hip joint center*
FEL: *femoral lateral epicondyle*
FEM: *femoral medial epicondyle*
FE: *midpoint of femoral epicondyles*
Sy: *middle of symphisis*

Fig. 1 Anatomical and functional landmarks for surgical and kinematic parameters

Anatomical reconstruction

Based on computed tomography (CT) images, we reconstruct subject-specific models of hips by segmentation. The CT protocol is designed to maximize image quality while reducing at best the dose—by using varying slice thickness (e.g., pelvis: [0.5–1] mm, femur: [2–3] mm) and acquiring only proximal and distal parts of the femurs.

Automatic thresholding coupled with bone filling segments most of the bones but we perform some manual segmentation to refine results in pathological areas with abnormal morphology and intensities. The manual refinement requires in average 5 min of time. The segmentation is carried out with Mimics software v16.0 (Materialise NV, Leuven, Belgium).

Various anatomical and functional landmarks (Fig. 1) are extracted from the reconstructed models to define key parameters of the surgical planning and the kinematics. For instance, landmarks on the pelvis are used to express pelvic tilt ("Pelvic tilt") and implant orientation while femoral neck anteversion is derived from landmarks on femoral epicondyles. Similarly, the location of the hip joint center (HJC)—estimated by a functional method [19]—is required to compute the joint coordinate system and to estimate hip joint rotations.

Pelvic tilt

Pelvic tilt is defined as the angle α between the anterior pelvic plane (APP) and the coronal plane [4] (Fig. 2a). It is an impor-

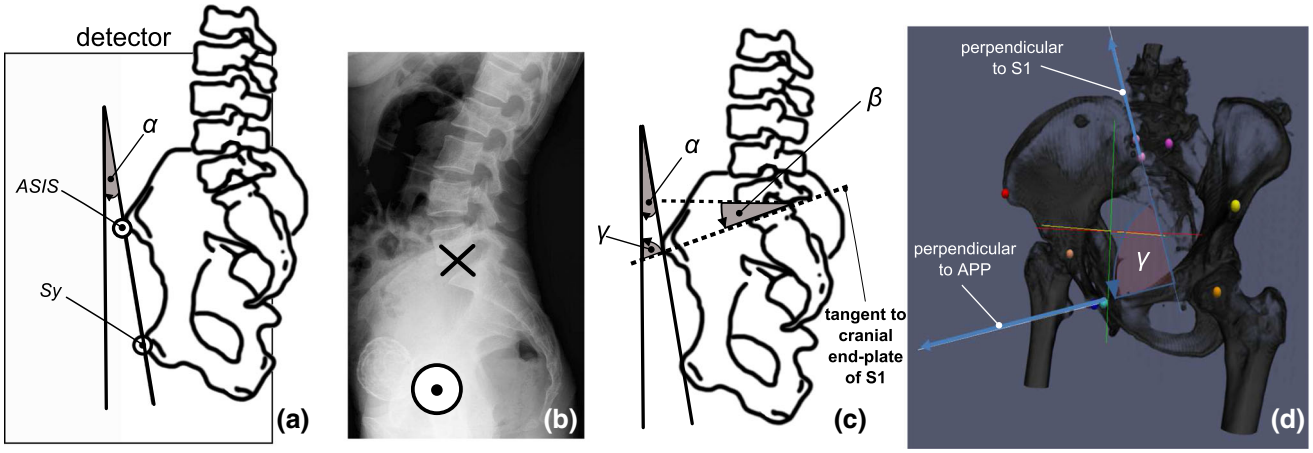

Fig. 2 Pelvic tilt computation. **a** The pelvic tilt is defined as the angle α between the coronal plane and the anterior pelvic plane (APP) passing through the $ASIS$ and Sy anatomical landmarks. Here, the α angle is positive since the pelvis is anteverted. **b** Our alternative radiograph protocol: the centering point ($\times$) is located below the iliac crest on the lumbar spine and the success criterion is the alignment of the femoral heads ($\odot$). **c** The pelvic tilt is linked to the sacral slope β (angle between horizontal direction and cranial end-plate tangent of S1) and the γ angle by $\alpha = \gamma + \beta - \pi/2$. **d** The γ angle is independent of patient position and can be directly computed from the pelvic bone morphology

tant indicator of pelvis version that should be used to correct the chosen value of cup anteversion [32,44,48]. We used the ASIS and Sy anatomical landmarks (Fig. 1) to compute the APP [33].

Lateral radiographs are commonly used to measure pelvic tilt since patients can be acquired in weight-bearing position. To accurately measure the angle by avoiding beam divergence [58], left and right ASIS should be superimposed and centered with respect to the detector [4] (Fig. 2a). This results in a significantly large portion of the detector being directly exposed which yields too short exposure time and a bad image quality when using automatic exposure control.

To avoid the use of an invasive fluoroscopy guidance to tackle beam divergence, we devised an alternative protocol based on the acquisition of lateral lumbar spine radiographs (Fig. 2b). In this protocol, we do not need to acquire the ASIS as produced radiographs are used to compute the sacral slope. It is defined as the angle β between the horizontal direction and the cranial end-plate tangent of S1 (Fig. 2c).

As reported by Lazennec et al. [29], the β angle is accurately computed in lateral radiographs—with the same accuracy than would be obtained with the modality EOS (EOS imaging SA, Paris, France). Similar to radiographs, the EOS scans patients in standing position but does not produce images with projective distortion—which theoretically makes it a better candidate to compute pelvic descriptors. However, Lazennec et al. [29] could not find any statistical difference when measuring the sacral slope with EOS and standard radiographs.

The value of pelvic tilt α is linked to the sacral slope β with the following formula (Fig. 2c):

$$\alpha = \gamma + \beta - \pi/2 \quad (1)$$

The presence of divergence or the possible absence of the ASIS in the radiographs prevents the direct computation of the γ angle. However, the γ angle is not dependent on the patient position and can be expressed as the angle between the normals of the S1 cranial plate and the APP (Fig. 2d). Hence, we can easily compute this angle from the reconstructed models of the hip ("Anatomical reconstruction").

Kinematics

To perform realistic motion simulations of prosthetic models, a motion database of daily activities was created. Four young active healthy subjects (1 female, 3 males; mean age, weight and height: 28.0 years, 74.2 kg and 181.5 cm) underwent magnetic resonance imaging (MRI) and motion capture.

Kinematic data were recorded using a Vicon MXT40S motion capture system (Oxford Metrics, UK) consisting of 24 cameras sampling at 120 Hz. The volunteers were equipped with retroreflective markers (Ø14 mm) placed directly onto the skin. Six markers were placed on pelvic anatomical landmarks (e.g., ASIS, Fig. 1) and two clusters of six markers were stuck on the lateral and frontal parts of both thighs. Additional markers were distributed over the body to provide a global visualization of the motion.

The following activities were recorded (3 trials each): walk, stand-to-sit, lie down on the floor, lace the shoes while seated and pick an object on the floor while seated or standing. These activities were chosen to reflect a variety of routine movements. Some are also known to be prone to hip implants failure (e.g., dislocation, impingements) [40,45]. If more specific patient's activities (e.g., sport movements) would be required, the patient could perform a dedicated motion capture session to enrich the motion database.

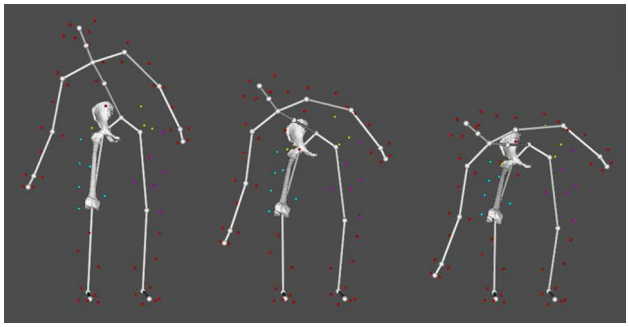

Fig. 3 Kinematic animation of the right hip joint during activity of "picking an object on the floor," showing the markers set-up (small colored spheres) and a virtual skeleton used to better visualize and analyze the motion as a whole

The hip joint kinematics was computed from the recorded marker data (Vicon markers reconstruction error < 0.5 mm). To solve the issue of soft tissue artifacts (STA) that could hinder accurate kinematic estimation [30], we used a validated optimized fitting algorithm (accuracy: translational error $\approx$ 0.5 mm, rotational error $< 3°$) which accounted for STA and patient-specific anatomical constraints [10,11]. Indeed, computed motion was applied to the volunteer's hip joint 3D models reconstructed from their MRI data [51]—which allowed accounting for the subject's anatomy and kinematic parameters (e.g., hip joint center). Figure 3 shows examples of computed postures.

The hip ROM was quantified for each volunteer and for all recorded daily activities, thanks to two bone coordinate systems (one for the pelvis, one for the femur) defined on the reconstructed models and derived from the anatomical landmarks ("Anatomical reconstruction"), according to standards of the International Society of Biomechanics [59]. Given the computed bone poses from motion capture data, hip angles (flex/ext, abd/add and IR/ER) were determined at each point of the movement [11]. Eventually, the ROM of the four volunteers' trials were averaged for each activity, and the final values were stored in a database to be later used in the simulation software.

We decided to use a motion database for two main reasons: (1) to acquire target ROMs that THA should restore in terms of mobility, since patient undergoing this surgery have limited ROMs or simply cannot perform a motion capture due to their musculoskeletal disorder and (2) to avoid any additional financial burden to patients since acquiring patient motion might not be reimbursed by the health insurance.

Dynamic planning

Based on reconstructed models and surgical parameters computed from landmarks ("Anatomical reconstruction"), surgeons perform a virtual planning of THA. Implant size and positioning are selected and a virtual bone resection is immediately applied to the models, as exemplified in Fig. 4. This virtual planning is performed online and provides an efficient feedback to prepare a first planning based on morphological aspects.

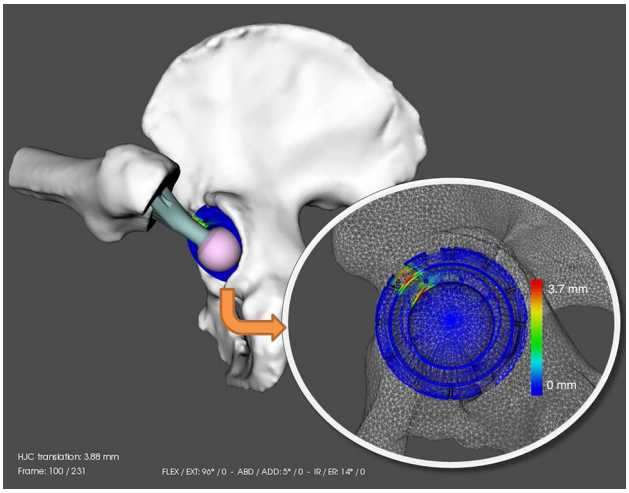

Fig. 4 Detection of the impingement region during simulation of a prosthetic hip. The colors represent the area of increased contact (*blue* no contact, *red* highest contact). Here, the simulation shows a prosthetic impingement between the stem and the cup/liner during lacing the shoes

The initial planning is subsequently refined by performing a dynamic simulation of the prosthetic 3D models driven by the motion database. The goal of this simulation is to detect potential risk of impingement and joint instability during everyday activities. The pre-computed hip angles stored in the database are first applied at each time step to the virtual prosthetic hip in its anatomical coordinate systems [12].

A collision detection algorithm [10,11] is then used to virtually locate abnormal contacts between both prosthetic and bony components (Fig. 4). Moreover, femoral head translations (subluxation) are computed to evaluate the joint congruence [12]. Based on the simulation's results, the surgeon adapts and refines the initial implant configuration and selects the optimal planning for the surgery.

Intra-operative guidance

Guides are components that are placed intra-operatively on bones to support the bone resection process. Their surface must accurately match the patient anatomy to ensure a good anchoring, and their shape and positioning are derived from the surgical planning. Guides are thus personalized for the patient and the surgery, and are produced by rapid prototyping based on 3D meshes.

We devised a computer-assisted process for the creation of these meshes, exemplified in Fig. 5. Based on information of the surgical planning (e.g., cutting plane P for the femoral neck) and on constraints provided by the operator (e.g., anchoring points a_1 and a_2 specified on bone), generic

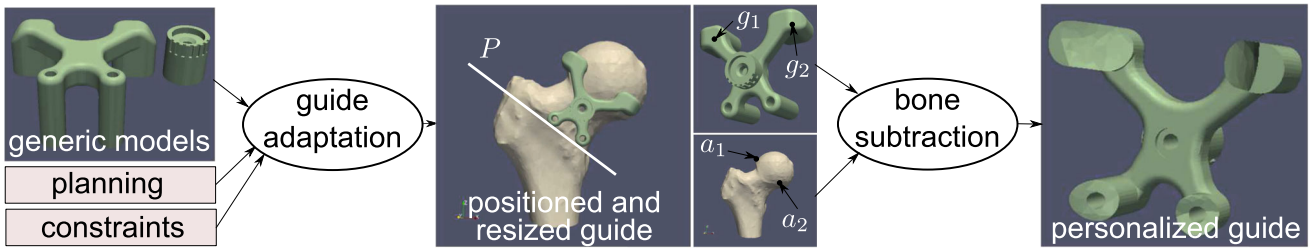

Fig. 5 Guide adaptation process with an example of prototype for a femoral guide. From left to right: a generic model of the guide is resized and positioned on the bone surface based on information of the planning (e.g., femoral cutting plane P) and constraints provided by an operator (e.g., points g_1 and g_2 of the superior "pads" of the model to be located at anchoring points a_1 and a_2). The generic model is composed of sub-parts to easily resize the guide—while avoiding geometrical complications such as overlapping triangles. The bone surface is subsequently subtracted from the guide model to yield the final personalized guide

models of guides are automatically resized and positioned with respect to the reconstructed bones. The geometry of a guide is divided into different sub-parts that are independently deformed with thin-plate spline transforms (TPS) [17]—this subdivision mainly preventing geometrical complications such as overlapping triangles that could result from TPS.

Finally, the bone surface is removed from the adapted guide models based on Boolean mesh subtraction to obtain individualized meshes closely fitting patient anatomy. We used the CARVE library (http://carve-csg.com) to perform Boolean mesh operations.

Post-operative assessment

For validation purposes, we acquired and processed post-operative CT images of operated patients to accurately assess the quality of the surgery with respect to the planning—by reconstructing 3D models of the bones and implants. Patients underwent a post-operative dual energy CT scan designed to reduce artifacts of metallic implants. Instead of directly segmenting the collected images, we rigidly registered the pre-operative bone models ("Anatomical reconstruction") and CAD models of the implants to the CT images.

The optimization of the model transformations was indirectly performed by controlling the motion of the corresponding models as they were rigid bodies evolving in a system built upon Newtonian laws of motion [51]. We defined external forces based on image gradient to attract models toward boundaries of interest [51]. To regulate the simultaneous evolution of several models, we implemented collision response to avoid inter-penetrating models and constrained the head of the stem to remain inside the socket of the cup's liner.

Bone segmentation was corrected to account for resected areas. First the implant models were subtracted from the bone models, then the bony parts effectively removed by the surgery were manually identified in the image and subtracted from the models.

Experiments

First, we ran a pre-operative experiment to investigate the impact of pelvic tilt on THA planning, by performing a dynamic analysis on one patient ("Pre-operative experiment on pelvic tilt"). Then, we ran two post-operative experiments with three patients based on post-operative CT images and motion capture data ("Post-operative experiments").

Pre-operative experiment on pelvic tilt

The purpose of this experiment was to quantitatively assess the impact of significant pelvic tilts in the dynamic planning. We considered a pelvic tilt as being significant when $|\alpha| > 5°$ (Eq. 1). Such value of 5° would produce an approximate error of 3.5° in effective cup anteversion [32] (for planned radiographic anteversion (RA) of 15° and inclination (RI) of 45°)—yielding a cup configuration close to the limits of the recommended "safe zone" [45].

We measured on one patient a retroverted pelvic tilt of −17.8° based on our radiographic protocol ("Pelvic tilt"). Two sets of prosthetic 3D models were produced whether or not the pelvic tilt was accounted for in the planning. Dynamic simulations ("Dynamic planning") were then performed with the two sets of models in order to compare the incidence of impingements during motion. To investigate more variations of ROM, all individual motion trials of the healthy volunteers were simulated for each daily activity instead of the averaged trials stored in the database.

Post-operative experiments

A pilot study was conducted with three male patients undergoing THA (mean age, weight and height: 65.0 years, 91.3 kg and 178.0 cm)—after approval from local ethics committees and written informed consent given by the patients. All patients benefited from the *MyHip* pre-operative planning. During their surgery performed with the anterior approach, only femoral guides were used since support for acetabular guidance was still under development.

Two post-operative experiments were conducted. The first experiment ("evaluation of intra-operative guidance") studied the efficiency of the intra-operative guidance with respect to surgical outcomes, while the second one ("Dynamic simulation") applied a dynamic analysis on reconstructed post-operative hips based on kinematics acquired from post-operative motion capture sessions or extracted from our motion database.

Evaluation of intra-operative guidance

Based on our registration-based approach ("Post-operative assessment"), pre-operative bone and implant models were simultaneously and rigidly registered to the corresponding CT image. We first assessed the accuracy of the bone segmentation by comparing the bone registration results with manual segmentations performed by a trained radiographer, based on the average symmetric distance (SD) [23]. Then, we measured (i) the differences in position and orientation of the virtual and effective cutting planes of femurs and (ii) the positioning of the stem with respect to the femur between the planning and the post-operative reconstruction. Based on these measures, the quality of the planning execution was studied along with associated surgical outcomes such as leg length discrepancy.

Dynamic simulation

After a minimum of four months after surgery, the three patients participated to a motion capture session. Marker data were collected during the activities of daily living with the same motion capture system and markers protocol as those used in the pre-operative stage. The captured data were post-processed and the patients' hip ROM were calculated based on the method described in Section "Kinematics."

Using the patient's motion as input and the models of their prosthetic hips reconstructed from the post-operative CT images ("evaluation of intra-operative guidance"), a dynamic simulation was performed to assess the prevalence of impingement during their practice. Again, the collision detection algorithm [10,11] was used to detect any abnormal contact ("Dynamic planning"). All patients' trials were simulated. To evaluate the patients' mobility compared to healthy subjects, additional simulations were performed with motion data from the database.

Results

Impact of pelvic tilt on planning

In the pre-operative experiment on pelvic tilt impact ("Pre-operative experiment on pelvic tilt"), the dynamic simulation was performed for the planning with and without tilting consideration. For both plannings, impingements were observed during lacing the shoes in the antero-superior position of the acetabulum. Contacts occurred either between the stem and acetabular rim (20 %), the femur and anterior superior iliac spine (20 %) or a combination of both (60 %). Subluxation was slightly higher when the pelvic tilt was ignored (mean $\pm$ standard deviation: 1.0 ± 1.5 mm without tilt vs. 0.7 ± 1.0 mm with tilt).

Moreover, impingements between the prosthetic components were more intense. In particular, the stem and cup/liner also encountered collisions, which could result in extra joint damage.

Evaluation of intra-operative guidance

In the first post-operative experiment ("Evaluation of intra-operative guidance"), the simultaneous registration of bone and implant models required in average 3 min to converge (Intel Xeon Quad-Core at 2.1 Ghz, 8 Gb of RAM), while the subsequent manual correction for resected bone was quickly performed within 5–10 min.

The rigid registration of models combined with inter-model constraints (collisions, liner-head constraint) allowed us to tackle image regions with significant metallic artifacts that would have been very difficult to segment manually (Fig. 6a, b). Indeed, since some regions around bone and implants presented little image artifacts, the approach was more effective in these regions and could constraint the registration in areas with more artifacts—yielding a robust process.

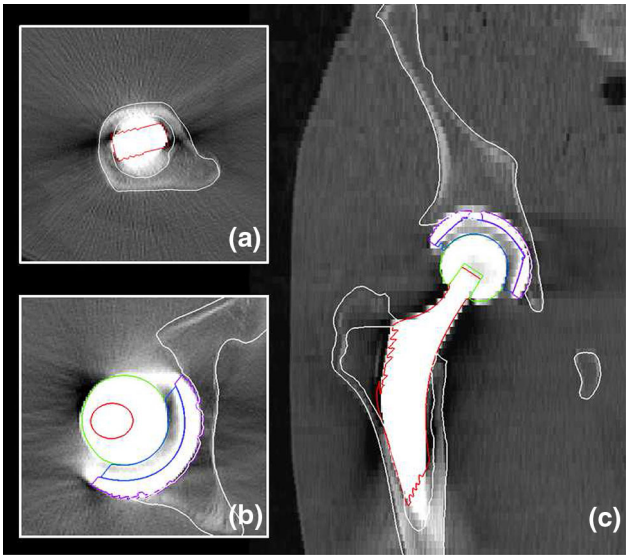

Fig. 6 Example of segmentation of a post-operative CT image by rigid registration of pre-operative models, whose contours are overlaid on **a**–**b** axial and **c** coronal slices. Our constrained registration is particularly useful in regions with strong metallic artifacts, exemplified in the axial slices

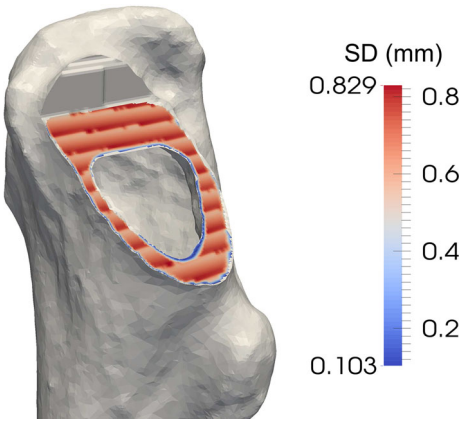

Fig. 7 Example of segmented femur for which the cutting plane area is color mapped with the surface distance between planned and effective resection. Highest errors take place along lines related to the staircase effect of manual segmentation

Despite we used pre-operative bone models and the images presented resected areas and image artifacts, we observed an accurate bone segmentation (Fig. 6). Compared to the manual reference segmentation, we measured an average SD of 0.36 ± 0.20 mm.

We measured small differences in the position and orientation of the virtual and effective cutting planes of femurs. We computed for the cutting plane area an average surface error of 0.68 ± 0.08 mm. As shown in Fig. 7, this small error was partially related to the "staircase" effect of the reconstruction of the manually segmented area. Since the accuracy of the bone segmentation was very satisfactory (≈ 0.36 mm), it did not significantly bias the computation of the cutting plane error.

Finally, we compared the positioning of the stem with respect to the femur between the planning and the post-operative reconstruction, by measuring an average distance of 4.4 mm between the centers of the planned and post-operative head of the stem.

Post-operative dynamic simulation

In the second post-operative experiment ("Dynamic simulation"), no impingement could be noted for any patient using their own motion. When the motion database was used, bony impingements were observed during lacing the shoes and prosthetic impingements occurred during picking an object while standing for all patients. The average subluxation was 2.63 ± 2.25 mm and 1.01 ± 1.31 mm, respectively. The contacts were all located in the antero-superior position of the acetabulum.

Interestingly, patients did not have the same ROM compared to the one from the motion database of healthy subjects. Patients performed the different daily activities with lower hip flexion ($-13 \pm 11.2°$) and higher abduction ($+14 \pm 4.4°$). In addition, one patient could not perform the full ROM of one motion (lace the shoes) because of hip and back pain.

Discussion

Dose exposure in radiological acquisitions

Volunteers of our pilot study underwent various radiological acquisitions: the pre-operative CT for anatomical reconstruction ("anatomical reconstruction"), the lateral radiograph for pelvic tilt computation ("pelvic tilt") and finally the post-operative CT for post-operative assessment ("evaluation of intra-operative guidance"). In clinical routine, the *MyHip* approach does not include post-operative CT acquisitions as surgeons commonly assess the implant position by using post-operative radiographs—to reduce dose exposure. In this study, the Computed Tomography Dose Index (CTDI) and the Entrance Surface Dose (ESD, for radiographs) were within the recommended National Diagnostic Reference Levels provided by the Swiss Federal Office of Public Health.

In our pre-operative CT protocol, we sought for the best trade-off between image quality and delivered dose, and we preferred not to use MR images as an alternative modality despite it is not invasive. In fact, despite equivalent bone segmentation accuracy with MR or CT images has been reported with cadavers [6,49], MR scanning time is longer—possibly yielding image motion artifacts with patients [49]. Furthermore, MR segmentation generally requires more complex segmentation approaches as trabecular and cortical bone intensities vary and are dependent on the MR protocol [51]. Finally, surgical outcomes are generally worse when MR images are used for arthroplasty planning instead of the CT modality (e.g., superiority of CT-based plannings [20] in post-operative neutral alignment of total knee arthroplasty compared to an MR-based approach [42]).

Pelvic tilt computation and consideration

Our experiment on the impact of pelvic tilt ("Impact of pelvic tilt on planning") showed that if the tilt was ignored during planning, there was an increased risk of observing significant subluxation and impingement in the prosthetic hip. These results are consistent with other studies that showed the necessity to consider pelvic tilt in THA [32,44,48].

Our imaging protocol to measure pelvic tilt ("Pelvic tilt") is currently performed in various clinics and hospitals, and the feedback from radiographers and physicians is so far very positive. The main advantage of the protocol that we were reported was its close similarity with standard protocols for lumbar spine acquisition. These protocols being mastered by radiographers, the integration of the new protocol in clinical

practice is greatly facilitated without any significant loss in productivity.

Besides this positive qualitative assessment, our imaging protocol also brings some robustness against possible positioning errors performed by radiographers such as lateral flexion and pelvis rotation. Imai et al. [24] showed that errors up to 6° in lateral flexion or rotation did not impact significantly the accuracy of the sacral slope measurement from lateral radiographs. In [55], results showed that even with large rotations up to 30°, the measurement was still reliable. Experienced radiographers confirmed to us that they could achieve an alignment of the femoral heads with errors below 6°.

Study [24] also reported an accuracy of 3° to compute the sacral slope from lateral radiographs. We showed in Eq. (1) that pelvic tilt and sacral slope were related to the γ angle. Since this angle can be computed accurately from the reconstructed models or the CT images, the computation of the pelvic tilt is expected to be as accurate as the measurement of the sacral slope.

Use of intra-operative guidance

Currently, the femoral guide provides assistance for the bone resection but not for the placement of the femoral component. Even if such assistance was available, many surgeons still prefer to be able to perform some modifications based on information only available intra-operatively (e.g., penetration and adherence of the stem in the femur). Still, the analysis of differences between planned and executed femoral arthroplasty provides insightful information.

The absence of significant differences between planned and performed femoral cut (≈0.68 mm of surface error, Section "evaluation of intra-operative guidance") highlighted the surgeons' capability to correctly replicate the planned bone cutting by using the femoral guide. As a result, guides offer a cost-effective alternative to more complex computer-assisted surgical systems, since they offer accuracy and reproducibility for an operative time equivalent to a traditional surgery. Indeed, despite these advanced systems provide improved reliability and accuracy, they are more expensive and usually yield longer operative times [36].

Despite the planned bone resection was well executed, surgeons did not fully respect the suggested placement of the femoral component as we measured an average error of 4.4 mm between planned and executed positions of the stem head ("evaluation of intra-operative guidance"). This error may impact any planned correction of leg length discrepancy (LLD)—a magnitude of LLD over 20 mm being often associated with post-operative signs of discomfort or functional disabilities [22]. The value of problematic LLD being patient-specific, other studies [41] proposed a more conservative threshold of 10 mm. Knowing that THAs usually yield an average LLD of 5–6 mm [27,35], the measured difference of 4.4 mm is likely to lead to an LLD below this conservative threshold.

We also assessed the impact of the automated creation of the femoral guides ("intra-operative guidance") from a productivity perspective. We surveyed the operators responsible for creating the models of the guides based on the planning—who commonly performed a manual positioning and resizing of the models. They reported that the time required to design the models decreased from 25 min to 3 min (in average).

Despite we reconstructed the acetabular components from the post-operative images ("Evaluation of intra-operative guidance"), we did not perform a similar post-operative analysis since the involved patients did not benefit from an acetabular guide. Furthermore, some surgeons use to align the cup with respect to the transverse ligament, ignoring the traditional rule of thumb of 45°–15° for inclination and anteversion. A further study would be necessary to understand the impact of this anatomical alignment, especially with respect to dynamic aspects as conducted in our experiments.

Consideration of hip kinematics

As in our previous studies [12,13], we studied the effects of implant positioning, pelvic tilt and motion on impingements, joint congruence and ROM—using computer simulations and motion capture data. A strong correlation between the frequency of impingements and implant characteristics was reported. This confirmed the importance of performing a dynamic planning to select the best implants configuration based on the patient's morphology, posture and activity lifestyle.

In the post-operative experiment ("post-operative dynamic simulation"), we investigated the surgical outcomes in terms of kinematics and impingements. Patient's motion was free of collisions, but not when testing with ROM of healthy subjects. Simulations revealed interesting motion adaptations in order to execute the different activities. In particular, patients adopted less hip flexion with more abduction, which seems to be a good strategy to avoid impingement. However, it is unknown if those adaptations resulted from the hip replacement, since we could not compare the patient's post-operative ROM to motion data acquired before the surgery. This aspect could be addressed in future work—such a study providing useful information about patient's mobility, stability and kinematic changes after THA.

Finally, we were unable to post-operatively evaluate whether the use of intra-operative acetabular guidance to accurately reproduce the planning minimizes the frequency of impingement during motion, since the guide was still under development. The results of our post-operative study showed that the patients' hips were in good function. However, a more comprehensive study including more patients

undergoing THA under the *MyHip* framework is necessary to evaluate the support of acetabular guidance. This kind of study is already planned by our research team.

Conclusion

We presented the computer-assisted *MyHip* framework to plan and execute THA. Based on patient-specific data including anatomical and dynamic information (posture, kinematics), we refined traditional planning by simulating the prosthetic hip and detecting some possible causes of implant failures. We showed how surgical guides can be designed with computer assistance and how they effectively assist surgeons in performing more accurate surgical gestures—yielding a more cost-effective surgery.

So far, more than 230 *MyHip* surgeries have been successfully performed with the femoral guide. Results are very encouraging, but future work is needed to fully validate the overall approach. In particular, the acetabular guide is now available and we are extending our experiments to account for a larger number of subjects and testing conditions.

Acknowledgments Authors would like to thank all members of the *MyHip* consortium, as well as the patients and volunteers who agreed to participate to this study. This research work was supported by the *MyHip: Patient-Specific Pre-operative Planning and Intra-operative Surgical Guidance for Total Hip Arthroplasty* project funded by the Swiss Commission for Technology and Innovation (CTI No. 13573.1 PFFLE-LS).

Compliance with ethical standard All procedures performed in studies involving human participants were in accordance with the ethical standards of the institutional and/or national research committee and with the 1964 Helsinki Declaration and its later amendments or comparable ethical standards.

Conflicts of interest All authors declare that they have no conflict of interest.

Informed consent Informed consent was obtained from all individual participants included in the study.

References

1. Asgari S, Hamouda A, Mansor S, Singh H, Mahdi E, Wirza R, Prakash B (2004) Finite element modeling of a generic stemless hip implant design in comparison with conventional hip implants. Finite Elem Anal Des 40(15):2027–2047
2. Beaumont E, Beaumont P, Odermat D, Fontaine I, Jansen H, Prince F (2010) Clinical validation of computer-assisted navigation in total hip arthroplasty. Adv Orthoped 2011
3. Beckmann J, Lüring C, Tingart M, Anders S, Grifka J, Köck F (2009) Cup positioning in THA: current status and pitfalls. a systematic evaluation of the literature. Arch Orthop Trauma Surg 129(7):863–872
4. Blondel B, Parratte S, Tropiano P, Pauly V, Aubaniac JM, Argenson JN (2009) Pelvic tilt measurement before and after total hip arthroplasty. J Orthop Traumatol Surg Res 95(8):568–572
5. Bowsher J, Hussain A, Williams P, Shelton J (2006) Metal-on-metal hip simulator study of increased wear particle surface area due to 'severe' patient activity. Proc IME H J Eng Med 220(2): 279–287
6. Van den Broeck J, Vereecke E, Speetjens R, Vander Sloten J (2014) Segmentation accuracy of long bones. Med Eng Phys 36(7):949–953
7. Burroughs B, Hallstrom B, Golladay G, Hoeffel D, Harris W (2005) Range of motion and stability in total hip arthroplasty with 28-, 32-, 38-, and 44-mm femoral head sizes: an in vitro study. J Arthroplasty 20(1):11–19
8. Callaghan J, Pedersen D, Johnston R, Brown T (2003) Clinical biomechanics of wear in total hip arthroplasty. Iowa Orthop J 23:1–12
9. Callanan M, Jarrett B, Bragdon C, Zurakowski D, Rubash H, Freiberg A, Malchau H (2011) The John Charnley award: risk factors for cup malpositioning: quality improvement through a joint registry at a tertiary hospital. Clin Orthop Relat Res 469(2):319–329
10. Charbonnier C, Assassi L, Volino P, Magnenat-Thalmann N (2009) Motion study of the hip joint in extreme postures. Vis Comput 25(9):873–882
11. Charbonnier C, Kolo F, Duthon V, Magnenat-Thalmann N, Becker C, Hoffmeyer P, Menetrey J (2011) Assessment of congruence and impingement of the hip joint in professional ballet dancers. Am J Sports Med 39(3):557–566
12. Charbonnier C, Chagué S, Bernardoni M, Panzoni M, Hoffmeyer P, Christofilopoulos P (2014) Sexual activity after total hip arthroplasty: a motion capture study. J Arthroplasty 29(3):640–647
13. Charbonnier C, Chagué S, Schmid J, Kolo F, Bernardoni M, Christofilopoulos P (2014) Analysis of hip range of motion in everyday life: a pilot study. Hip Int 25(1):82–90
14. Chemello C, Costacurta G (2014) Patient Specific Instruments is realy useful? Prospective study of 50 prenavigated total knee replacement. In: Proceedings of CAOS
15. Dao-Lena S, P M (2014) Patient specific guides for total knee arthroplasty. A cadaveric study. In: Abstracts of CAOS
16. De Thomasson E, Mazel C, Guingand O, Terracher R (2002) Value of preoperative planning in total hip arthroplasty. Revue de chirurgie orthopedique et reparatrice de l'appareil moteur 88(3):229–235
17. Duchon J (1977) Splines minimizing rotation-invariant semi-norms in sobolev spaces. In: Constructive theory of functions of several variables. Springer, pp 85–100
18. Eggli S, Pisan M, Müller M (1998) The value of preoperative planning for total hip arthroplasty. J Bone Joint Surg Br 80(3):382–390
19. Gilles B, Kolo F, Magnenat-Thalmann N, Becker C, Duc S, Menetrey J, Hoffmeyer P (2009) MRI-based assessment of hip joint translations. J Biomech 42(9):1201–1205
20. Goldberg T, Curry WT, Bush JW (2013) CT-based patient-specific instrumentation is accurate for TKA: a single-surgeon, prospective trial. Bone Joint J Orthop Proc Supp 95(34):325–325
21. Gross S, Abel E (2001) A finite element analysis of hollow stemmed hip prostheses as a means of reducing stress shielding of the femur. J Biomech 34(8):995–1003
22. Gurney B (2002) Leg length discrepancy. Gait Posture 15(2):195–206
23. Heimann T, Van Ginneken B, Styner MA, Arzhaeva Y, Aurich V, Bauer C, Beck A, Becker C, Beichel R, Bekes G et al (2009) Comparison and evaluation of methods for liver segmentation from CT datasets. IEEE Trans Med Imaging 28(8):1251–1265
24. Imai N, Miyasaka D, Horigome Y, Suzuki H, Takubo R, Endo N (2014) Are measurements of sacral slopes reliable? Am J Clin Med Res 2(3):57–60

25. Jun Y, Choi K (2010) Design of patient-specific hip implants based on the 3D geometry of the human femur. Adv Eng Softw 41(4): 537–547
26. Kluess D, Martin H, Mittelmeier W, Schmitz KP, Bader R (2007) Influence of femoral head size on impingement, dislocation and stress distribution in total hip replacement. Med Eng Phys 29(4):465–471
27. Konyves A, Bannister G (2005) The importance of leg length discrepancy after total hip arthroplasty. J Bone Joint Surg Br 87(2):155–157
28. Lattanzi R, Viceconti M, Zannoni C, Quadrani P, Toni A (2002) Hip-Op: an innovative software to plan total hip replacement surgery. Inform Health Soc Care 27(2):71–83
29. Lazennec J, Rousseau M, Rangel A, Gorin M, Belicourt C, Brusson A, Catonné Y (2011) Pelvis and total hip arthroplasty acetabular component orientations in sitting and standing positions: measurements reproductibility with eos imaging system versus conventional radiographies. Orthop Traumatol: Surg Res 97(4):373–380
30. Leardini A, Chiari L, Croce UD, Cappozzo A (2005) Human movement analysis using stereophotogrammetry-part 3: soft tissue artifact assessment and compensation. Gait Posture 21:212–225
31. Learmonth I, Young C, Rorabeck C (2007) The operation of the century: total hip replacement. Lancet 370(9597):1508–1519
32. Lembeck B, Mueller O, Reize P, Wuelker N (2005) Pelvic tilt makes acetabular cup navigation inaccurate. Acta Orthop 76(4):517–523
33. Lewinnek G, Lewis J, Tarr R, Compere C, Zimmerman J (1978) Dislocations after total hip-replacement arthroplasties. J Bone Joint Surg 60(2):217–220
34. Malik A, Maheshwari A, Dorr LD (2007) Impingement with total hip replacement. J Bone Joint Surg 89(8):1832–1842
35. Maloney WJ, Keeney JA (2004) Leg length discrepancy after total hip arthroplasty. J Arthroplasty 19(4):108–110
36. Manzotti A, Cerveri P, De Momi E, Pullen C, Confalonieri N (2011) Does computer-assisted surgery benefit leg length restoration in total hip replacement? Navigation versus conventional freehand. Int Orthop 35(1):19–24
37. Mattei L, Di Puccio F, Piccigallo B, Ciulli E (2011) Lubrication and wear modelling of artificial hip joints: a review. Tribol Int 44(5):532–549
38. Minoda Y, Kadowaki T, Kim M (2006) Acetabular component orientation in 834 total hip arthroplasties using a manual technique. Clin Orthop Relat Res 445:186–191
39. Murray D (1993) The definition and measurement of acetabular orientation. J Bone Joint Surg 75(2):228–232
40. Nadzadi M, Pedersen D, Yack H, Callaghan J, Brown T (2003) Kinematics, kinetics, and finite element analysis of commonplace maneuvers at risk for total hip dislocation. J Biomech 36(4):577–591
41. Nam D, Sculco PK, Abdel MP, Alexiades MM, Figgie MP, Mayman DJ (2013) Leg-length inequalities following THA based on surgical technique. Orthopedics 36(4):e395–400
42. Nunley RM, Ellison BS, Zhu J, Ruh EL, Howell SM, Barrack RL (2012) Do patient-specific guides improve coronal alignment in total knee arthroplasty? Clin Orthop Relat Res 470(3):895–902
43. Otomaru I, Kobayashi K, Okada T, Nakamoto M, Kagiyama Y, Takao M, Sugano N, Tada Y, Sato Y (2009) Expertise modelling for automated planning of acetabular cup in total hip arthroplasty using combined bone and implant statistical atlases. In: Proceedings of MICCAI, vol LNCS 5761. Springer, pp 532–539
44. Parratte S, Pagnano M, Coleman-Wood K, Kaufman K, Berry D (2009) The 2008 Frank Stinchfield award: variation in postoperative pelvic tilt may confound the accuracy of hip navigation systems. Clin Orthop Relat Res 467(1):43–49
45. Pedersen D, Callaghan J, Brown T (2005) Activity-dependence of the "safe zone" for impingement versus dislocation avoidance. Med Eng Phys 27(4):323–328
46. Peter R, Lübbeke A, Stern R, Hoffmeyer P (2011) Cup size and risk of dislocation after primary total hip arthroplasty. J Arthroplasty 26(8):1305–1309
47. Petrella A, Stowe J, DLima D, Rullkoetter P, Laz P (2009) Computer-assisted versus manual alignment in THA: a probabilistic approach to range of motion. Clin Orthop Relat Res 467(1):50–55
48. Philippot R, Wegrzyn J, Farizon F, Fessy MH (2009) Pelvic balance in sagittal and lewinnek reference planes in the standing, supine and sitting positions. J Orthop Traumatol Surg Res 95(1):70–76
49. Rathnayaka K, Sahama T, Schuetz MA, Schmutz B (2011) Effects of CT image segmentation methods on the accuracy of long bone 3D reconstructions. Med Eng Phys 33(2):226–233
50. Sanchez-Sotelo J, Haidukewych G, Boberg C (2006) Hospital cost of dislocation after primary total hip arthroplasty. J Bone Joint Surg 88(2):290–294
51. Schmid J, Kim J, Magnenat-Thalmann N (2011) Robust statistical shape models for MRI bone segmentation in presence of small field of view. Med Image Anal 15:155–168
52. Shaarani S, McHugh G, Collins D (2013) Accuracy of digital preoperative templating in 100 consecutive uncemented total hip arthroplasties: a single surgeon series. J Arthroplasty 28(2):331–337
53. Stewart K, Pedersen D, Callaghan J, Brown T (2004) Implementing capsule representation in a total hip dislocation finite element model. Iowa Orthop J 24:1
54. Turley G, Williams M, Wellings R, Griffin D (2013) Evaluation of range of motion restriction within the hip joint. Med Biol Eng Comput 51(4):467–477
55. Tyrakowski M, Wojtera-Tyrakowska D, Siemionow K (2014) Influence of pelvic rotation on pelvic incidence, pelvic tilt, and sacral slope. Spine 39(21):E1276–E1283
56. Wixson R (2007) Computer-assisted total hip navigation. Instr Course Lect 57:707–720
57. Wixson R, MacDonald M (2005) Total hip arthroplasty through a minimal posterior approach using imageless computer-assisted hip navigation. J Arthroplasty 20(3):51–56
58. Wolf A, DiGioia AI, Mor A, Jaramaz B (2005) Cup alignment error model for total hip arthroplasty. Clin Orthop Relat Res 437:132–137
59. Wu G, Siegler S, Allard P, Kirtley C, Leardini A, Rosenbaum D, Whittle M, D'Lima D, Cristofolini L, Witte H, Schmid O, Strokes I (2002) ISB recommendation on definitions of joint coordinate system of various joints for the reporting of human joint motion - part I: Ankle, hip and spine. J Biomech 35(4):543–548

Orthopaedics & Traumatology: Surgery & Research 100 (2014) 715–719

Available online at
ScienceDirect
www.sciencedirect.com

Elsevier Masson France
EM|consulte
www.em-consulte.com/en

Original article

A patient-specific measurement technique to model shoulder joint kinematics

C. Charbonnier[a,*], S. Chagué[a], F.C. Kolo[b], J.C.K. Chow[c], A. Lädermann[d,e]

[a] Artanim Foundation, Medical Research Department, Geneva, Switzerland
[b] Rive Droite Radiology Center, Geneva, Switzerland
[c] Department of Geomatics Engineering, University of Calgary, Calgary, Canada
[d] Division of Orthopaedics and Trauma Surgery, La Tour Hospital, Geneva, Switzerland
[e] Faculty of Medicine, University of Geneva, Geneva, Switzerland

ARTICLE INFO

Article history:
Accepted 24 June 2014

Keywords:
Shoulder kinematics
Glenohumeral translation
Global optimization
Motion capture
Fluoroscopy

ABSTRACT

Background: Measuring dynamic in vivo shoulder kinematics is crucial to better understanding numerous pathologies. Motion capture systems using skin-mounted markers offer good solutions for non-invasive assessment of shoulder kinematics during dynamic movement. However, none of the current motion capture techniques have been used to study translation values at the joint, which is crucial to assess shoulder instability. The aim of the present study was to develop a dedicated patient-specific measurement technique based on motion capture and magnetic resonance imaging (MRI) to determine shoulder kinematics accurately.
Hypothesis: Estimation of both rotations and translations at the shoulder joint using motion capture is feasible thanks to a patient-specific kinematic chain of the shoulder complex reconstructed from MRI data.
Materials and methods: We implemented a patient-specific kinematic chain model of the shoulder complex with loose constraints on joint translation. To assess the effectiveness of the technique, six subjects underwent data acquisition simultaneously with fluoroscopy and motion capture during flexion and empty-can abduction. The reference 3D shoulder kinematics was reconstructed from fluoroscopy and compared to that obtained from the new technique using skin markers.
Results: Root mean square errors (RMSE) for shoulder orientation were within 4° (mean range: 2.0°–3.4°) for each anatomical axis and each motion. For glenohumeral translations, maximum RMSE for flexion was 3.7 mm and 3.5 mm for empty-can abduction (mean range: 1.9–3.3 mm). Although the translation errors were significant, the computed patterns of humeral translation showed good agreement with published data.
Discussion: To our knowledge, this study is the first attempt to calculate both rotations and translations at the shoulder joint based on skin-mounted markers. Results were encouraging and can serve as reference for future developments. The proposed technique could provide valuable kinematic data for the study of shoulder pathologies.
Level of evidence: Basic Science Study.

1. Introduction

Measuring dynamic in vivo shoulder kinematics is crucial to better understanding numerous pathologies and sport injuries, but remains a challenging problem due to the complicated anatomy and large range of motion. Unfortunately, the motion of the shoulder joints cannot be explored with standard magnetic resonance imaging (MRI) or computed tomography (CT) because these are limited to static measurement and might therefore miss some specificities of dynamic motion. Fluoroscopy-based measurement provides sufficient accuracy for dynamic shoulder analysis [1], but uses ionizing radiation. Motion capture systems using skin-mounted markers are a good solution to determine shoulder kinematics non-invasively during dynamic movement [2,3]. However, these systems are subject to soft-tissue artefacts (STA) due to muscle contraction and skin sliding, causing the markers to move

* Corresponding author. Medical Research Department, Artanim Foundation, 41b, Route des Jeunes, 1227 Carouge, Switzerland. Tel.: +41 22 596 45 40; fax: +41 22 320 07 76.
E-mail address: caecilia.charbonnier@artanim.ch (C. Charbonnier).

http://dx.doi.org/10.1016/j.otsr.2014.06.015
1877-0568/

with respect to the underlying bone. In the upper extremity, the scapula is particularly affected. To solve this issue, several techniques were proposed, such as the scapula locator device [4], the acromion marker cluster [5,6] or the use of a large number of markers to track skin deformation and infer scapular motion [7].

Nevertheless, none of the current motion capture techniques have been used to study translation values at the shoulder joint. This information is crucial to assessing shoulder instability and to understanding many motion-related disorders (e.g., shoulder impingement). One reason for this lack is that studies using the current techniques concentrated either on analysis of a single shoulder bone (scapula) or on humeral motion relative to the thorax rather than to its proximal bone. Yet, it is important to consider the contribution of each bone in assessing shoulder kinematics, taking account of the whole kinematic chain of the shoulder complex from thorax to humerus via the clavicle and scapula, as this could help reduce overall STA error [8,9]. Another important aspect is the ability to combine the anatomical and kinematic data of the patient: if the patient's anatomy (3D models) can be integrated into the kinematic model, the true bone axes and centre of rotation of the patient's actual shoulder can be used. Furthermore, this data fusion enables direct assessment of the patient's anatomy in motion.

Our hypothesis was that both rotations and translations at the shoulder joint could be assessed on motion capture thanks to MRI reconstruction of the patient-specific kinematic chain of the shoulder complex. The purpose of this study was thus:

- to develop a dedicated patient-specific measurement technique to determine shoulder kinematics accurately;
- to assess the effectiveness of the technique by comparing the resulting 3D kinematics with that obtained by simultaneous X-ray fluoroscopy during functional activity.

2. Materials and methods

2.1. Subjects

Six adult healthy males with no pathologic shoulder instability or limitation of range of motion were recruited (age = 39.6 ± 7.0 years; height = 181.1 ± 5.9 cm: weight = 81.6 ± 4.4 kg) for the study. Exclusion criteria were history of shoulder injury or shoulder surgery, and contraindications for MRI. The dominant arm (right arm, except for one subject) was used throughout testing. Ethical approval was gained from the local Institutional Review Board, and all participants gave their written informed consent.

2.2. MRI bone models

All subjects underwent MR shoulder arthrography to assess all images prospectively for rotator cuff and labral lesions (results not reported in this article). MRI was performed with a 1.5 T HDxT system (General Electric Healthcare, Milwaukee, WI, USA). A shoulder-dedicated surface coil was used. Three 3D MRI volumes were acquired:

- a cosmic 3D fast gradient echo sequence with fat saturation (section thickness, 1.8 mm; no gaps; TR/TE, 6.1/3.0 ms; flip angle, 45°) capturing from the acromion to approximately the mid-part of the scapula;
- a cosmic 3D fast gradient echo sequence (section thickness, 4 mm; no gaps; TR/TE, 5.7/2.8 ms) capturing from the acromion to approximately the mid-shaft of the humerus;
- a lava 3D fast gradient echo sequence (section thickness, 5.2 mm; no gaps; TR/TE, 3.7/1.7 ms) capturing from the acromion to the elbow.

The MRI volumes were registered and manually segmented by a musculoskeletal radiologist (FCK) using ITK-SNAP software [10]. Based on the segmented contours, 3D models of the shoulder bones (humerus, scapula, clavicle and sternum) were reconstructed for each volunteer. Local coordinate systems (Fig. 1) were then established based on the definitions suggested by the International Society of Biomechanics [11] to represent the thorax, clavicle, scapula and humerus segments, using anatomical landmarks identified on the reconstructed bone models and MR images. The glenohumeral joint centre was calculated using a sphere-fitting method [12].

2.3. Data collection

Participants were equipped with spherical retroreflective markers (Fig. 2) placed directly on the skin. Four markers (Ø14 mm) were attached to the thorax (sternal notch, xyphoid process, C7 and T8 vertebra), four (Ø6.5 mm) on the clavicle, and four (Ø14 mm) on the upper arm – two placed on anatomical landmarks (lateral and medial epicondyles) and two as far as possible from the deltoid. For the scapula, 1 marker (Ø14 mm) was fixed on the acromion. In

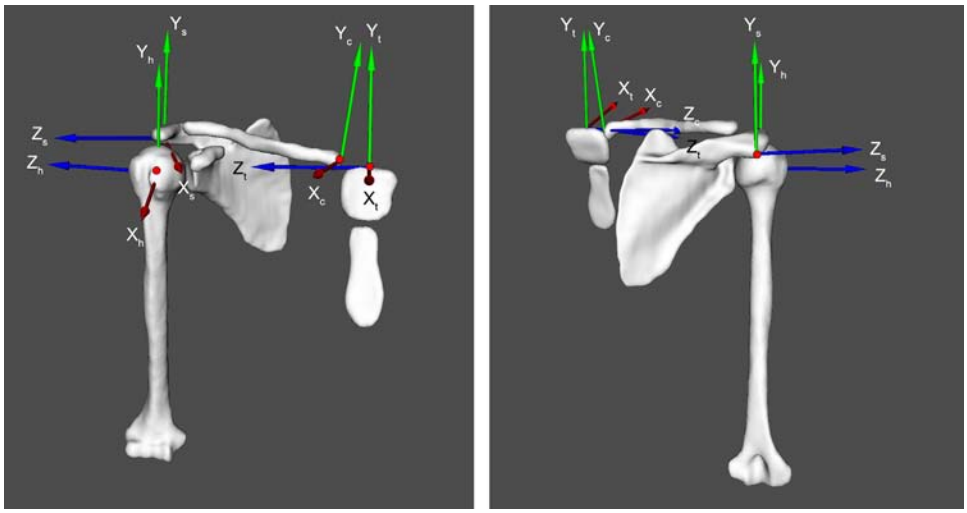

Fig. 1. Bone coordinate systems for the thorax ($X_tY_tZ_t$), clavicle ($X_cY_cZ_c$), scapula ($X_sY_sZ_s$) and humerus ($X_hY_hZ_h$).

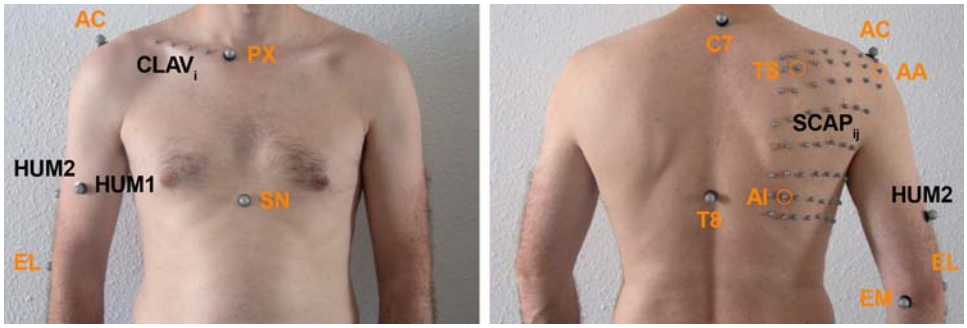

Fig. 2. Marker placement, including markers placed on anatomical landmarks (orange) and technical markers (black). PX = xyphoid process, SN = sternal notch, AC = acromion, TS = trigonum spinae, AA = angulus acromialis, AI = angulus inferior, EL = lateral epicondyle, EM = medial epicondyle.

addition, the scapula was covered with a regular grid of 56 markers (Ø6.5 mm); this number was determined so as to have enough markers to cover the scapula while limiting the time required to place them.

Kinematic data were collected simultaneously from an X-ray fluoroscopy unit (MultiDiagnostEleva, Philips Medical Systems, Netherlands) operating at 30 Hz and a Vicon MXT40S motion capture system (Vicon, Oxford Metrics, UK) consisting of 8 cameras sampling at 120 Hz. Prior to data collection, the fluoroscopy system was calibrated for image distortion and radiographic projection parameters using a calibration object [13]. A calibration frame was also acquired with 10 non-coplanar retroreflective markers, visible in both systems, to compute the pose of the coordinate system of the Vicon system relative to the fluoroscopy coordinate system by a 4×4 homogenous matrix. During testing, subjects were positioned in front of the fluoroscope with the torso at approximately 30° to the X-ray beam, so that the scapular plane was parallel to the fluoroscope. They were instructed to perform 2 tasks: 3 consecutive arm flexions from neutral to maximum flexion, and 3 consecutive empty-can abductions from neutral to maximum abduction in the scapular plane. These standard movements were chosen because they have been widely investigated in the literature, facilitating comparison with previous studies. Subjects were not constrained during motion, to allow natural arm movement.

2.4. Calculation of shoulder kinematics using X-ray fluoroscopy

The 3D poses of the scapula and humerus were obtained using a 3D-to-2D shape-matching technique [14] (Fig. 3). The 3D MRI-based models were projected and iteratively matched to the 2D X-ray images using custom software. After manual initialization of the bone positions, a non-linear optimization algorithm based on an edge-to-edge metric was used to calculate the optimal poses of the bones. 3D clavicle and thorax motion was not determined because of the limited field of view of the fluoroscopy system (structures were not sufficiently visible). A previous validation study [15] had shown that best-case accuracy for fluoroscopy measurements was 0.53 mm for in-plane translation (parallel to image plane), 1.6 mm for out-of-plane translation (perpendicular to image plane), and 0.54° for rotation in all planes.

2.5. Calculation of shoulder kinematics using skin markers

The main problem in estimating kinematics from skin markers is STAs: skin deformation and displacement due to muscle activity cause parasitic marker movements with respect to the underlying bones [16]. Thus, rigid bone motion cannot be robustly estimated, unless STAs are effectively reduced. It was demonstrated that global optimization could help reduce overall STA error [8,9]; this method minimizes overall STA error by taking account of the anatomical

Fig. 3. 3D-to-2D shape-matching technique used to determine 3D motion of the scapula and humerus during dynamic arm movements.

constraints of the entire kinematic chain. We therefore developed a patient-specific kinematic chain comprising 4 rigid bodies (thorax, clavicle, scapula and humerus) using the individual subject's 3D MRI-based models. The position and orientation of the thorax relative to the global coordinate system was determined with 6 degrees of freedom (DoF), and the sternoclavicular (SC), acromioclavicular (AC) and glenohumeral (GH) joints were each defined as ball-and-socket joints (3 DoF) with loose constraints on translation. Joint translation was thus permitted but limited.

The optimal pose of the kinematic chain was obtained by finding the best transform RT_s for each segment s that minimized the following equation:

$$\min \sum_{s=1}^{4} \left(\sum_{i=1}^{n_s} \alpha_{si} \left\| RT_s x_{si} - y_{si} \right\|^2 \right) + \sum_{s=1}^{3} \beta_s \|t_s\|^2 \quad (1)$$

This corresponds to the minimization of 2 terms:

- the distance between the model-based (x_{si}) and the measured (y_{si}) marker coordinates in the segment's cluster (n_s markers in segment's cluster s) with a weighting factor α_{si} to reflect different degrees of STA, as described by Lu and O'Connor [8];
- the translation penalty at each joint, with a weighting factor β_s to control the amount of possible translation at the joint and t_s the

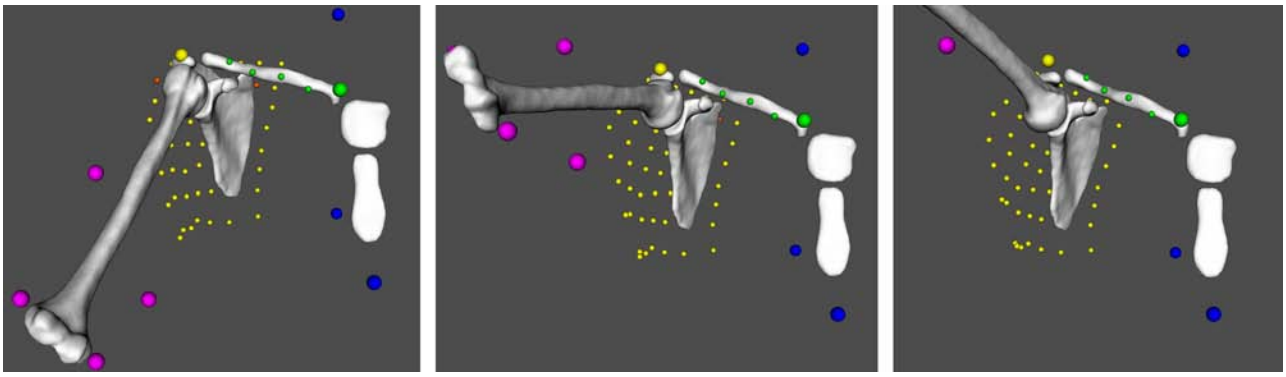

Fig. 4. Kinematic animation of the shoulder joints during empty-can abduction, including the marker setup (small colored spheres).

relative translation of the segment *s* with respect to its proximal bone.

For simplicity, equal weighting factors (α_{si}) were assigned to the markers of the thorax, clavicle and humerus clusters. Since STAs are significantly less in the flat portion of the acromion [6], scapular grid markers were weighted inversely to their distance from the acromion. The weighting factors β_s were chosen to allow translation values of the same order of magnitude as reported in the literature.

Eq. (1) was solved using a non-linear sequential quadratic programming algorithm [17]. Fig. 4 shows examples of computed motions.

2.6. Data analysis

Humeral motion with respect to the scapula was determined for both measurement methods with the following order of rotation: shoulder abduction/adduction (X_s), flexion/extension (Z', floating axis) and internal/external rotation (Y_h). This sequence was used because it is the best in terms of gimbal lock and amplitude coherence [18]. For the 2 motor tasks, the mean, standard deviation (SD) and root mean square error (RMSE) of the difference between the 2 measurement methods were calculated, as well as the motion amplitude (i.e., total measured motion) yielded by the fluoroscopic measurements.

3. Results

RMSEs for shoulder orientation were within 4° for each anatomical axis and each motion (Table 1). Minimal errors were observed for shoulder abduction/adduction and flexion/extension during flexion (mean ± SD: 2.0° ± 1.7° and 2.0° ± 2.4°, respectively). The range of glenohumeral translation was smallest in the superior-inferior direction (amplitude: 4.6 mm for flexion; 5.1 mm for abduction). Maximal amplitude reached 6 mm during abduction in the lateral-medial direction. Mean error ranged between 1.9 and 3.3 mm. Maximum RMSE for flexion was 3.7 mm and 3.5 mm for empty-can abduction. Overall, orientation errors were lower for flexion, whereas translation errors were comparable for both motor tasks.

4. Discussion

We present a patient-specific measurement technique based on the fusion of motion capture and MRI data. Kinematics was assessed using a patient-specific kinematic chain model of the shoulder complex with loose constraints on joint translation. To our knowledge, this methodology is the first attempt to calculate both rotation and translation at the shoulder joint using skin-mounted markers.

Orientation RMSEs were within 4°, which is good and acceptable for clinical use in the study of shoulder pathology. For comparison, Karduna et al. [19] reported RMSEs of 10° for a scapula tracker and 11.4° for an acromial method against bone pins; Warner et al. [6]

Table 1
Mean ± SD errors, root mean square errors (RMSE) of shoulder kinematics between fluoroscopy-based and marker-based measurement. The motion amplitude (total measured motion) obtained from fluoroscopic measurement is also reported.

Movement	Glenohumeral rotation			
	Rotation (°)	Amplitude	Mean ± SD	RMSE
Flexion	Abduction/adduction (X)	105.0	2.0 ± 1.7	2.7
	Flexion/extension (Z)	53.5	2.0 ± 2.4	2.7
	Internal/external rotation (Y)	68.6	3.1 ± 2.5	3.9
Empty-can abduction	Abduction/adduction (X)	92.6	3.4 ± 2.3	4.0
	Flexion/extension (Z)	32.6	2.8 ± 2.2	3.5
	Internal/external rotation (Y)	54.2	3.1 ± 2.4	3.9
Movement	Glenohumeral translations			
	Translation (mm)	Amplitude	Mean ± SD	RMSE
Flexion	Anterior/posterior translation (X)	5.8	1.9 ± 1.2	2.2
	Lateral/medial translation (Z)	5.9	2.9 ± 1.6	3.3
	Superior/inferior translation (Y)	4.6	3.1 ± 2.1	3.7
Empty-can abduction	Anterior/posterior translation (X)	5.7	2.1 ± 1.8	2.8
	Lateral/medial translation (Z)	6.0	3.3 ± 1.3	3.5
	Superior/inferior translation (Y)	5.1	3.1 ± 1.5	3.5

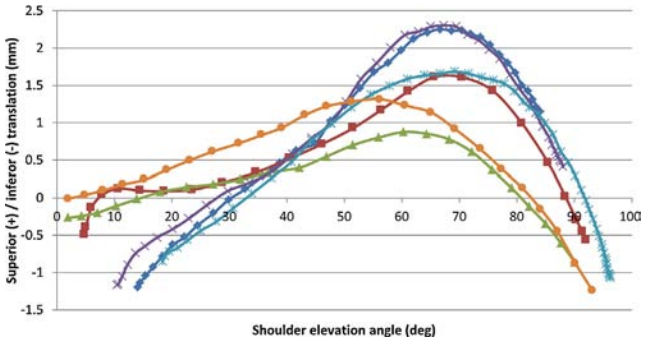

Fig. 5. Superior-inferior translation of the humeral head as a function of shoulder elevation angle during empty-can abduction. Each curve corresponds to 1 of the 6 participants.

found RMSEs of 3.5° to 7.3° comparing an acromion marker cluster to a scapula locator. We were not able to find any comparative data in the literature specific to the relative motion of the humerus with respect to the scapula.

Difficulties were encountered in determining glenohumeral translation due to the great mobility of the joint. Although our data contained some significant translational errors, particularly in superior-inferior direction, the patterns of humeral translation were in good agreement with previous reports. For example, the data computed from the skin markers showed that the humeral head translated superiorly during the early phase of arm elevation and inferiorly toward maximum elevation (Fig. 5), as previously reported [14,20]. Nevertheless, improvement is still needed. One direction could be to replace loose translational constraints with a full biomechanical simulation (e.g., finite element models) of the capsular ligaments, taking account of their 3D shapes and mechanical properties.

Two sources of error that may contribute to the differences in shoulder kinematics as determined by fluoroscopy versus motion capture should be considered: Firstly, MRI-based models were used for the 3D-to-2D matching technique rather than CT-based models, which may have impaired the quality of the shape-matching results [15]. MRI was chosen because we wanted to review soft-tissue lesions as part of a future study. Secondly, single-plane fluoroscopy provides poor measurement accuracy for out-of-plane translation. Biplane fluoroscopy provides smaller measurement error [1], but subjects are exposed to twice as much radiation and the equipment is rarely available in a clinical setting.

5. Conclusion

The results of this study showed that the proposed technique could provide valuable kinematic data at the shoulder joint. Most importantly, we demonstrated that a first estimate of joint translation was feasible using an external measurement system, such as motion capture. This original technique may open new horizons leading to improved understanding of shoulder pathologies and opening up new possibilities of analyzing large ranges of shoulder motion, for instance during sports movements.

Disclosure of interest

The authors declare that they have no conflicts of interest concerning this article.

Acknowledgments

This work was supported by grants from La Tour Hospital, Geneva, Switzerland, and from the European Society for Shoulder and Elbow Surgery (SECEC-ESSSE).

References

[1] Zhu Z, Massimini DF, Wang G, Warner JJP, Li G. The accuracy and repeatability of an automatic 2D–3D fluoroscopic image-model registration technique for determining shoulder joint kinematics. Med Eng Phys 2012;34:1303–9.
[2] Jackson M, Michaud B, Tetreault P, Begon M. Improvements in measuring shoulder joint kinematics. J Biomech 2012;45:2180–3.
[3] Klotz MCM, Kost L, Braatz F, et al. Motion capture of the upper extremity during activities of daily living in patients with spastic hemiplegic cerebral palsy. Gait Posture 2012;38:148–52.
[4] Johnson GR, Stuart PR, Mitchell S. A method for the measurement of three-dimensional scapular movement. Clin Biomech 1993;8:269–73.
[5] Andel C, Hutten K, Eversdijk M, Veeger D, Harlaar J. Recording scapular motion using an acromion cluster. Gait Posture 2009;29:123–8.
[6] Warner MB, Chappell PH, Stokes MJ. Measuring scapular kinematics during arm lowering using the acromion marker cluster. Hum Mov Sci 2012;31:386–96.
[7] Mattson JM, Russo SA, Rose WC, Rowley KM, Richards JG. Identification of scapular kinematics using surface mapping: a validation study. J Biomech 2012;45:2176–9.
[8] Lu TW, O'Connor JJ. Bone position estimation from skin marker co-ordinates using global optimisation with joint constraints. J Biomech 1999;32:129–34.
[9] Roux E, Bouilland S, Godillon-Maquinghen A-P, Bouttens D. Evaluation of the global optimisation method within the upper limb kinematics analysis. J Biomech 2002;35:1279–83.
[10] Yushkevich PA, Piven J, Hazlett HC, et al. User-guided 3D active contour segmentation of anatomical structures: significantly improved efficiency and reliability. Neuroimage 2006;31:1116–28.
[11] Wu G, Helm FCT, Veegerc HEJ, et al. ISB recommendation on definitions of joint coordinate systems of various joints for the reporting of human joint motion – part II: shoulder, elbow, wrist and hand. J Biomech 2005;38:981–92.
[12] Schneider PJ, Eberly DH. Geometric Tools for Computer Graphics. The Morgan Kaufmann Series in Computer Graphics and Geometric Modeling; 2003.
[13] Lu TW, Tsai TY, Kuo MY, Hsu HC, Chen HL. In vivo three-dimensional kinematics of the normal knee during active extension under unloaded and loaded conditions using single-plane fluoroscopy. Med Eng Phys 2008;30:1004–10.
[14] Matsuki K, Matsuki KO, Yamaguchi S, et al. Dynamic in vivo glenohumeral kinematics during scapular plane abduction in healthy shoulders. J Orthop Sports Phys Ther 2012;42:96–104.
[15] Moro-oka T, Hamai S, Miura H, et al. Can magnetic resonance imaging–derived bone models be used for accurate motion measurement with single-plane three-dimensional shape registration. J Ortho Res 2007;25:867–72.
[16] Leardini A, Chiari L, Croce U, Della, Cappozzo A. Human movement analysis using stereophotogrammetry. Part 3: soft tissue artifact assessment and compensation. Gait Posture 2005;21:212–25.
[17] Lawrence CT, Tits AL. A computationally efficient feasible sequential quadratic programming algorithm SIAM. J Optim 2001;11:1092–118.
[18] Bonnefoy-Mazure A, Slawinski J, Riquet A, Lévèque J-M, Miller C, Chèze L. Rotation sequence is an important factor in shoulder kinematics. Application to the elite players' flat serves. J Biomech 2012;43:2022–5.
[19] Karduna AR, McClure PW, Michener LA, Sennett B. Dynamic measurements of three-dimensional scapular kinematics: a validation study. J Biomech Eng 2001;123:184–90.
[20] Massimini DF, Boyer PJ, Papannagari R, Gill TJ, Warner JP, Li G. In vivo glenohumeral translation and ligament elongation during abduction and abduction with internal and external rotation. J Orthop Surg Res 2012;7:29–38.

Int J CARS
DOI 10.1007/s11548-014-1135-4

ORIGINAL ARTICLE

Shoulder motion during tennis serve: dynamic and radiological evaluation based on motion capture and magnetic resonance imaging

Caecilia Charbonnier · Sylvain Chagué · Frank C. Kolo · Alexandre Lädermann

Received: 30 July 2014 / Accepted: 30 November 2014

Abstract
Purpose Rotator cuff and labral lesions in tennis players could be related to posterosuperior internal impingement or subacromial impingement during tennis serve. However, it is unknown which of these impingements are responsible for the lesions found in the tennis player's shoulder. Moreover, there is a lack of validated noninvasive methods and dynamic studies to ascertain impingement during motion.
Methods Ten intermediate or ex-professional tennis players were motion captured with an optical tracking system while performing tennis serves. The resulting computed motions were applied to patient-specific shoulder joints' 3D models based on magnetic resonance imaging (MRI) data. During motion simulation, impingements were detected and located using computer-assisted techniques. An MRI examination was also performed to evaluate the prevalence of shoulder lesions and to determine their relevance with the simulation findings.
Results Simulation showed that internal impingement was frequently observed compared to subacromial impingement when serving. The computed zones of internal impingement were mainly located in the posterosuperior or superior region of the glenoid. These findings were relevant with respect to radiologically diagnosed damaged zones in the rotator cuff and glenoid labrum.
Conclusions Tennis players presented frequent radiographic signs of structural lesions that seem to be mainly related to posterosuperior internal impingement due to repetitive abnormal motion contacts. The present study indicates that the practice of tennis serve could lead with time to cartilage/tendon hyper compression, which could be damageable for the glenohumeral joint.

Keywords Shoulder kinematics · Motion capture · MRI · 3D Simulation · Impingement · Tennis

C. Charbonnier (✉) · S. Chagué
Medical Research Department, Artanim Foundation, 41b route des Jeunes, Carouge, 1227 Geneva, Switzerland
e-mail: caecilia.charbonnier@artanim.ch

F. C. Kolo
Rive Droite Radiology Center, Geneva, Switzerland

A. Lädermann
Division of Orthopaedics and Trauma Surgery, La Tour Hospital, Geneva, Switzerland

A. Lädermann
Faculty of Medicine, University of Geneva, Geneva, Switzerland

Introduction

Impingement of the shoulder is a common cause of shoulder pain in tennis players due to repetitive overhead arm movements [10,20,27]. Impingement occurs during tennis serves, leading with time to rotator cuff and/or labral tears [1,10,20,27]. Two different impingements have been described: (1) the posterosuperior internal impingement [35] of the rotator cuff tendons (supraspinatus/ infraspinatus) and glenoid labrum between the greater tuberosity of the humeral head and the posterosuperior aspect of the glenoid when the arm is in extreme abduction, extension and external rotation [12] during the late cocking stage of the serve; (2) the subacromial impingement of the rotator cuff between the anterior acromion [25] or lateral acromion [26] and the superior humeral head.

To our knowledge, impingements during tennis serve have never been dynamically evaluated in vivo. It is therefore unknown which of the aforementioned impingements are responsible for the lesions found in the tennis player's shoul-

Published online: 14 December 2014

der. According to the impingement theory, shoulder damage occurs at the zone of impingement, but the concurrence of the actual impingement zone and resulting joint damage in the same patient has not yet been confirmed. Moreover, there is a lack of validated noninvasive methods to ascertain impingement during motion. Existing imaging methods only include a static interpretation of the joint damage [e.g., computed tomography (CT), magnetic resonance imaging (MRI)], while dynamic imaging protocols (e.g., MRI, fluoroscopy) are affected by technical limitations (e.g., confined area of measurement, low acquisition speed).

Motion capture systems using skin-mounted markers provide a good solution to noninvasively record large ranges of motion during high-velocity movements, such as in tennis strokes. However, drawbacks are related to soft tissue artifacts (STA) affecting kinematic estimation [17,37], in particular precise joint translation that is crucial to assess glenohumeral impingement. In previous work [6], we have demonstrated that this issue could effectively be tackled. Combined with computer-assisted techniques and anatomical models obtained from medical images, we believe that motion capture can offer novel insights into the analysis and comprehension of shoulder impingement.

As the serve is among the most important strokes in tennis, it has been the subject of significant biomechanical interest. Motion capture systems were used to investigate the kinematics and kinetics of lower and upper limb joint motion [11,28,38,39] as a function of serve type [28], body mass index [39] and racket type [11,38]. Attention has also been afforded to the interaction of the ball and racket during the serve [30,38]. Despite these advancements, recent research has not devoted specific attention to the direct consequences of the practice of tennis serve on the internal joint structures. This study intended to be a step in this direction.

In this paper, we present a methodology to perform functional simulations of patient-specific shoulder joints during extreme and complex positions, as well as the results of a study conducted with tennis players. The purpose of this research was to visualize and simulate in 3D shoulder motion during tennis serve and to detect and locate potential impingement during their practice, using optical motion capture and computer-assisted techniques. In addition, this study aimed at evaluating the prevalence of shoulder lesions in this group of tennis players based on MRI and at determining their relevance with the simulation findings.

Materials and methods

Subjects

Ten intermediate or ex-professional tennis players (one female, nine males) volunteered for the study. The mean age, weight, height and body mass index of the ten volunteers were 39.7 years, 76.7 kg, 180.2 cm and 23.5 kg/m^2, respectively. Exclusion criteria were reported previous shoulder injuries, shoulder surgery or contraindications for MRI.

At the time of the examination, two subjects presented shoulder pain and nine previously suffered from the shoulder at other moment of their career. All subjects had a clinically functional rotator cuff.

The dominant arm was used throughout testing. This was the right arm for all participants, except one who was left-hand dominant. Institutional ethical approval and informed consent were obtained prior to data collection.

MRI and three-dimensional reconstruction

All volunteers underwent a MR shoulder arthrography. The MRI examinations were conducted after a fluoroscopically guided arthrography with a contrast agent and with an anterior approach. MRI was performed with a 1.5 T HDxT system (General Electric Healthcare, Milwaukee, WI, USA). A dedicated shoulder surface coil was used. The following MRI sequences were acquired: (1) a sagittal T1-weighted fast spin echo sequence (section thickness 3.5 mm; gap 0.5 mm; TR/TE ms 380/11), (2) a coronal T2-weighted fast spin echo sequence with fat saturation (section thickness 4 mm; gap 0.5 mm; TR/TE ms 1920/101.6), (3) a sagittal T2-weighted fast spin echo sequence with fat saturation (section thickness 3.5 mm; gap 0.5 mm; TR/TE ms 5680/103.6), (4) a coronal T1-weighted fast spin echo sequence with fat saturation (section thickness 4 mm; gap 0.5 mm; TR/TE ms 320/13), (5) an axial T1-weighted fast spin echo sequence with fat saturation (section thickness 4 mm; gap 0.5 mm; TR/TE ms 640/26.8), (6) an axial Cosmic® 3D fast gradient echo sequence with fat saturation (section thickness 1.8 mm; no gaps; TR/TE ms 6.1/3.0), (7) an axial Cosmic® 3D fast gradient echo sequence (section thickness 4 mm; no gaps; TR/TE ms 5.7/2.8) and (8) an axial Lava® 3D fast gradient echo sequence (section thickness 5.2 mm; no gaps; TR/TE ms 3.7/1.7).

Two musculoskeletal radiologists, blinded to the clinical evaluation, assessed independently all MRI arthrograms for shoulder pathology. The rotator cuff abnormalities [33], the labral lesions [36] and the bony changes [24] were reviewed. Rotator cuff lesions were classified as partial articular surface tendon avulsion lesion, bursal-sided partial thickness tear, interstitial tear or complete tear (Fig. 1). The glenoid labrum was considered as normal, degenerated (abnormal signal intensity), torn (abnormal linear intensity extending to the glenoid surface), detached (abnormal linear intensity coursing at the interface between bone and labrum at the level or posterior to the attachment of biceps tendon) or as ossification of the labrum (continuity of the labrum with glenoid

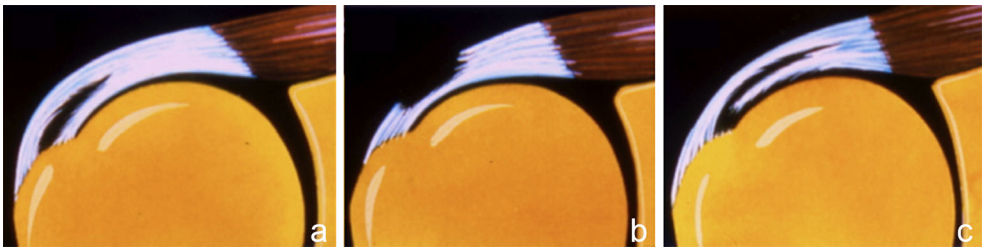

Fig. 1 **a** Interstitial tear, **b** bursal-sided partial thickness tear and **c** partial articular supraspinatus tendon avulsion (PASTA) lesion

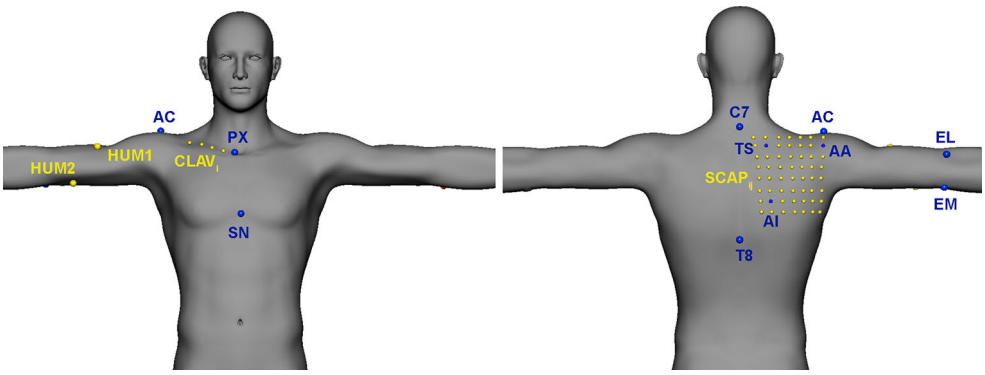

Fig. 2 Markers placement including markers placed on anatomical landmarks (*blue*) and technical markers (*yellow*). *PX* xyphoid process, *SN* sternal notch, *AC* acromion, *TS* trigonum spinae, *AA* angulus acromialis, *AI* angulus inferior, *EL* lateral epicondyle, *EM* medial epicondyle

bone marrow). The absence or presence of bony changes such as Bankart lesions [2] or intra-osseous cysts was reported.

The 3D MRI images were manually segmented by one of the musculoskeletal radiologists (FCK), and a virtual 3D model of the shoulder complex was reconstructed using Mimics software (Materialize NV, Leuven, Belgium). For each tennis player, patient-specific 3D models of the shoulder bones (humerus, scapula, clavicle and sternum), cartilage surfaces and labrum were obtained.

To compute joint motion, local coordinate systems were established based on the definitions suggested by the International Society of Biomechanics [40] to represent the thorax, clavicle, scapula and humerus segments. They were created using anatomical landmarks identified on the reconstructed bone models and MRI images. The glenohumeral joint center was calculated using a sphere-fitting method [32].

Motion recording

The tennis players participated to a motion capture session. They were equipped with a dedicated shoulder markers protocol [6] (Fig. 2), including 69 spherical retroreflective markers placed directly onto the skin using double-sided adhesive tape. The setup included four markers (Ø 14 mm) on the thorax (sternal notch, xyphoid process, C7 and T8 vertebra), four markers (Ø 6.5 mm) on the clavicle, four markers (Ø 14 mm) on the upper arm—two placed on the lateral and medial epicondyles and two as far as possible from the deltoid—and 57 markers on the scapula ($1 \times$ Ø 14 mm on the acromion and a 7×8 grid of Ø 6.5 mm). Additional markers were distributed over the body (non-dominant arm and legs) to provide a global visualization of the motion.

After appropriate warm-up, participants performed three trials of the following variants of tennis serve: flat serve, when the ball is hit down and through with little to no spin; and kick serve, when the ball is hit with an upward motion, imparting top-spin on the ball. Motion was recorded using a Vicon MXT40S motion capture system (Vicon, Oxford Metrics, UK) consisting of 24 cameras sampling at 240 Hz. The same investigators (CC, SC) attached all markers and performed all measurements.

Kinematics modeling

Shoulder kinematics was computed from the recorded markers' trajectories. Measuring shoulder motion using skin-mounted markers is a challenging task. The first issue is related to the accuracy of the measurements which is prone to error due to the non-rigid movement of the soft tissue interface between the skin markers and the underlying bone, commonly referred to as soft tissue artifact [17]. In the upper extremity, the scapula is particularly affected [37]. The second issue is related to the ability to estimate both shoulder joint rotation and translation using an external measurement system—information about joint translation is crucial to properly assess glenohumeral impingement.

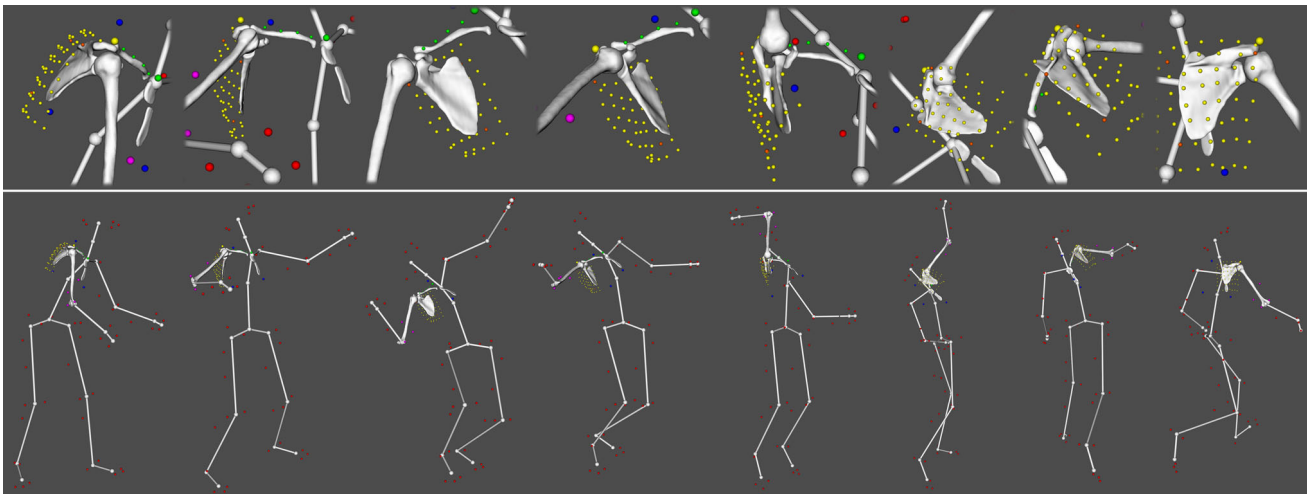

Fig. 3 Kinematic animation of the shoulder (here the right shoulder joints) during flat serve. *Top images* show a zoom in the shoulder for each position. Position 4 is commonly known as the cocking stage

To address these two issues, we used a previously developed and validated biomechanical model based on a patient-specific kinematic chain consisting of four rigid bodies (thorax, clavicle, scapula and humerus) using the tennis player's shoulder 3D models reconstructed from their MRI data. To register internal anatomical structures to the marker cluster frames, a calibration was performed based on a standard CAST (calibrated anatomical system technique) protocol [31]. The optimal pose of the kinematic chain was then obtained using a global optimization algorithm (to minimize STA error globally [29]) with loose constraints on joint translations. More details about the model and its validation can be found in [6]. The accuracy of the model for glenohumeral orientation was within 4° for each anatomical plane and within 3 mm for glenohumeral translation. Moreover, previous results showed that the translation patterns computed with the model were in good agreement with related works [21,22].

As a result, the motion of the tennis player's shoulder 3D models could be visualized at each point of the movement. Figure 3 shows an example of computed bone poses during tennis serve. A ball and stick representation of the overall skeleton was also added to improve the analysis and visualization of the motion.

Impingement detection

During motion simulation, internal and subacromial impingements were evaluated at the critical position—the late cocking stage of the serve (see Fig. 3). For internal impingement, a collision detection algorithm [4,5] was used to virtually locate contacts between the humeral cartilage, the glenoid cartilage and the glenoid labrum. Moreover, the surface-to-surface distance (i.e., penetration depth) was computed in order to estimate the overall impingement. This distance represented the topographic extent of the cartilage or labral compression and was reported in millimeter.

To document areas of increased compression, the penetration depth distribution on the surface of the cartilages and labrum was represented using a color scale (Fig. 4a). The blue color was assigned when no collision was detected (penetration depth = 0), while other colors showed the compression zone. The red color denoted the area with the highest compression (penetration depth = max).

To describe and report the exact location of the impingement zone, the glenoid was divided into eight sectors (position 1, anterior; position 2, anterosuperior; position 3, superior; position 4, posterosuperior; position 5, posterior; position 6, posteroinferior; position 7, inferior; position 8, anteroinferior), as depicted in Fig. 4b. The impingement zones were, hence, assigned numbers correlating with their position.

For subacromial impingement, the minimum humero-acromial distance that is typically used for the evaluation of such impingement was measured [8,14,34]. This distance was calculated in 3D based on the simulated bone models positions and was reported in millimeter. A color scale was also used to map the variations of distance on the scapula surface, with the red color denoting the zone of minimum distance and other colors denoting the areas of increased distance (Fig. 5).

Eventually, the following two criteria were applied: (1) Increased penetration depth results in increased soft tissue compression. Thus, when performed repetitively, the greater the penetration depth is, the more potentially damageable for the joint the internal impingement can be; (2) given the thickness of the potential impinged tissues, subacromial impingement was considered when the computed humero-acromial

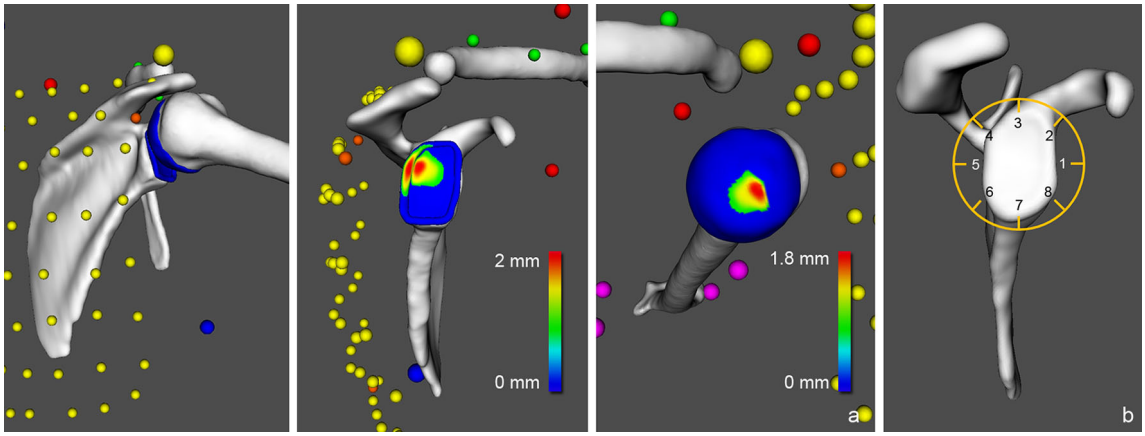

Fig. 4 **a** Visualization of the contact zone during motion (posterior, lateral and medial views). The *colors* represent the penetration depth distribution: the *blue color* is assigned when no collision is detected (penetration depth = 0), while *other colors* show the compression zone. The *red color* denotes the area with the highest compression (penetration depth = max). The humerus and humeral cartilage, respectively, the scapula, glenoid cartilage and labrum are not shown in the lateral and medial views for clarity. **b** Glenoid was divided into eight sectors (position 1, anterior; position 2, anterosuperior; position 3, superior; position 4, posterosuperior; position 5, posterior; position 6, posteroinferior; position 7, inferior; position 8, anteroinferior) to report the location of the impingement zone

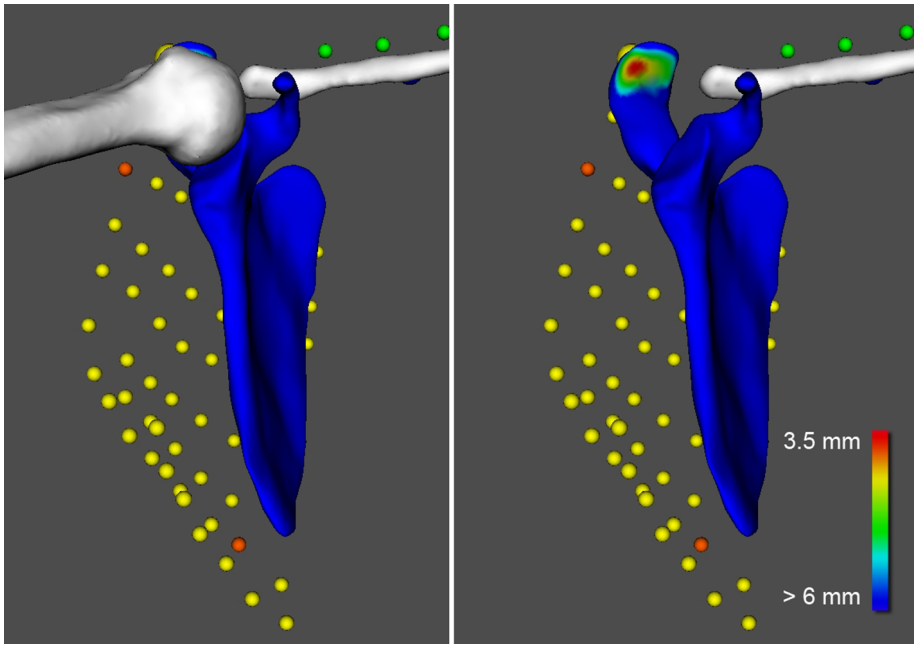

Fig. 5 Visualization of the humero-acromial distance during motion (anterior view). The *colors* represent the variations of distance between the acromion and humeral head. The *red color* denotes the zone of minimum distance. The humerus is not shown in the second view for clarity

distance was <6 mm, as suggested in previous studies [8,19].

Statistical analysis

A statistical analysis was conducted for the two variants of tennis serve. For internal impingement, we computed the frequency of impingement, the mean values and the standard deviations (SD) of the penetration depth, and we created histograms displaying the frequency of distribution of the zone of impingement. For subacromial impingement, we calculated the frequency of impingement and the mean and SD of the minimum humero-acromial distance.

For the radiological analysis, the prevalence of rotator cuff abnormalities, labral lesions and bony changes were calculated, as well as the frequency of distribution of the location of diagnosed labral lesions. Cohen's kappa coefficient (K) was calculated to assess the interobserver agreement regarding the image analysis. The statistical software package R, version 3.1.1, was employed.

Table 1 Rotator cuff lesions

Position	Rotator cuff condition in tennis players ($n = 10$)*				
	Normal	Partial articular	Partial bursal	Interstitial	Complete
Supraspinatus	5	3	0	3	0
Infraspinatus	7	3	0	0	0
Subscapularis	8	2	0	0	0
Teres minor	10	0	0	0	0
Total lesions		8	0	3	0

* Data are the number of subjects

Table 2 Labral lesions

Position	Labrum condition in tennis players ($n = 10$)*				
	Normal	Degeneration	Tear	Detachment	Ossification
Anterior	10	0	0	0	0
Superior	7	0	3	0	0
Posterosuperior	7	2	2	0	0
Posterior	8	2	0	0	0
Posteroinferior	10	0	0	0	0
Inferior	8	0	0	2	0
Anteroinferior	10	0	0	0	0
Total lesions		4	5	2	0

* Data are the number of subjects

Fig. 6 **a** Coronal T2-weighted MRI image with fat saturation showing a PASTA lesion (*arrow*). **b** Coronal T1-weighted MRI image with fat saturation showing a posterosuperior labral lesion (*arrow*)

Results

MRI findings

The *K* value for interobserver agreement of shoulder lesion evaluation on MRI arthrograms was 0.86, representing excellent agreement [9]. We found eleven rotator cuff lesions in six subjects (Table 1)—three interstitial of the supraspinatus, three partial articular supraspinatus tendon avulsions (PASTA), three partial articular infraspinatus tendon avulsions and two articular of the subscapularis. All lesions were located on the articular side.

Distribution of labral lesions in the different positions around the glenoid (Table 2) showed more pronounced labral lesions at the posterosuperior and superior positions. There was no radiographic evidence of bony changes such as Bankart lesions or intra-osseous cysts.

Figure 6 shows two typical lesions found in the tennis players' shoulders: a PASTA lesion and a posterosuperior labral lesion (torn labrum).

Simulation findings

For the flat serve, internal impingement was observed in 76 % of the tennis players' shoulders. The majority of the contacts (60 %) was located in the posterosuperior position of the glenoid (Fig. 7). The mean penetration depths varied

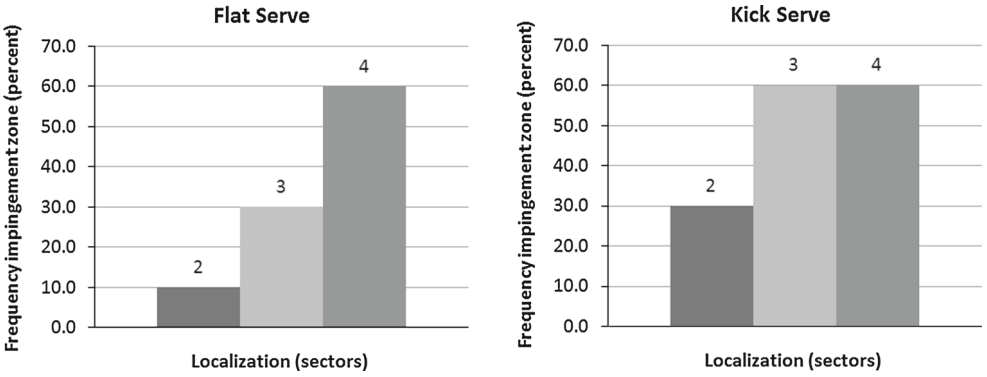

Fig. 7 Histograms showing the distribution of frequency of the computed internal impingement zones for each serve

Table 3 Computed penetration depths (mm) by movement ($n = 30$)*

Movements	Humeral cartilage Mean ± SD (range)	Glenoid cartilage Mean ± SD (range)	Glenoid labrum Mean ± SD (range)
Flat serve	1.18 ± 0.25 (0.79–1.61)	1.43 ± 1.30 (0.79–1.76)	1.85 ± 0.48 (1.12–2.71)
Kick serve	1.23 ± 0.20 (1.05–1.62)	1.53 ± 0.24 (1.08–1.87)	1.90 ± 0.34 (1.65–2.71)

* Data are the number of trials (3 trials per subject)

from 1.43 to 1.85 mm, depending on the cartilage considered. For the kick serve, internal impingement occurred in 75 % of the cases. The contacts were distributed between the posterosuperior (60 %), superior (60 %) and anterosuperior (30 %) positions of the glenoid (Fig. 7). The computed penetration depths were of similar intensity (mean range 1.53–1.90 mm). For both serves, the most intense penetration depths were obtained for the glenoid labrum, with peak values of 2.71 mm. Interestingly, when those contacts occurred, they were located in the posterosuperior region of the glenoid. Table 3 summarizes for the reader mean values and standard deviations of computed penetration depths by movement.

Subacromial impingement was detected during flat serve for 29 % of the tennis players' shoulders. Ten percent were located in the anterior part of the acromion, and 19 % were located in the lateral part of the acromion. The mean ± SD of the minimum humero-acromial distance was 7.43 ± 3.12 mm. During kick serve, subacromial impingement was slightly more frequent (38 % of the tennis players' shoulders), with 13 and 25 % of the cases located, respectively, in the anterior and lateral parts of the acromion. The mean ± SD of the minimum humero-acromial distance was 6.88 ± 3.47 mm.

Discussion

In this study, we have presented a methodology to perform functional simulations of the shoulder joints in extreme and complex positions. To our knowledge, shoulder impingement during tennis serve has never been dynamically evaluated. Using this patient-specific measurement technique, impingement was actively assessed and demonstrated in vivo. The results of this study showed that the detected internal impingements were mostly located in the posterosuperior or superior quadrant of the glenoid and that subacromial impingement was less frequent when serving. MRI revealed eleven rotator cuff lesions and more pronounced labral lesions at the posterosuperior and superior positions of the glenoid. All lesions were located in the articular side, suggesting an internal impingement as origin.

In the present study, nine of the ten tennis players presented radiographic signs of structural lesions that could be related to impingement syndrome due to overhead arm movements. However, the precise causes for these lesions remain unclear. Two main theories can be put forward. The first theory holds that repetitive contacts between the rotator cuff insertion and the posterosuperior glenoid rim—when the arm is placed in the cocked position of 90° abduction, full external rotation and extension [12]—may be responsible for rotator cuff tears and superior labral lesions [12,23,35]. The second theory holds that subacromial impingement may occur in overhead athletes because of narrowing of the subacromial space due to glenohumeral instability and/or muscle imbalance [15,18,27].

As shown by the results of this study, internal impingement was frequent when serving (75–76 % of the tennis players' shoulders). For both tennis serves, the computed zones of impingement were mainly located in the posterosuperior or superior quadrant of the glenoid and this was relevant with respect to the MRI findings. Subacromial impingement remained low. We did not note shoulder instability in this population, as demonstrated in our previous study [7,16]. Moreover, all subjects had a competent rotator cuff. The repeti-

tive posterosuperior internal impingements seem thus to be the most plausible explanation for these lesions that are not always symptomatic, as previously observed [13].

The computed penetration depths varied from 1.43 to 1.90 mm in average for both tennis serves, with peak values of 2.71 mm for the labrum in posterosuperior position. Knowing that the glenoid labrum has superiorly and posteriorly an average height of 6–11 mm [3], the labrum is already compressed in our simulation during the late cocking stage of the serve—and this without accounting for the rotator cuff insertion that may also impinge between the greater tuberosity of the humeral head and the posterosuperior labrum. It is therefore most likely that our results underestimated labral compressions. In fact, the true extent of compression cannot be determined without a more advanced simulation, taking into account the 3D shapes of the rotator cuff tendons and the soft tissues deformation under loads. Future work should, hence, include a 3D reconstruction of the rotator cuff from MRI data, as well as a physically based simulation of the chondrolabral and tendon structures. A clinical trial could also be performed to validate the impingement estimates. Nevertheless, according to our data, there is little doubt that the glenohumeral articular surface is exposed to high mechanical stress.

There are potential limitations to the accuracy of the global setup. Indeed, errors in our methodology could originate from the kinematics computation from motion capture data (translational error <3 mm and rotational error $<4°$). Since the measurements are external (no direct access to the joint), motion capture is generally subject to greater errors than other techniques (e.g., dynamic MRI and fluoroscopy). However, this modality is not harmful and allows the recording of large ranges of high-velocity motion, such as tennis strokes. The second limitation of this study is the use of the humeroacromial distance to assess subacromial impingement, which does not take into account precise measurements of the thickness of the impinged soft tissues. Again, one improvement could be to perform a more advanced simulation accounting for the 3D shapes and movements of the rotator cuff tendons.

In summary, we conclude from our data that tennis players presented frequent radiographic signs of structural lesions that seem to be mainly related to posterosuperior internal impingement due to repetitive abnormal motion contacts. We believe that recurrent posterosuperior internal impingement could lead with time to cartilage/tendon hyper compression and therefore could be a potential factor of damages of the glenoid labrum and rotator cuff tendons.

This study[1] offers novel insights into the analysis of shoulder impingement that could, with future studies, be generalized to other shoulder pathologies and sports. This method[2] may open new horizons, leading to improvement in impingement comprehension.

Acknowledgments This work was supported by grants from La Tour Hospital, Geneva, Switzerland, and from the European Society for Surgery of the Shoulder and the Elbow (ESSSE).

Conflict of interest The authors declare that they have no conflict of interest.

References

1. Abrams G, Renstrom P, Safran M (2012) Epidemiology of musculoskeletal injury in the tennis player. Br J Sports Med 46:492–498
2. Bankart A (1923) Recurrent or habitual dislocation of the shoulder-joint. Br Med J 2(3285):1132–1133
3. Carey J, Small C, Pichora D (2000) In situ compressive properties of the glenoid labrum. J Biomed Mater Res 51(4):711–716
4. Charbonnier C, Assassi L, Volino P, Magnenat-Thalmann N (2009) Motion study of the hip joint in extreme postures. Vis Comput 25(9):873–882
5. Charbonnier C, Kolo F, Duthon V, Magnenat-Thalmann N, Becker C, Hoffmeyer P, Menetrey J (2011) Assessment of congruence and impingement of the hip joint in professional ballet dancers. Am J Sports Med 39(3):557–566
6. Charbonnier C, Chagué S, Kolo F, Chow J, Lädermann A (2014) A patient-specific measurement technique to model the kinematics of the glenohumeral joint. Orthop Traumatol: Surg Res 100(7): 715–719
7. Charbonnier C, Chagué S, Kolo F, Lädermann A (2014) Analysis of shoulder impingement and stability in tennis players. In: Proceedings of the 13th International Symposium on 3D Analysis of Human Movement, Lausanne, Switzerland
8. Chopp J, Dickerson C (2012) Resolving the contributions of fatigue-induced migration and scapular reorientation on the subacromial space: an orthopaedic geometric simulation analysis. Hum Mov Sci 31:448–460
9. Cohen J (1960) A coefficient of agreement for nominal scales. Educ Psychol Meas 20:37–46
10. Cools A, Declercq G, Cagnie B, Cambier D, Witvrouw E (2008) Internal impingement in the tennis player: rehabilitation guidelines. Br J Sports Med 42:165–171
11. Creveaux T, Dumas R, Hautier C, Macé P, Chèze L, Rogowski I (2013) Joint kinetics to assess the influence of the racket on a tennis player's shoulder. J Sports Science Med 12:259–266
12. Davidson P, Elattrache N, Jobe C, Jobe F (1995) Rotator cuff and posterior-superior glenoid labrum injury associated with increased glenohumeral motion: a new site of impingement. Shoulder Elb Surg 4(5):384–390
13. Girish G, Lobo L, Jacobson J, Morag Y, Miller B, Jamadar D (2011) Ultrasound of the shoulder: asymptomatic findings in men. AJR Am J Roentgenol 197:713–719
14. Graichen H, Hinterwimmer S, Eisenhart-Rothe R, Vogl T, Englmeier KH, Eckstein F (2005) Effect of abducting and adducting muscle acitivity on glenohumeral translation, scapular kinematics and subacromial space width in vivo. J Biomech 38(4):755–760
15. Hallstrom E, Karrholm J (2006) Shoulder kinematics in 25 patients with impingement and 12 controls. Clin Orthop Relat Res 448: 22–27

[1] This study won the *Best Technical Paper Award* at the 14th Annual Meeting of the International Society for Computer Assisted Orthopaedic Surgery (CAOS) in Milan, 2014.

[2] A video summarizing the method and complementary information about this work can be found at http://www.artanim.ch/Shoulder3D.

16. Lädermann A, Chagué S, Kolo F, Charbonnier C (2014) Kinematics of the shoulder joints in tennis players. J Sci Med Sport (in Press)
17. Leardini A, Chiari L, Croce UD, Cappozzo A (2005) Human movement analysis using stereophotogrammetry Part 3: soft tissue artifact assessment and compensation. Gait Posture 21:212–225
18. Ludewig P, Cook T (2002) Translations of the humerus in persons with shoulder impingement symptoms. J Orthop Sports Phys Ther 32(6):248–259
19. Maeseneer MD, Roy PV, Shahabpour M (2006) Normal MR imaging anatomy of the rotator cuff tendons, glenoid fossa, labrum, and ligaments of the shoulder. Radiol Clin N. Am 44:479–487
20. Manske R, Grant-Nierman M, Lucas B (2013) Shoulder posterior internal impingement in the overhead athlete. Int J Sports Phys Ther 8(2):194–204
21. Massimini D, Boyer P, Papannagari R, Gill T, Warner J, Li G (2012) In-vivo glenohumeral translation and ligament elongation during abduction and abduction with internal and external rotation. J Orthop Surg Res 7:29–38
22. Matsuki K, Matsuki K, Yamaguchi S, Ochiai N, Sasho T, Sugaya H, Toyone T, Wada Y, Takahashi K, Banks S (2012) Dynamic in vivo glenohumeral kinematics during scapular plane abduction in healthy shoulders. J Orthop Sports Phys Ther 42(2):96–104
23. Meister K (2000) Internal impingement in the shoulder of the overhand athlete: pathophysiology, diagnosis, and treatment. Am J Orthop 29(6):433–438
24. Meister K, Andrews J, Batts J, Wilk K, Baumgarten T (1999) Symptomatic thrower's exostosis arthroscopic evaluation and treatment. Am J Sports Med 27(2):133–136
25. Neer C (1972) Anterior acromioplasty for chronic impingement syndrome in the shoulder: a preliminary report. J Bone Joint Surg Am 54:41–50
26. Nyffeler R, Werner C, Sukthankar A, Schmid M, Gerber C (2006) Association of a large lateral extension of the acromion with rotator cuff tears. J Bone Joint Surg Am 88(4):800–805
27. Page P (2011) Shoulder muscle imbalance and subacromial impingement syndrome in overhead athlete. Int J Sports Phys Ther 6(1):51–58
28. Reid M, Elliott B, Alderson J (2007) Shoulder joint loading in the high performance flat and kick tennis serves. Br J Sports Med 41:884–889
29. Roux E, Bouilland S, Godillon-Maquinghen AP, Bouttens D (2002) Evaluation of the global optimisation method within the upper limb kinematics analysis. J Biomech 35:1279–1283
30. Sakurai S, Reid M, Elliott B (2013) Ball spin in the tennis serve: spin rate and axis of rotation. Sports Biomech 12(1):23–29
31. Salvia P, Jan SVS, Crouan A, Vanderkerken L, Moiseev F, Sholukha V, Mahieu C, Snoeck O, Rooze M (2009) Precision of shoulder anatomical landmark calibration by two approaches: a CAST-like protocol and a new anatomical palpator method. Gait Posture 29(4):587–591
32. Schneider P, Eberly D (2003) Geometric Tools for Computer Graphics. The Morgan Kaufmann Series in Computer Graphics and Geometric Modeling
33. Snyder S, Pachelli A, Pizzo WD, Friedman M, Ferkel R, Pattee G (1991) Partial thickness rotator cuff tears: results of arthroscopic treatment. Arthroscopy 7(1):1–7
34. Timmons M, Lopes-Albers AD, Borgsmiller L, Zirker C, Ericksen J, Michener L (2013) Differences in scapular orientation, subacromial space and shoulder pain between the full can and empty can tests. Clin Biomech 28:395–401
35. Walch G, Boileau P, Noel E, Donell S (1992) Impingement of the deep surface of the supraspinatus tendon on the posterior glenoid rim: an arthroscopic study. J Shoulder Elb Surg 1:238–245
36. Waldt S, Burkart A, Imhoff A, Bruegel M, Rummeny E, Woertler K (2005) Anterior shoulder instability: accuracy of MR arthrography in the classification of anteroinferior labroligamentous injuries. Radiology 237(2):578–583
37. Warner M, Chappell P, Stokes M (2012) Measuring scapular kinematics during arm lowering using the acromion marker cluster. Hum Mov Sci 31:386–396
38. Whiteside D, Elliott B, Lay B, Reid M (2014) The effect of racquet swing weight on serve kinematics in elite adolescent female tennis players. J Science Med Sport 17(1):124–128
39. Wong F, Keung J, Lau N, Ng D, Chung J, Chow D (2014) Effects of body mass index and full body kinematics on tennis serve speed. J Hum Kinet 40:21–28
40. Wu G, van der Helm F, Veegerc H, Makhsouse M, Royf PV, Angling C, Nagelsh J, Kardunai A, McQuadej K, Wangk X, Wernerl F, Buchholzm B (2005) ISB recommendation on definitions of joint coordinate systems of various joints for the reporting of human joint motion—part II: shoulder, elbow, wrist and hand. J Biomech 38:981–992

COMPUTER METHODS IN BIOMECHANICS AND BIOMEDICAL ENGINEERING, 2017
https://doi.org/10.1080/10255842.2017.1390568

Taylor & Francis
Taylor & Francis Group

Multi-body optimization with subject-specific knee models: performance at high knee flexion angles

Caecilia Charbonnier[a], Sylvain Chagué[a], Frank C. Kolo[b], Victoria B. Duthon[c] and Jacques Menetrey[d]

[a]Medical Research Department, Artanim Foundation, Meyrin, Switzerland; [b]Rive Droite Radiology Center, Geneva, Switzerland; [c]Faculty of Medicine, Centre de Médecine de l'appareil locomoteur et du sport, Orthopedics and Trauma Service, University Hospitals of Geneva, Geneva, Switzerland; [d]Centre de Médecine de l'appareil locomoteur et du sport, Orthopedics and Trauma Service, University Hospitals of Geneva, Geneva, Switzerland

ABSTRACT

When estimating knee kinematics from skin markers and stereophotogrammetry, multi-body optimization (MBO) has provided promising results for reducing soft tissue artefacts (STA), but can still be improved. The goal of this study was to assess the performance of MBO with subject-specific knee models at high knee flexion angles (up to 110°) against knee joint kinematics measured by magnetic resonance imaging. Eight subjects were recruited. MBO with subject-specific knee models was more effective in compensating STA compared to no kinematic and spherical constraints, in particular for joint displacements. Moreover, it seems to be more reliable over large ranges of knee flexion angle. The ranges of root mean square errors for knee rotations/displacements were 3.0°–9.2°/1.3–3.5 mm for subject-specific knee models, 6.8°–8.7°/6.0–12.4 mm without kinematic constraint and 7.1°–9.8°/4.9–12.5 mm for spherical constraints.

ARTICLE HISTORY
Received 25 September 2016
Accepted 6 October 2017

KEYWORDS
Soft tissue artefact; knee; multi-body optimization; joints and ligament constraints; subject-specific modeling; high knee flexion

Introduction

Stereophotogrammetry and the use of skin markers are a widely recognized technique to analyze human movement. The aim is to deduce the kinematics of the bone segments under investigation from the trajectories of the skin markers. However, such technique is subject to soft tissue artifacts (STA) due to muscle contractions and skin sliding, causing the markers to move with respect to the underlying bone (Leardini et al. 2005). In the lower extremity, the thigh is particularly affected. To solve this issue, several techniques were proposed. Some of them computed the optimal bone pose from a marker cluster by considering each segment separately (Söderkvist and Wedin 1993; Chèze et al. 1995), while other methods, such as multi-body optimization (MBO) (Lu and O'Connor 1999; Duprey et al. 2010; Bergamini et al. 2011; Clément et al. 2015; Gasparutto et al. 2015; Richard et al. 2016; Clément et al. 2017; Richard et al. forthcoming), aimed at optimally estimating the location of bone segments, modelled as a kinematic chain of rigid bodies connected by articulating joints, by minimizing the distances between the model-determined and the measured marker trajectories. A recent review on the use and applications of MBO is given in Leardini et al. (forthcoming).

The use of MBO for determining knee kinematics provided promising results (Duprey et al. 2010; Clément et al. 2015; Gasparutto et al. 2015; Richard et al. 2016), but validation of the method remains limited. In particular, MBO methods rely on the determination of a predefined kinematic model with specific joint constraints. Simple kinematic constraints (spherical or hinge joints) were introduced, but showed mixed results. Stagni et al. (2009), Andersen et al. (2010), Clément et al. (2017) and Richard et al. (forthcoming) obtained significant errors at the knee level evidencing limitations in reducing STA, especially its effect on joint translations. Opposite results were found in Gasparutto et al. (2015) and Richard et al. (2016) where spherical constraints performed better than models with no kinematic constraint, leading the authors to conclude that imposing joint constraints could be valuable. These studies suggested that more advanced models implementing anatomical constraints, together with accurate parameter identification, could improve results.

Anatomical constraints were thus proposed by taking into account the articular surfaces and the ligaments.

CONTACT Caecilia Charbonnier caecilia.charbonnier@artanim.ch

Duprey et al. (2010) and Clément et al. (2017) modeled the knee using parallel mechanisms with sphere-on-plane contacts (Feikes et al. 2003) and three isometric ligaments of constant length: anterior cruciate ligament (ACL), posterior cruciate ligament (PCL) and medial collateral ligament (MCL). This concept was further developed in Bergamini et al. (2011), Gasparutto et al. (2013, 2015) taking into account the four major ligaments (ACL, PCL, MCL and the lateral medial collateral ligament (LCL)) and different deformable conditions: minimal ligament length variations or prescribed ligament length variations as a function of knee flexion angle. The latter study concluded that anatomical constraints helped reduce STA compared to no kinematic constraint or degree-of-freedom (DoF) coupling curves (Walker et al. 1988). To account for ligament deformability, a 'soft' constraint (i.e. stiffness matrix) and a penalty-based method were also introduced in Richard et al. (2016). The authors suggested as in Gasparutto et al. (2015) that for a better definition of joint models, personalization should be considered for further improvements.

The importance of improving the accuracy of kinematic models to reduce the errors in calculated joint kinematics using personalization from medical imaging has been demonstrated previously (Scheys et al. 2011; Clément et al. 2015; Valente et al. 2015; Kainz et al. 2016; Sreenivasa et al. 2016). In particular, Clément et al. (2015) evaluated the performance of knee joint models with subject-specific kinematic constraints in healthy and osteoarthritis subjects during quasi-static squats. Different kinematic chains of four lower limb segments were compared using various combinations of joint models (a mix of no kinematic constraint, spherical joints and parallel mechanisms with customized minimal ligaments length variation). Results showed that personalization improved STA compensation, especially for the knee internal/external rotation, abduction/adduction, antero-posterior and proximal-distal displacements in both groups of tested subjects. This is to our knowledge the only work to date assessing personalized knee models in MBO for STA compensation. Therefore, further investigation is required to attest their validity.

Another aspect common to all previously cited studies is that the knee ranges of motion (ROM) of the activities considered in the *in vivo* experiments were limited to small flexion angles (usually between 40° and 65°). Indeed, these studies focused on typical clinical movements (e.g. gait, running, limited squat), but for many sport activities (e.g. dance, gymnastic, judo, hockey) higher ROM is usually performed. The performance of MBO at higher knee flexion angles should be hence verified and we expected that the more advanced models such as parallel mechanism would provide better results, since they are able to more realistically model the complex physiological kinematic behavior of the knee that comes into play at higher ROM (i.e. knee roll-back) (Duprey et al. 2010; Leardini et al. forthcoming).

The objective of this study was thus to assess against *in vivo* knee joint kinematics measured by Magnetic Resonance Imaging (MRI) the performance of MBO with subject-specific knee models. Here, we introduced more refined knee joint models to reproduce, at best, specific knee geometry: the standard sphere-on-plane contacts were replaced by surface-on-plane contacts, and the ligaments attachment sites were defined with reference to MRI. Moreover, the performance of MBO is evaluated at high knee flexion angles, up to 110°. For comparison, MBO methods with no kinematic and with spherical constraints were also studied.

Materials and methods

Subjects

The measurements were made on the right knee of eight healthy young active participants (five females, three males). The mean age, weight and height were 27.1 years, 61.3 kg and 166 cm, respectively. Because of the technical protocol, a height criterion was used. The subjects higher than 180 cm were excluded. Other exclusion criteria were reported previous knee injuries, knee surgery or contraindications for MRI. Institutional ethical approval and informed consent were obtained prior to data collection.

Experimental protocol

All volunteers were MRI scanned with a 1.5 T Optima MR450w GEM system (General Electric Healthcare, Milwaukee, WI, USA). A flexible surface coil was used and images were acquired at several unloaded knee flexions: 0°, 45°, 90° and 110°. At neutral knee flexion (0°), the subjects were placed in supine position. One 3D intermediate weighted fast spin echo without fat saturation (Cube®) sequence (section thickness 0.8 mm; no gaps; TR/TE ms 1500/27.9) centered on the knee and three 3D fast gradient echo (Lava®) sequences (section thickness 3 mm; no gaps; TR/TE ms 4.2/2.0) were achieved covering a region of interest from the pelvis to the ankle, as shown in Figure 1(A). For the other flexion angles, the subjects were lying on the right side to ensure sufficient room to center the knee joint in the magnetic bore. A hand-held goniometer was used to position the subject's lower limb at the desired knee flexion. For each position, one 3D intermediate weighted fast spin echo without fat saturation (Cube®) sequence and two 3D fast gradient echo (Lava®) sequences were acquired (Figure 1(B)). It is

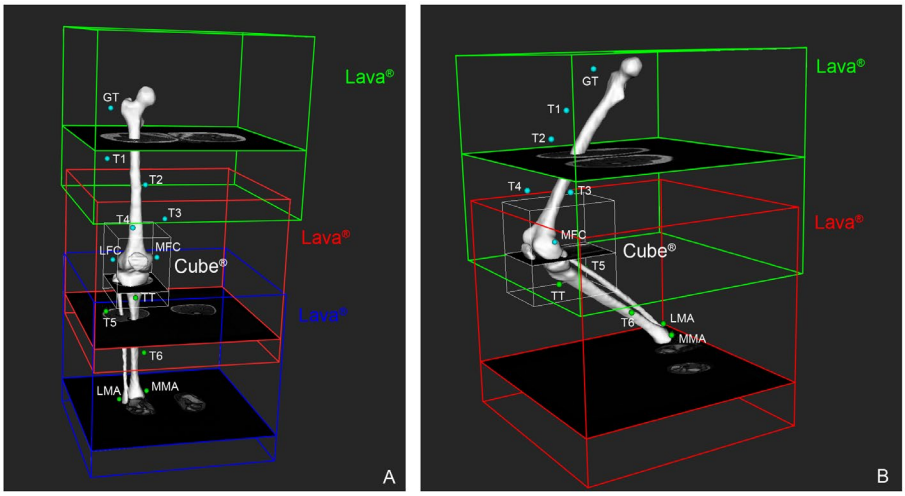

Figure 1. MRI volumes acquired (A) in neutral knee flexion (frontal view) and (B) at 90° knee flexion (lateral view).
Notes: Markers are also shown. GT = greater trochanter, LFC = lateral femoral epicondyle, MFC = medial femoral epicondyle, TT = tibial tuberosity, MMA = medial malleoli, LMA = lateral malleoli, T1–T6 = technical markers.

worth mentioning that changing orientation of the body in the MRI scanner resulted in soft tissues shape changes.

The subjects were equipped with external MRI-compatible markers set placed directly onto the skin using adhesive tape. We used spherical capsules (∅10 mm) of Burgenstein Vitamin E (Antistress AG, Switzerland) because of their highly visible MRI signal. The femur marker set included three markers placed on anatomical landmarks (greater trochanter, lateral and medial femoral epicondyles) and four markers distributed on the lateral and frontal parts of the thigh (see Figure 1). For the tibia, three markers were placed on anatomical landmarks (tibial tuberosity, medial and lateral malleoli), one on the lateral part and one on the medial part of the shank. Markers were placed as much as possible on skin areas susceptible to show less sensitivity to STA according to previous studies (Stagni et al. 2005; Akbarshahi et al. 2010; Kuo et al. 2011; Tsai et al. 2011). The same investigator (CC) attached all markers and performed all measurements.

Kinematic knee models

Bone geometry was obtained from 3D reconstruction based on the 3D images in neutral knee flexion. The MRI volumes were registered and manually segmented using Mimics software (Materialize NV, Leuven, Belgium). For each volunteer, subject-specific 3D models of the femur and tibia were thus obtained.

Parallel mechanism was modeled with four ligaments (ACL, PCL, MCL, LCL) and two surface-on-plane contacts, providing more accurate constraints than the standard sphere-on-plane contacts, since it takes into account the femur geometry and not an approximation. The surface-on-plane constraints forced the lateral and medial femoral condyles surfaces to maintain contact with the tibial plateaus, modeled as a 3D plane. The contact surfaces and the normal and point of planes were determined on the subject-specific knee bone models. To account for the articular cartilages, the tibial plateaus plane was then translated superiorly along its normal by the average thickness of the cartilages. We estimated this value to 4 mm (2 mm for the femoral and tibial cartilages, respectively) based on literature measuring cartilage thickness at the joint (Cohen et al. 1999; Shepherd and Seedhom 1999).

Table 1. Coefficients of the polynomial interpolation* used to fit ligament length variations (% of elongation compared to the length at neutral knee flexion) with respect to the knee flexion angle θ.

	ACL ($l = 1$)	PCL ($l = 2$)	MCL ($l = 3$)	LCL ($l = 4$)
α_0^l	0.9963	0.9996	0.9974	1.0037
α_1^l	0.0012	−0.0045	−0.0004	−0.0003
α_2^l	1.58e−05	−2.54e−05	−1.23e−05	−1.09e−05
LOO-XVE	0.052	0.060	0.042	0.046

Note: The last column provides the leave-one-out cross validation error (LOO-XVE) for each ligament evaluating how well the polynomial interpolation would generalize to an independent data-set. *$d^l(\theta) = a_0^l + a_1^l\theta + a_2^l\theta^2$;

The origins and insertions of the four ligaments were defined for each subject by first identifying on the high-resolution 3D Cube® images the attachment surface and then taking its barycenter. Ligament length variations measured in all subjects during the experiment were fitted with polynomial functions of the knee flexion angle θ. Table 1 provides for each ligament the computed coefficients of the polynomial interpolation. A leave-one-out analysis was performed for each ligament to evaluate how well the polynomial interpolation would generalize to an independent data-set. The computed leave-one-out cross validation errors are given in Table 1, showing that the

ligament length variation models were not overfitting the data.

Multi-body optimization and constraints

The aim of MBO is to minimize the sum of square distances between model-determined and measured skin marker positions by optionally taking into account a certain number of kinematic constraints (Lu and O'Connor 1999; Duprey et al. 2010; Gasparutto et al. 2015; Richard et al. 2016; Clément et al. 2017; Richard et al. forthcoming). In this study, MBO was applied to two segments – the femur and the tibia. Three different kinematic models were considered: First, no kinematic constraint (*N*) was imposed to the knee joint (full 6 DoF), equivalent to a least square segment pose estimation, such as the singular value decomposition (SVD) (Söderkvist and Wedin 1993). Second, a spherical joint constraint (*S*) (Lu and O'Connor 1999) was introduced limiting movement to rotation only (3 DoF). The center of rotation was taken as the midpoint between the lateral and medial femoral epicondyles. Third, parallel mechanism constraints (*P*) were applied considering the two surface-on-plane contacts and the four ligament length variations, implemented as a penalty-based method (Gasparutto et al. 2013; Charbonnier et al. 2014) as follows:

$$\min \sum_{s=1}^{2} \left(\sum_{i=1}^{n_s} \alpha_{si} ||T_s x_{si} - y_{si}||^2 \right) + \beta \sum_{e=1}^{2} D_e^2 + \sum_{l=1}^{4} \gamma_l \left(L_l - Lref_l\right)^2 \quad (1)$$

The optimal pose T_s (i.e. 3 rotational components (r_x, r_y, r_z) and 3 translational components (t_x, t_y, t_z)) for each segment *s* corresponds to the minimization of three terms:

- the square distances between the model-based (x_{si}) and the measured (y_{si}) marker coordinates in the segment's cluster (n_s markers in segment's cluster *s*) with a weighting factor α_{si} to reflect different degrees of STA, as described by Lu and O'Connor (1999);
- the square distance D_e^2 between the lateral ($e = 1$) or medial ($e = 2$) condyle surface and the tibial plateaus plane translated superiorly along its normal by 4 mm for the given pose with a weighting factor β, where D_e is the minimum of the distances between each point of the condyle and the tibial plateaus plane (note that under the modelling assumption that cartilage thickness is constant over the whole articular surfaces and between subjects, this term tends to zero);
- the square difference between the computed ligament length L_l for the ligament l and the reference ligament length $Lref_l$ obtained by multiplying the rest length (measured at neutral knee flexion) with the estimated variation calculated for the given pose with the polynomial interpolation (see Table 1) and weighted by γ_l to reflect different ligament contributions. Given the large ROM studied, prescribed ligament length variations were preferred over minimized ligament length variations around the average length.

The model-based (x_{si}) marker coordinates were established in neutral knee flexion. For all kinematic models and for simplicity, equal weighting factors ($\alpha_{si} = \frac{1}{n_s}$) were assigned to the markers of the femur and tibia. No different weighting factor was applied between the surface-on-plane constraints ($\beta = \frac{1}{2}$), nor between the ligaments ($\gamma_l = \frac{1}{4}$). Overall, the distribution of weights between the three terms of Equation (1), which are all homogeneous to a squared distance, was chosen so that each term was of the same order of magnitude. The initial guess used in MBO was computed from the skin markers using SVD. Equation (1) was solved by a non-linear BFGS optimization (Byrd et al. 1995).

Validation procedure

In order to assess the performance of the three models used in MBO to compensate for STA at several knee flexions, model-based knee kinematics derived from the skin markers was compared to the knee kinematics derived from the MRI scans. The MR series were processed, the bones segmented and the reference bone positions and orientations were calculated by registering the subject-specific knee bone models to each MRI pose using the iterative closest point algorithm (Besl and McKay 1992). Skin markers visible on the MR images were manually labelled and the centers of gravity of each marker were determined.

After MBO, descriptive statistics and in particular the root mean square errors (RMSEs) between the model-based and the reference kinematics were computed for each method at each flexion angle and for the overall ROM (i.e. cumulated data for the three flexion angles). Knee joint angles and displacements were calculated with the femur and tibia segment coordinate systems defined following the recommendations of the ISB (Wu et al. 2002) using anatomical landmarks identified on the subject-specific knee bone models by virtual palpation. The center of the femoral head was calculated using a sphere fitting method (Schneider and Eberly 2003).

Results

RMSEs between the model-based knee kinematics computed by the three MBO methods and the reference kinematics at 45°, 90° and 110° of knee flexion and for the entire ROM are shown in Figure 2. Figure 3 presents box-and-whisker plots of the kinematic errors. Information about the actual ROM at the different knee flexion angles is also reported in Table 2.

Overall, the lowest RMSEs in all anatomical planes were obtained with the parallel mechanism constraints. Compared to constraints *N* and *S*, the model *P* was particularly good in minimizing displacements errors (between 1.3 and 3.5 mm vs. 6.0 and 12.4 mm and 4.9 and 12.5 mm for *N* and *S*, respectively). RMSEs for flexion/extension and abduction/adduction obtained with model *P* were also smaller (5.8° and 3.0°, respectively), but were comparable for internal/external rotation compared to the other models (9.2°). For constraints *N* and *S*, the RMSEs among the joint angles showed comparable results (difference of 1°), while the model *S* was more accurate than the model *N* for lateral-medial and proximal-distal displacements, but less accurate for the anterior-posterior shift.

In terms of inter-subject variability, model *P* demonstrated globally the best median and inter-quartile of errors (Figure 3), in particular for abduction/adduction and proximal-distal displacements. For all flexion angles, constraints *N* and *S* exhibited comparable variability across subjects, but model *S* depicted smaller inter-quartile ranges than model *N* for displacement errors.

RMSEs for flexion/extension increased for constraints *N* and *S* with higher knee flexion angles, whereas RMSEs were in the similar range over all flexion angles for model *P*. For the other anatomical planes, as well as for displacements, parallel mechanism constraints seem to have more stable errors across the whole ROM. Interestingly, RMSEs for internal/external rotation were high for the three methods.

Discussion

In this study, we compared three MBO methods with different joint constraints against *in vivo* knee joint kinematics measured by MRI at high knee flexion angles. Moreover, we introduced anatomical constraints based on subject-specific knee joint models, taking into account

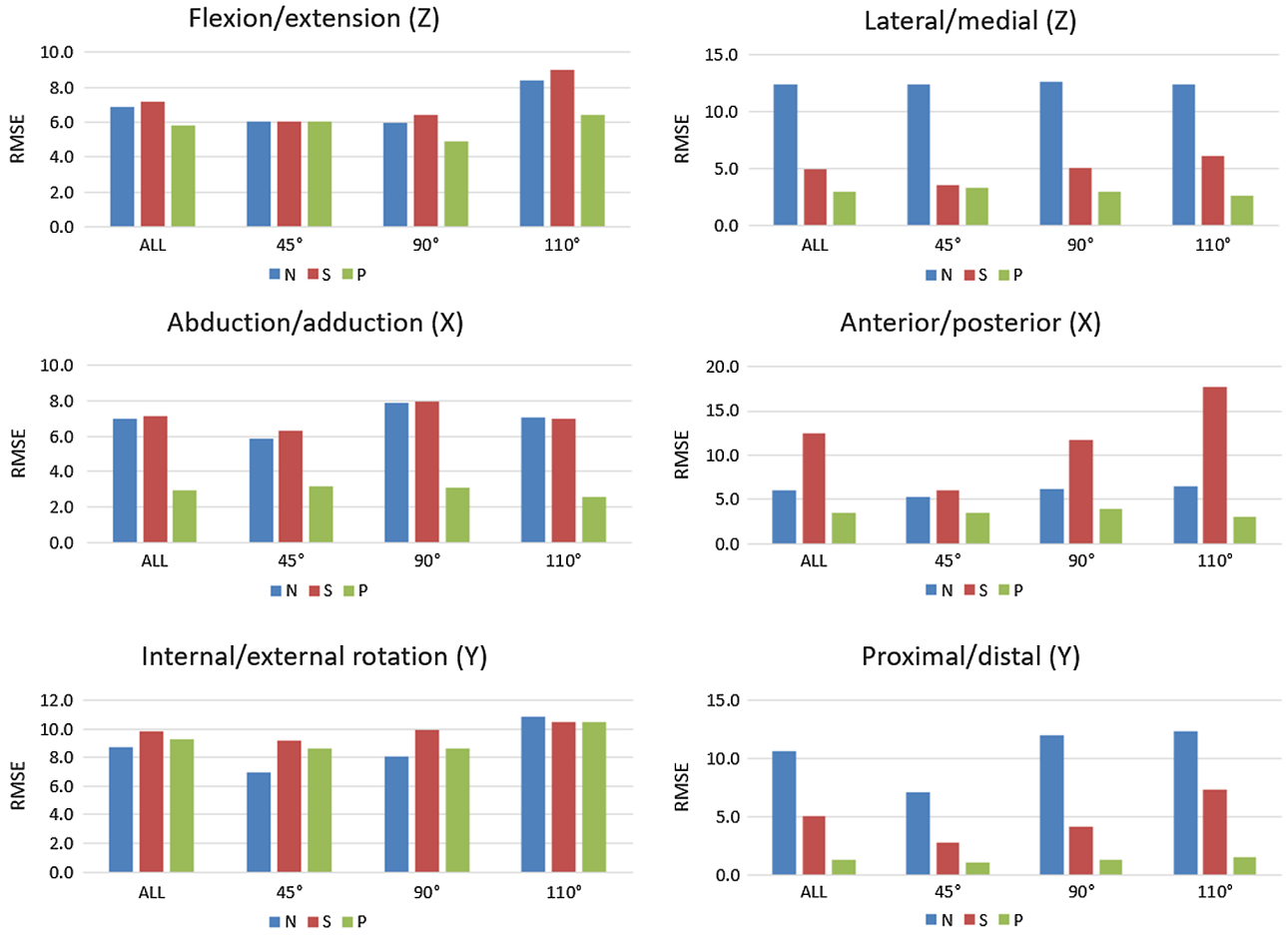

Figure 2. RMSEs for the three MBO methods at various knee flexion angles (45°, 90° and 110°) and for the overall ROM.

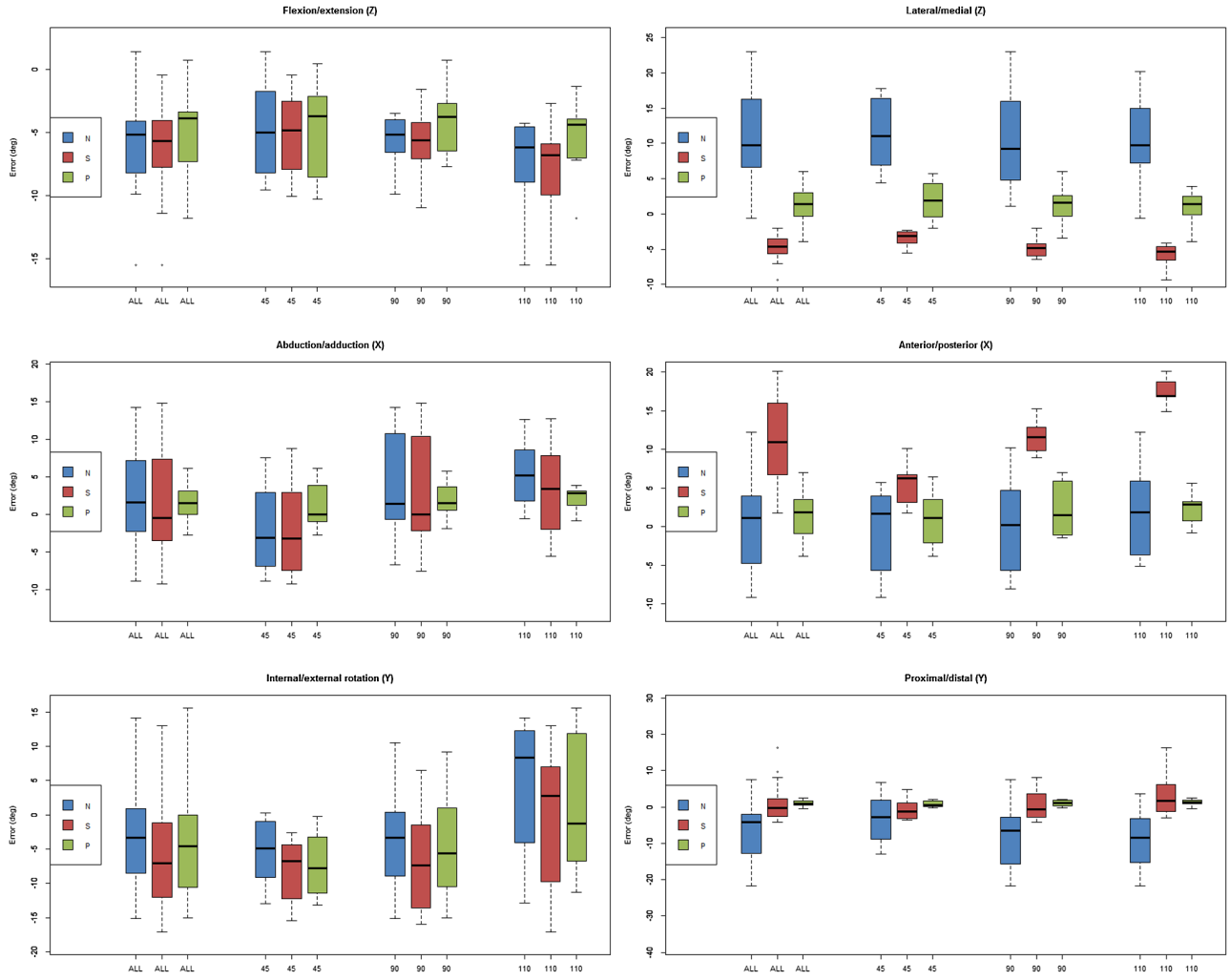

Figure 3. Box-and-whisker plots of the kinematic errors for the three MBO methods at various knee flexion angles (45°, 90° and 110°) and for the overall ROM.

Table 2. Mean ± standard deviation of the actual ROM at 45°, 90° and 110° of knee flexion.

Flexion angle	AA (°)	IE (°)	LM (mm)	AP (mm)	PD (mm)
45°	7.8 ± 4.0	1.0 ± 7.8	−3.1 ± 1.3	6.4 ± 3.6	0.0 ± 3.5
90°	6.4 ± 4.4	7.2 ± 6.2	−4.6 ± 1.4	12.1 ± 2.6	1.7 ± 5.4
110°	4.9 ± 3.2	9.1 ± 6.2	−6.0 ± 1.8	17.4 ± 1.7	3.6 ± 6.5

Notes: Abduction (−)/adduction (+), AA; internal (+)/external (−) rotation, IE; lateral (+)/medial (−) displacement, LM; anterior (+)/posterior (−) displacement, AP; and proximal (+)/distal (−) displacement, PD.

personalized ligaments attachment sites and knee bone geometry. This is the first *in vivo* study evaluating the performance of MBO methods at high knee flexion angles, up to 110°.

Defining a kinematic model to be used in MBO in order to derive accurate knee joint kinematics based on skin markers is critical. The use of no kinematic constraint or spherical constraints was thoroughly analyzed (Stagni et al. 2009; Andersen et al. 2010; Gasparutto et al. 2015; Richard et al. 2016; Clément et al. 2017; Richard et al. forthcoming) showing mixed results but most often inaccurate model-based kinematics. For instance, Stagni et al. (2009) reported mean RMSEs between 8° and 13° for knee rotations and between 5 and 20 mm for knee displacements during squatting. In the same activity, Clément et al. (2017) recorded mean RMSEs around 3–8° for knee rotations but less errors for knee displacements (2–3 mm). Our results for the spherical model were similar showing large RMSEs for all anatomical planes and in particular for joint displacements. According to our findings, the use of parallel mechanisms with subject-specific knee models gave lower error ranges, except for internal/external rotation. Indeed, RMSEs for internal/external rotation were not improved but comparable with the methods with no kinematic or with spherical constraints and were also high. Whereas the two latter models impose no limitation in rotational movement, parallel mechanisms attempt to reproduce the biomechanical behavior of the knee

ligaments that play a role in stabilizing the joint and thus limiting excessive ROM, which did not improve results for internal/external rotation in the present study. One explanation could be that the subjects were lying on the side during the MRI acquisitions. Abnormal STA were likely to be induced by soft tissue compression of the leg in contact with the MRI table, as well as by the change of gravity compared to the MRI acquisitions in supine position for the neutral knee flexion.

For quasi-static squats studied at five knee positions (0°, 30°, 40°, 50° and 60°), Clément et al. (2015) compared model-based kinematics measured using the KneeKG™ – a motion capture device designed to limit STA (Lustig et al. 2012) – with the kinematics measured by biplanar radiographic imaging system (EOS®) on 10 subjects. Using subject-specific kinematic constraints, they reported RMSEs of 2.2 ± 1.2° and 5.2 ± 3.8° for abduction/adduction and internal/external rotation, respectively, and 4.3 ± 2.4 mm, 3.2 ± 2.1 mm and 2.4 ± 1.1 mm for medial/lateral, anterior/posterior and proximal/distal displacements, respectively. The use of the subject-specific kinematic constraints in the present study gave better accuracy for joint displacements, but greater errors for joint angles. These greater errors could be explained by the fact that the KneeKG™ device tackled STA more effectively than the marker set used in the present study. Moreover, we investigated larger ROM up to 110°, thus more important STA could be expected. Finally, Clément et al. (2015) used a complete lower limb model (4 segments and 3 joints, from the hip to the foot) in MBO, resulting in better optimization performances as previously reported (Duprey et al. 2010).

Another foreseen finding of the present study is that the parallel mechanism constraints seem to have more stable errors across the whole ROM and less inter-subject variability. Compared to simple kinematic constraints, errors did not increase with knee flexion angle, and the results of model *P* demonstrated the best median and inter-quartile of errors. Indeed, these mechanisms seemed to model appropriate physiological knee patterns (i.e. femoral roll-back, limited abduction/adduction), as previously evidenced (Duprey et al. 2010; Leardini et al. forthcoming). Furthermore, they have the unique advantage of being customizable with subject-specific knee joint geometry, hence offering the possibility to adapt the model to pathologies and to conduct clinical studies. STA being known to be subject-specific (Leardini et al. 2005), adding more personalized anatomical constraints is also expected to reduce more effectively the inter-subject variability of the model-derived kinematics.

We acknowledge some limitations in the present study. First, we assessed the performance of MBO methods in reducing STA errors against *in vivo* knee joint kinematics measured by MRI during static and non-weight-bearing knee poses, which does not represent dynamic activities for which STA would be different (due to inertia effects, muscle contractions, etc.). In the literature, two types of technique are generally used as gold standard to evaluate methods for STA compensation. The first type uses strongly invasive metallic rods inserted directly into the bone and instrumented with cluster of markers to derive true bone movements, such as intra-cortical pins (Benoit et al. 2006; Gasparutto et al. 2015; Richard et al. forthcoming). The second type uses fluoroscopic acquisitions (Stagni et al. 2005; Lin et al. 2016; Richard et al. 2016; Richard et al. forthcoming) which has two main drawbacks: firstly, the 3D movement is estimated from biplanar radiographs and secondly the method uses ionizing radiation. Conversely, MRI acquisitions are not invasive and provides full 3D images of the joint with visualization of the soft tissues, but the volumes of the knee need to be acquired in static positions. Therefore, we consider this technique more suitable for a study involving healthy volunteers. Another limitation was that the parallel mechanisms used in MBO to compute model-based knee kinematics of the subjects were based on polynomial functions built from the validation data obtained from the same subjects, which represents a source of bias. Eventually, instead of using a constant cartilage thickness in the sphere-on-plane constraints, cartilages could have been segmented on MRI to obtain subject-specific and accurate thickness estimation of these structures, but this would have required an invasive arthro-MRI (with injection of contrast agent) to allow for a reliable segmentation of the soft tissues.

Conclusion

The results of this study seem to confirm the findings of Clément et al. (2015) and indicate that MBO combined with subject-specific knee models can improve knee kinematics estimation based on skin markers, in particular for the determination of joint displacements. In addition, this method seems to be more reliable over large ranges of knee flexion angle, since it models more precisely the physiological behavior of the knee joint. Although this method should be further validated with large ROM during dynamic movements, it provides promising results for the study of pathologies or injuries related to sport activities requiring high knee flexion.

Disclosure statement

No potential conflict of interest was reported by the authors.

References

Akbarshahi M, Schache A, Fernandez J, Baker R, Banks S, Pandy M. 2010. Non-invasive assessment of soft-tissue artifact and its effect on knee joint kinematics during functional activity. J Biomech. 43:1292–1301.

Andersen M, Benoit D, Damsgaard M, Ramsey D, Rasmussen J. 2010. Do kinematic models reduce the effects of soft tissue artefacts in skin marker-based motion analysis? An *in vivo* study of knee kinematics. J Biomech. 43:268–273.

Benoit DL, Ramsey DK, Lamontagne M, Xu L, Wretenberg P, Renström P. 2006. Effect of skin movement artifact on knee kinematics during gait and cutting motions measured *in vivo*. Gait Posture. 24(2):152–164.

Bergamini E, Pillet H, Hausselle J, Thoreux P, Guerard S, Camomilla V, Cappozzo A, Skalli W. 2011. Tibio-femoral joint constraints for bone pose estimation during movement using multi-body optimization. Gait Posture. 33(4):706–711.

Besl P, McKay N. 1992. A method for registration of 3-D shapes. IEEE Trans Pattern Anal Mach Intell. 14(2):239–256.

Byrd R, Lu P, Nocedal J, Zhu C. 1995. A limited memory algorithm for bound constrained optimization. SIAM J Sci Comput. 16(5):1190–1208.

Charbonnier C, Chagué S, Kolo F, Chow, J, Lädermann A. 2014. A patient-specific measurement technique to model the kinematics of the glenohumeral joint. Orthop Traumatol Surg Res. 100:715–719.

Chèze L, Fregly B, Dimnet J. 1995. A solidification procedure to facilitate kinematic analyses based on video system data. J Biomech. 28:879–884.

Clément J, Dumas R, Hagemeister N, De Guise JA. 2015. Soft tissue artifact compensation in knee kinematics by multi-body optimization: Performance of subject-specific knee joint models. J Biomech. 48:3796–3802.

Clément J, Dumas R, Hagemeister N, de Guise J. 2017. Can generic knee joint models improve the measurement of osteoarthritic knee kinematics during squatting activity? Comput Methods Biomech Biomed Eng. 20(1):94–103.

Cohen Z, McCarthy D, Kwak S, Legrand P, Fogarasi F, Ciaccio E, Ateshian G. 1999. Knee cartilage topography, thickness, and contact areas from MRI: *in vitro* calibration and *in vivo* measurements. Osteoarthritis and Cartilage. 7(1):95–109.

Duprey S, Cheze L, Dumas R. 2010. Influence of joint constraints on lower limb kinematics estimation from skin markers using global optimization. J Biomech. 43(14):2858–2862.

Feikes J, O'Connor J, Zavatsky A. 2003. A constraint-based approach to modelling the mobility of the human knee joint. J Biomech. 36(1):125–129.

Gasparutto X, Dumas R, Jacquelin E. 2013. Multi-body optimisation with deformable ligament constraints: influence of ligament geometry. Comput Methods Biomech Biomed Eng. 15:191–193.

Gasparutto X, Sancisi N, Jacquelin E, Parenti-Castelli V, Dumas R. 2015. Validation of a multi-body optimization with knee kinematic models including ligament constraints. J Biomech. 48:1141–1146.

Kainz H, Modenese L, Lloyd D, Maine S, Walsh H, Carty C. 2016. Joint kinematic calculation based on clinical direct kinematic versus inverse kinematic gait models. J Biomech. 49(9):1658–1669.

Kuo M-Y, Tsai T-Y, Lin C-C, Lu T-W, Hsu H-C, Shen W-C. 2011. Influence of soft tissue artifacts on the calculated kinematics and kinetics of total knee replacements during sit-to-stand. Gait Posture. 33(3):379–384.

Leardini A, Chiari L, Croce UD, Cappozzo A. 2005. Human movement analysis using stereophotogrammetry Part 3: soft tissue artifact assessment and compensation. Gait Posture. 21:212–225.

Leardini A, Belvedere C, Nardini F, Sancisi N, Conconi M, Parenti-Castelli V. Forthcoming. Kinematic models of lower limb joints for musculo-skeletal modelling and optimization in gait analysis. J Biomech. 62:77–86.

Lin C-C, Lu T-W, Lu H-L, Kuo M-Y, Hsu H-C. 2016. Effects of soft tissue artifacts on differentiating kinematic differences between natural and replaced knee joints during functional activity. Gait Posture. 46:154–160.

Lu T, O'Connor J. 1999. Bone position estimation from skin marker co-ordinates using global optimisation with joint constraints. J Biomech. 32:129–134.

Lustig S, Magnussen RA, Cheze L, Neyret P. 2012. The KneeKG system: a review of the literature. Knee Surg Sports Traumatol Arthroscopy. 20(4):633–638.

Richard V, Lamberto G, Lu T, Cappozzo A, Dumas R. 2016. Knee kinematics estimation using multi-body optimisation embedding a knee joint stiffness matrix: a feasibility study. PLoS ONE. 11(6):e0157010.

Richard V, Cappozzo A, Dumas R. Forthcoming.Comparative assessment of knee joint models used in multi-body kinematics optimisation for soft tissue artefact compensation. J Biomech. 62:95–101.

Scheys L, Desloovere K, Spaepen A, Suetens P, Jonkers I. 2011. Calculating gait kinematics using MR-based kinematic models. Gait Posture. 33(2):158–164.

Schneider P, Eberly D. 2003. Geometric tools for computer graphics. The Morgan Kaufmann Series in computer graphics and geometric modeling. San Francisco: Morgan Kaufmann.

Shepherd D, Seedhom B. 1999. Thickness of human articular cartilage in joints of the lower limb. Ann Rheum Dis. 58(1):27–34.

Söderkvist I, Wedin P. 1993. Determining the movements of the skeleton using well-configured markers. J Biomech. 26:1473–1477.

Sreenivasa M, Chamorro C, Gonzalez-Alvarado D, Rettig O, Wolf S. 2016. Patient-specific bone geometry and segment inertia from MRI images for model-based analysis of pathological gait. J Biomech. 49(9):1918–1925.

Stagni R, Fantozzi S, Cappello A, Leardini A. 2005. Quantification of soft tissue artefact in motion analysis by combining 3D fluoroscopy and stereophotogrammetry: a study on two subjects. Clin Biomech. 20:320–329.

Stagni R, Fantozzi S, Cappello A. 2009. Double calibration vs. global optimisation: performance and effectiveness for clinical application. Gait Posture. 29(1):119–122.

Tsai T-Y, Lu T-W, Kuo M-Y, Lin C-C. 2011. Effects of soft tissue artifacts on the calculated kinematics and kinetics of the knee during stair-ascent. J Biomech. 44(6):1182–1188.

Valente G, Pitto L, Stagni R, Taddei F. 2015. Effect of lower-limb joint models on subject-specific musculoskeletal

models and simulations of daily motor activities. J Biomech. 48(16):4198–4205.

Walker P, Rovick J, Robertson D. 1988. The effects of knee brace hinge design and placement on joint mechanics. J Biomech. 21(11):965–974.

Wu G, Siegler S, Allard P, Kirtley C, Leardini A, Rosenbaum D, Whittle M, D'Lima D, Cristofolini L, Witte H, et al. 2002. ISB recommendation on definitions of joint coordinate system of various joints for the reporting of human joint motion – part I: ankle, hip, and spine. J Biomech. 35(4):543–548.

Chapter 3

Conclusion

[7]Leonardo da Vinci, c. 1490. Male head in profile with proportions, Gallerie dell'Accademia, Venice.

3.1 Contributions

Our main research focus has been over the last six years the biomechanical modeling of human joints (hip, knee and shoulder complex) using motion tracking and simulation techniques to explore the mechanisms of motion-related disorders, such as femoroacetabular impingement in the prosthetic hip, knee ligaments biomechanics, glenohumeral instability and impingement or rotator cuff hyperelongation. Research has also been devoted to the improvement of the surgical planning, developing software solutions to better evaluate the impact of hip and shoulder implants design on the mobility of the joint and to better plan the surgical resection procedure in acromioplasty surgeries.

The originality of our research lies in the ability to fuse patient-specific 3D anatomical models and computer-assisted techniques to track and simulate moving joint structures. Our research has involved expertise in real time medical imaging, clinical image processing, segmentation and 3D reconstruction of hard and soft tissues (bones, cartilages, ligaments and muscles), soft tissue deformation, computer-assisted medical software and motion tracking based on different modalities: stereophotogrammetry and 3D-2D model to image registration (MRI, fluoroscopy).

Unlike most of the biomechanics research labs or gait labs, we do not make use of any generic human model scaled to the patient's anthropometric measurements (e.g., OpenSim[8]) to infer clinical outcomes. Contrariwise, we aim at modeling accurate patient-specific models from both an anatomical and kinematic point of view. Starting from patient's medical images, 3D joint models are generated using conventional segmentation and reconstruction software. Patient's movements are captured in a subsequent step and applied to the reconstructed joint. Here, we have devoted significant research to the improvement of accuracy and robustness in bone pose estimation when skin markers-based motion capture is considered, including the elaboration of optimized markers protocol, calibration techniques and STA minimization algorithms. As a result, the joint can be visualized in motion and in real time, allowing functional evaluation of soft tissues (e.g., tendons, muscles, cartilages), measurements or planning of surgical treatment in 3D.

Over the years, we have developed simulation software that have proven to be effective in the analysis of functional disorders in the native and prosthetic joints, and especially in the particular context of sports medicine and rehabilitation. Our objective is to further develop this research and extend the work to other pathologies or joints. The results of this research have been published in more than 70 peer-reviewed articles in journals and international conferences, and been awarded 4 international prizes and awards in the field of computer-assisted diagnosis and surgery.

3.2 Limitations

Despite the advances attributable to the presented research, we acknowledge some limitations that would be worth devoting particular attention in future research. Here is a review of the limitations of our work and potential new directions per topic.

[8]OpenSim, `http://opensim.stanford.edu/`, accessed March 2017

3.2.1 Complexity of the methodology

Most of the studies presented in the previous chapter included a small number of tested volunteers or patients due to the complexity of the analysis. Indeed, our methodology requires the subjects to undergo different acquisitions: MRI/CT scan for diagnosis and 3D reconstruction, motion capture for kinematic estimation and if required additional acquisitions for validation purposes (e.g., dynamic imaging). Except from the pre-operative or pre-treatment scans, these extra analyses are nowadays not covered by the health insurance. Moreover, the post-processing of the medical images and kinematic data, as well as the execution of the computer simulations and motion analysis, are time consuming and thus involve additional costs (i.e., the salaries of the engineers) with respect to standard patient care. All these costs must be for now covered by research funds. This prevents us from testing more subjects and thus deriving more valuable clinical outcomes. This also prevents us from implementing this methodology at a larger scale or as a standard of care.

One solution to reduce the complexity of the analysis would be to develop automatic software tools that allow to perform the maximum number of tasks without operator control. Typical tasks that could be automated include, for instance, the creation of generic anatomical models from medical images adapted to the patient's anatomy which would automate the computation of morphological descriptors or biomechanical parameters (e.g., joint center, AFs). In addition, to suppress the cost of the kinematic acquisition, the patient's joint could be at least simulated with a generic database of realistic movements (e.g., daily activities and not idealized motions only).

We recently took one step forward into this direction by developing the "Arthroplanner" computer-assisted planning solution for acromioplasty surgery [CCP+18, LCP+18] that allows to perform standard morphological bony measurements, as well as 3D simulations of the patient's joint using a database of everyday activities. The software perform the planning procedure based on successive automatic steps where the results at each step are just validated by the engineer before continuing to the next. The time required to execute the planning is drastically reduced ($\approx$ 40 minutes for one planning including 3D reconstruction), which renders the process cost-effective.

With such developments, our objective is to provide health care practitioners with new diagnostic and treatment planning tools which do not remain at the research state, but are effectively implemented in the clinical setting and used for the direct benefit of patients. We will hence dedicate further R&D in this direction and develop partnerships with industrial partners for the commercialization and distribution of such software.

3.2.2 Kinematic estimation

There are potential limitations to the accuracy of the kinematics computation from motion capture data. Indeed, we have translational errors of up to 3.7 mm and rotational errors of up to 6°, which is comparable to previously reported kinematic studies based on stereophotogrammetry. Here, a trade-off must be found: since the measurements are external (i.e., no direct access to the joint), motion capture is generally subject to greater errors than other techniques (e.g., dynamic MRI, fluoroscopy). However, this modality is not harmful and allows the recording of large ranges of motion, as well as multiple joints at the same time. This is also for now the unique solution to assess joint motion during sport activities. Possible improvements

could be the following:

- A possible extension could be investigated regarding our bone pose algorithms by introducing physically-based constraints that model more realistically the joint mechanics. The idea would be to model the soft tissues structures (ligaments, cartilages) and their mechanical properties, as well as to integrate forces (loads) and velocities to find the joint equilibrium for each instant frame. Our method would no longer be mathematically-based, but driven by a more advanced mechanical simulation able to model the dynamic behavior of the articulation. However, loads should be available, which can be difficult to measure according to the motor task (e.g., shoulder movements).
- The progress in 4D medical imaging could offer new opportunities to image in real time the joint in motion and in 3D. If we can produce three-dimensional images of the joint structures with sufficient quality without compromising acquisition speed, the use of motion capture becomes superfluous. Research is thus needed to exceed the limits of the current means of acquisition and to achieve this objective. However, we are still very far to be able to acquire sport movements in a scanner.

3.2.3 Nature of the simulation

Our proposed simulation techniques (contact and conflict analysis, elongation analysis) are non-physical and irrespective of many loads. As already explained in Section 1.5.1, physically-based simulations (e.g., finite element models, mass-spring models) could be more advanced and realistic methods accounting for the dynamics and physical properties of the joint tissues. However, to our knowledge, no physical model allowing simulation of the chondrolabral structures compression and ligaments/muscles elongation during complex motion exists. Indeed, current physically-based methods are difficult to set up and are limited to simple ROM simulation where loads can be estimated. Moreover, they require accurate tissue segmentation on medical images, which remains a complicated task with respect to muscles and ligaments. Contrariwise, although our simulation techniques are non-physical approaches, they are generalizable to different joints and allow real time simulation of osteoarticular structures during complex motion. Nevertheless, future work should investigate and push the boundaries of physically-based simulation to achieve the desired results.

3.3 Perspectives

Patient care starts with an accurate diagnosis of the disease, followed by treatment planning, actual treatment of the disease and finally rehabilitation to recover an acceptable health state. Over the past six years, our research has been mainly focused on two aspects of this process: the diagnosis by improving understanding of human joint structures and the surgical planning for the treatment of musculoskeletal disorders. Some work has also been devoted to the evaluation of the rehabilitation program. We believe that we can bring more in the future, notably in three specific areas (surgery, education/training and rehabilitation), thanks to our expertise in augmented reality (AR) and virtual reality (VR).

Recent advances in VR and AR headsets allow, respectively, users to either be immersed in computer-generated simulation or environment where they have the feeling to experience the virtual reality first-hand or to have access to digitally-created enhancements overlaid on the existing reality to make it more meaningful. VR/AR technologies are earning a lot of media attention and are considered as a new technological revolution,

as Internet and mobile were in the past. In medicine, these disruptive technologies can offer added value over traditional education, assessment and interventional approaches.

Artanim's group has specialized in the development of VR/AR applications with a focus on real time interaction and using cutting edge motion capture. The lab has gained over the years a strong knowledge in this field and is recognized both at the national[9] and international levels, in particular for its work on immersive and collaborative VR. By combining Artanim's expertise in motion capture, 3D anatomical modelling and VR/AR technologies, new solutions can be proposed to improve medical treatment. More specifically, we are already developing research projects that aim at creating VR applications to improve the rehabilitation program using gamification scenarios, as well as an innovative system based on AR technology for use in surgery and sports medicine to visualize and analyze patient's anatomy in real time and in motion. These perspectives are developed in the next sections.

3.3.1 Perspectives offered by virtual reality

VR technology can be used effectively to improve performance and participation for patients receiving rehabilitation programs. For instance, combining motion capture with interactive audiovisual feedback can support rehabilitation training with rewarding mechanisms (gamification) and reliable monitoring of patient's progress. In this perspective, VR rehabilitation platforms can be developed integrating customized VR software with low-cost commercially available devices such as HTC Vive[10] (Figure 3.1) to offer rehabilitation training approaches for hospital, clinic and home.

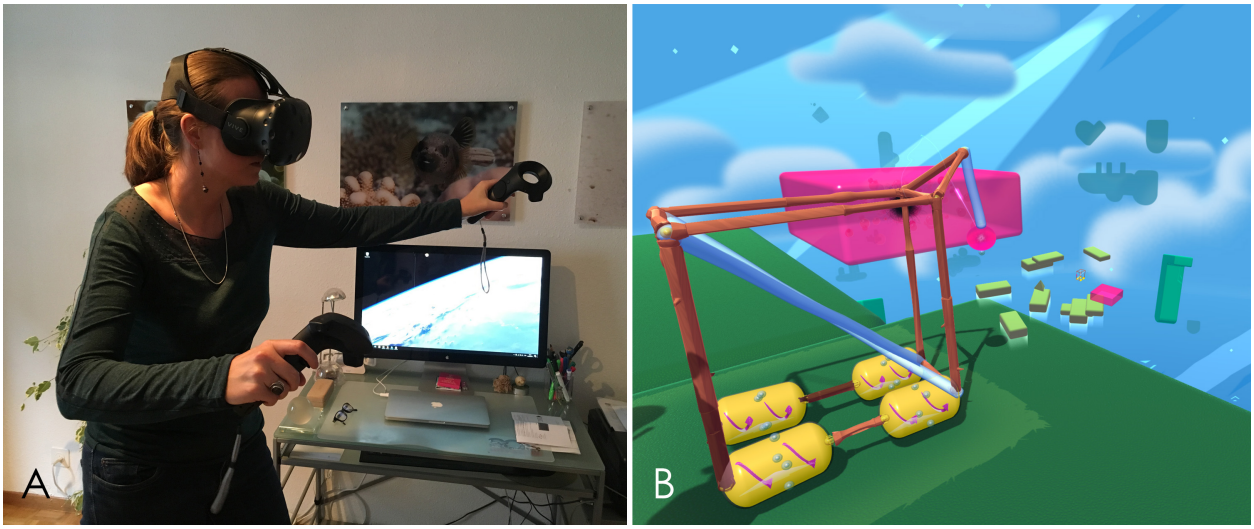

Figure 3.1: A) User equipped with HTC Vive showing the headset and the hand controllers. B) Example of a VR game that could be adapted for upper arm rehabilitation training: the game is a puzzle in which players construct machines from building materials to meet challenges. Image courtesy of Fantastic Contraption.

HTC Vive provides a VR headset to be immersed in the virtual world, two wireless hand controllers to interact with virtual objects and two optical cameras that track the position and orientation in space of

[9] Artanim is for instance at the initiative of the National Thematic Network on immersive technologies *Virtual Switzerland* funded by the Commission for Technology and Innovation, period 2017-2020, `http://virtualswitzerland.org/`, accessed March 2017

[10] HTC Vive, `https://www.vive.com/eu/`, accessed March 2017

the head and controllers. The system allows to walk around freely in a 3 x 3 meters play area. The setup is thus ideal for the creation of dedicated rehabilitation games which guide patients in their training program by using gamified goal-oriented tasks. The idea here is to transport the patient into a fun environment while re-educating him/her. Moreover, it is possible to monitor the patient's progress over the different training sessions by adding extra Vive trackers on the limb segments or by combining the HTC Vive with other motion capture devices (e.g., inertial sensors, Microsoft Kinect[11]) to capture comprehensive patient's movements. Using this technology, we plan in the next future to develop such rehabilitation programs in close collaboration with physiotherapists, sports medicine physicians and orthopedists.

VR technology has the potential to offer many more opportunities in different medical sectors, such as in neuroscience to understand specific brain mechanisms where VR can be used as an effective tool to fool the brain, in social phobias treatment to confront patients to their fear while being in secure conditions or for medical education to train surgeons at complex procedures or medical students at the complex anatomy of the human body.

3.3.2 Perspectives offered by augmented reality

In neurosurgery or orthopedic surgery, we are already planning surgical interventions in 3D using navigation tools. Surgical navigation systems have proven to be beneficial and cost-effective by offering real time feedback of the surgical field, enabling surgeons to adjust the surgical technique to improve post-operative outcomes and decrease intra-operative errors. However, the difficult hand-eye coordination required if the computer screen is in different orientation than the surgical field is the main limiting factor. To overcome this issue, the use of AR headset, such as the glasses proposed by Microsoft HoloLens[12], could greatly improve the accuracy and safety of the surgical gesture when using navigation systems, since patient's anatomy (3D models, images, other visual information) can be directly projected in agreement with the surgeon's visual system.

Microsoft HoloLens is made up of specialized components that together enable to visualize and interact with high definition holograms. Moreover, the system understands user gestures, gaze and speech, which is ideal for the use in the operating room environment. Despite the AR headset works with advanced sensors for position and orientation tracking, they are not accurate and robust enough for surgical interventions. Therefore, the solution is to combine the AR headset tracking with a commercial navigation system to allow precise superposition of 3D pre-operative planning information or medical images over the patient – a solution that we have called "HoloMed" and that we have undertaken to develop recently. Such a solution would provide surgeons with computer guidance to precisely execute the surgical planning or to avoid damaging critical anatomical structures.

To test the feasibility of the system, Artanim's group has developed a first prototype in the laboratory using the optical motion capture system instead of the navigation system. With the HoloLens glasses, the user can see and analyze the 3D reconstructed anatomical joint structures overlaid on the patient during the motion capture session (Figure 3.2) – like if the user has an "X-ray vision". Based on our existing algorithms, the software compute in real time the patient's joint kinematics from the markers positions, and the resulting bone poses are then streamed to the HoloLens and projected according to the user's point of view. This work

[11]Microsoft Kinect, `https://developer.microsoft.com/en-us/windows/kinect`, accessed March 2017
[12]Microsoft HoloLens, `https://www.microsoft.com/microsoft-hololens/`, accessed March 2017

is a first step toward the combination of AR headset with surgical navigation system, providing a real time monitoring and visualization tool of the anatomy in movement for sports medicine and rehabilitation. The next step is to effectively integrate the HoloLens with the navigation and to extensively test the developed solution, as small overlapping errors can compromise the foundation of the entire system. We believe that in a few years, it will not be possible to dissociate surgery from these AR technologies.

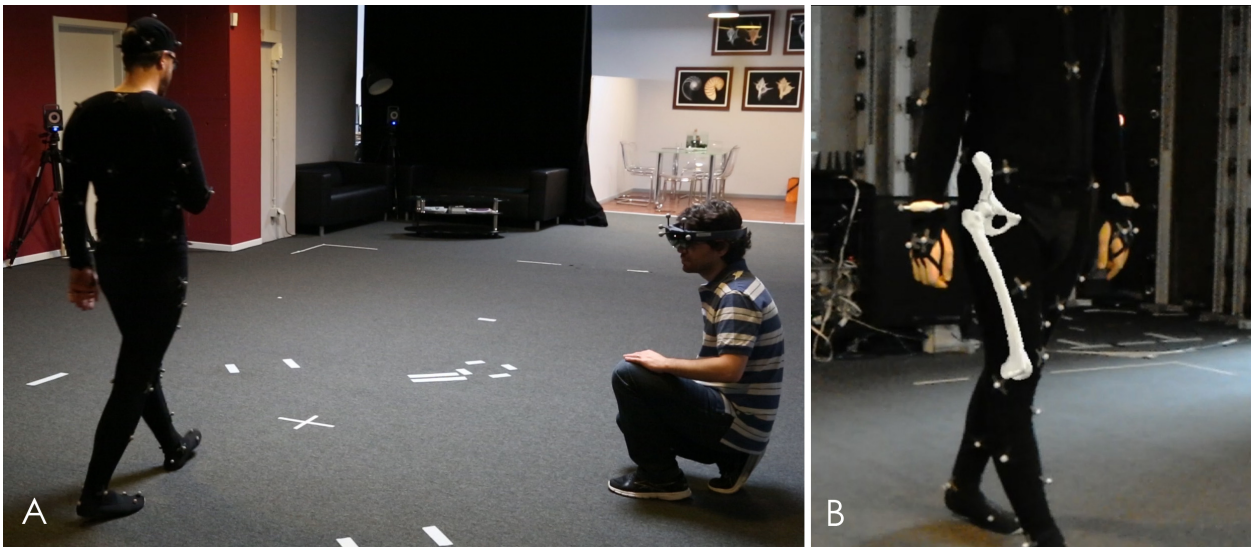

Figure 3.2: A) Motion capture session using the HoloLens headset. B) Superposition of the anatomical structures on top of the patient, as seen through the HoloLens. The projection follows the movement of the patient.

Appendix A

Acronyms

Acronyms used throughout the text and their definition:

AC: Acromioclavicular

ACL: Anterior Cruciate Ligament

AF: Anatomical Frame

AL: Anatomical Landmark

AR: Augmented Reality

CSA: Critical Shoulder Angle

CT: Computed Tomography

DoF: Degrees of Freedom

EMG: Electromyography

GH: Glenohumeral

ISB: International Society of Biomechanics

LCL: Lateral Collateral Ligament

MRI: Magnetic Resonance Imaging

MBO: Multi-Body Optimization

MCL: Medial Collateral Ligament

OA: Osteoarthritis

PCL: Posterior Cruciate Ligament

RMSE: Root Mean Square Errors

ROM: Range Of Motion

RSA: Shoulder Reverse Arthroplasty

SC: Sternoclavicular

STA: Soft Tissue Artifact

THA: Total Hip Arthroplasty

VR: Virtual Reality

Bibliography

[AA01] E Alexander and TP Andriacchi. Correcting for deformation in skin-based marker systems. *J Biomech*, 34:355–361, 2001.

[ABA03] EJ Alexander, C Bregler, and TP Andriacchi. Non-rigid modeling of body segments for improved skeletal motion estimation. *Comput Model Eng Sci*, 4(3-4):351–364, 2003.

[ABD+10] MS Andersen, DL Benoit, M Damsgaard, DK Ramsey, and J Rasmussen. Do kinematic models reduce the effects of soft tissue artefacts in skin marker-based motion analysis? An in vivo study of knee kinematics. *J Biomech*, 43:268–273, 2010.

[ACCL92] C Angeloni, A Cappozzo, F Catani, and A Leardini. Quantification of relative displacement between bones and skin and plate-mounted marker. In *Proc of the VIII Meeting on European Society of Biomechanics*, page 279, Roma, Italy, 1992.

[ACCL93] C Angeloni, A Cappello, F Catani, and A Leardini. Evaluation of soft tissue artifacts in the in-vivo determination of human knee instantaneous helical axis. In *Proc of the 2nd International Symposium on 3D Analysis of Human Movement*, pages 57–60, Poitiers, France, jul 1993.

[ACS+09] L Assassi, C Charbonnier, J Schmid, P Volino, and N Magnenat-Thalmann. From MRI to Anatomical Simulation of the Hip Joint. *Computer Animation and Virtual Worlds*, 20(1):53–66, 2009.

[BCL+98] M G Benedetti, F Catani, A Leardini, E Pignotti, and S Giannini. Data management in gait analysis for clinical applications. *Clin Biomech*, 13(3):204–215, 1998.

[BD05] SS Blemker and SL Delp. Three-dimensional representation of complex muscle architectures and geometries. *Ann Biomed Eng*, 33(5):661–673, 2005.

[BJTA15] A Barré, Brigitte M Jolles, N Theumann, and K Aminian. Soft tissue artifact distribution on lower limbs during treadmill gait: Influence of skin markers location on cluster design. *J Biomech*, 48(10):1965–1971, 2015.

[BMSL+13] A Bonnefoy-Mazure, Y Sagawa, P Lascombes, G De Coulon, and S Armand. Identification of gait patterns in individuals with cerebral palsy using multiple correspondence analysis. *Res Dev Disabil*, 34(9):2684–2693, 2013.

[BPH+11] E Bergamini, H Pillet, J Hausselle, P Thoreux, S Guerard, V Camomilla, A Cappozzo, and W Skalli. Tibiofemoral joint constraints for bone pose estimation during movement using multi-body optimization. *Gait & Posture*, 33(4):706–711, 2011.

[BPT+09] B Blondel, S Parratte, P Tropiano, V Pauly, J.-M. Aubaniac, and J.-N. Argenson. Pelvic tilt measurement before and after total hip arthroplasty. *J Orthop Traumatol Surg Res*, 95(8):568–572, 2009.

[BRL+06] DL Benoit, DK Ramsey, M Lamontagne, L Xu, P Wretenberg, and P Renström. Effect of skin movement artifact on knee kinematics during gait and cutting motions measured in vivo. *Gait & Posture*, 19(2):152–164, 2006.

[CAVMT09] C Charbonnier, L Assassi, P Volino, and N Magnenat-Thalmann. Motion Study of the Hip Joint in Extreme Postures. *Vis Comput*, 25(9):873–882, 2009.

[CBF09] S Chegini, M Beck, and SJ Ferguson. The effects of impingement and dysplasia on stress distributions in the hip joint during sitting and walking: A finite element analysis. *J Orthop Res*, 27(2):195–201, 2009.

[CCCL95] A Cappozzo, F Catani, U Della Croce, and A Leardini. Position and orientation of bones during movement: anatomical frame definition and determination. *Clin Biomech*, 10:171–178, 1995.

[CCCL97] A Cappello, A Cappozzo, U Della Croce, and A Leardini. Bone position and orientation reconstruction using external markers. *Three-Dimensional Analysis of Human Locomotion*, Chichester:147–171, 1997.

[CCK99] U Della Croce, A Cappozzo, and D C Kerrigan. Pelvis and lower limb anatomical landmark calibration precision and its propagation to bone geometry and joint angles. *Med Biol Eng Comp*, 37:155–161, 1999.

[CCK+14] C Charbonnier, S Chagué, F C Kolo, J C K Chow, and A Lädermann. A patient-specific measurement technique to model shoulder joint kinematics. *Orthop & Traumatol: Surg & Res*, 100(7):715–719, 2014.

[CCK+16] C Charbonnier, S Chagué, B Kevelham, F C Kolo, and A Lädermann. ArthroPlanner: A Surgical Planning Solution for Acromioplasty. In *30th International Congress of Computer Assisted Radiology and Surgery, Int J CARS*, Heidelberg, Germany, 2016.

[CCK+17] C Charbonnier, S Chagué, FC Kolo, VB Duthon, and J Menetrey. Multi-body Optimization with Subject-Specific Knee Models: Performance at High Knee Flexion Angles. *Comput Meth Biomech Biomed Eng*, 20(14):1571–1579, 2017.

[CCKL15] C Charbonnier, S Chagué, F C Kolo, and A Lädermann. Shoulder motion during tennis serve: dynamic and radiological evaluation based on motion capture and magnetic resonance imaging. *Int J CARS*, 10(8):1289–1297, 2015.

[CCL+96] A Cappozzo, F Catani, A Leardini, M G Benedetti, and U Della Croce. Position and orientation in space of bones during movement: experimental artefacts. *Clin Biomech*, 11(2):90–100, 1996.

[CCL+18] G Cunningham, C Charbonnier, A Lädermann, S Chagué, and D H Sonnabend. Are Codman exercises worthwhile? *Sports Med*, Submitted, 2018.

[CCP+14] C Charbonnier, S Chagué, M Ponzoni, M Bernardoni, P Hoffmeyer, and P Christofilopoulos. Sexual Activity after Total Hip Arthroplasty: A Motion Capture Study. *J Arthroplasty*, 29(3):640–647, 2014.

[CCP+18] C Charbonnier, S Chagué, D Preissmann, F C Kolo, O Rime, B Kevelham, and A Lädermann. ArthroPlanner: A Surgical Planning Solution for Acromioplasty. *Int J CARS*, In Press, 2018.

[CCS+15] C Charbonnier, S Chagué, J Schmid, F C Kolo, M Bernardoni, and P Christofilopoulos. Analysis of hip range of motion in everyday life: A pilot study. *Hip Int*, 25(1):82–90, 2015.

[CD12] J N Chopp and C R Dickerson. Resolving the contributions of fatigue-induced migration and scapular reorientation on the subacromial space: An orthopaedic geometric simulation analysis. *Hum Mov Sci*, 31:448–460, 2012.

[CDHdG15] J Clément, R Dumas, N Hagemeister, and J de Guise. Soft tissue artifact compensation in knee kinematics by multi-body optimization: Performance of subject-specific knee joint models. *J Biomech*, 48:3796–3802, 2015.

[CDHdG17] J Clément, R Dumas, N Hagemeister, and JA de Guise. Can generic knee joint models improve the measurement of osteoarthritic knee kinematics during squatting activity? *Comput Meth Biomech Biomed Eng*, 20(1):94–103, 2017.

[CFD95] L Chèze, B J Fregly, and J Dimnet. A solidification procedure to facilitate kinematic analyses based on video system data. *J Biomech*, 28:879–884, 1995.

[Cha10] C Charbonnier. *Extreme hip movements based on optical motion capture*. PhD thesis, Univesité de Genève, 2010.

[CKD+11] C Charbonnier, F C Kolo, V B Duthon, N Magnenat-Thalmann, C D Becker, P Hoffmeyer, and J Menetrey. Assessment of Congruence and Impingement of the Hip Joint in Professional Ballet Dancers. *Am J Sport Med*, 39(3):557–566, 2011.

[CLCC05] U Della Croce, A Leardini, L Chiari, and A Cappozzo. Human movement analysis using stereophotogrammetry Part 4: Assessment of anatomical landmark misplacement and its effects on joint kinematics. *Gait & Posture*, 21:226–237, 2005.

[CLK+18] C Charbonnier, A Lädermann, B Kevelham, S Chagué, P Hoffmeyer, and N Holzer. Shoulder Strengthening Exercises Adapted to Specific Shoulder Pathologies Can Be Selected Using New Simulation Techniques: A Pilot Study. *Int J CARS*, 13(2):321–330, 2018.

[CMTB+10] C Charbonnier, N Magnenat-Thalmann, C D Becker, P Hoffmeyer, and J Menetrey. An integrated platform for hip joint osteoarthritis analysis: Design, implementation and results. *Int J CARS*, 5(4):351–358, 2010.

[Cro06] U Della Croce. Soft tissue artifacts in movement analysis. In *Proc of the 9th International Symposium on 3D Analysis of Human Movement*, Valenciennes, France, jun 2006.

[CSFL05] A Cappello, R Stagni, S Fantozzi, and A Leardini. Soft Tissue Artifact Compensation in Knee Kinematics by Double Anatomical Landmark Calibration: Performance of a novel Method During Selected Motor Tasks. *IEEE Trans Biomed Eng*, 52(2):992–998, 2005.

[DBD+04] A Duhamel, J L Bourriez, P Devos, P Krystkowiak, A Destée, P Derambure, and L Defebvre. Statistical tools for clinical gait analysis. *Gait & Posture*, 20:204–212, 2004.

[DCD10] S Duprey, L Chèze, and R Dumas. Influence of joint constraints on lower limb kinematics estimation from skin markers using global optimization. *J Biomech*, 43(14):2858–2862, 2010.

[FRB05] B J Fregly, H A Rahman, and S A Banks. Theoretical accuracy of model-based shape matching for measuring natural knee kinematics with single-plane fluoroscopy. *J Biomech Eng*, 127(4):692–699, 2005.

[FSH+12] P Favre, M Senteler, J Hipp, S Scherrer, C Gerber, and J G Snedeker. An integrated model of active glenohumeral stability. *J Biomech*, 45:2248–2255, 2012.

[GDJ13] X Gasparutto, R Dumas, and E Jacquelin. Multi-body optimisation with deformable ligament constraints: influence of ligament geometry. *Comput Meth Biomech Biomed Eng*, 15:191–193, 2013.

[GHER+05] H Graichen, S Hinterwimmer, R.von Eisenhart-Rothe, T Vogl, K.-H. Englmeier, and F Eckstein. Effect of abducting and adducting muscle activity on glenohumeral translation, scapular kinematics and subacromial space width in vivo. *J Biomech*, 38(4):755–760, 2005.

[Gil07] B Gilles. *Anatomical and Kinematical Modelling of the Musculoskeletal System from MRI*. PhD thesis, Université de Genève, 2007.

[GKMT+09] B Gilles, F C Kolo, N Magnenat-Thalmann, C D Becker, S Duc, J Menetrey, and P Hoffmeyer. MRI-based Assessment of Hip Joint Translations. *J Biomech*, 42(9):1201–1205, 2009.

[GMMT06] B Gilles, L Moccozet, and N Magnenat-Thalmann. Anatomical modelling of the musculoskeletal system from MRI. In R Larsen, M Nielsen, and J Sporring, editors, *MICCAI 2006, LNCS*, volume 4190, pages 289–296. Springer-Verlag, 2006.

[GMT05] B Gilles and N Magnenat-Thalmann. Automatic reconstruction of the musculoskeletal system based on simplex meshes. In *MICCAI 2015, LNCS*, 2005.

[GS83] E S Grood and W J Suntay. A joint coordinate system for the clinical description of three-dimensional motions: application to the knee. *J Biomech Eng*, 105:136–144, 1983.

[GSJ+15] X Gasparutto, N Sancisi, E Jacquelin, V Parenti-Castelli, and R Dumas. Validation of a multi-body optimization with knee kinematic models including ligament constraints. *J Biomech*, 48:1141–1446, 2015.

[HBT+11] D K Hodge, C F Beaulieu, G H Thabit, G E Gold, A G Bergman, R K Butts, M F Dillingham, and R J Herfkens. Dynamic MR Imaging and Stress Testing in Glenohumeral Instability: Comparison With Normal Shoulders and ClinicalSurgical Findings. *J Magn Reson Imaging*, 13:748–756, 2011.

[HM09] T Heimann and H Meinzer. Statistical shape models for 3D medical image segmentation: A review. *Med Image Anal*, 13(4):543–563, 2009.

[HOS+97] J P Holden, J H Orsini, K L Siegel, T M Kepple, L H Gerber, and S J Stanhope. Surface movement errors in shank kinematics and knee kinetics during gait. *Gait & Posture*, 5:217–227, 1997.

[HYC04] J Houck, H J Yack, and T Cuddeford. Validity and comparisons of tibiofemoral orientations and displacement using a femoral tracking device during early to mid stance of walking. *Gait & Posture*, 19:76–84, 2004.

[JMTB12] M Jackson, B Michaud, P Tetreault, and M Begon. Improvements in measuring shoulder joint kinematics. *J Biomech*, 45(12):2180–2183, 2012.

[KCP+13] F C Kolo, C Charbonnier, C W A Pfirrmann, S R Duc, A Lubbeke, V B Duthon, N Magnenat-Thalmann, P Hoffmeyer, J Menetrey, and C D Becker. Extreme Hip Motion in Professional Ballet Dancers: Dynamic and Morphologic Evaluation Based on MRI. *Skeletal Radiology*, 42(5):689–698, 2013.

[KKB+12] M C M Klotz, L Kost, F Braatz, V Ewerbeck, D Heitzmann, S Gantz, T Dreher, and SI Wolf. Motion capture of the upper extremity during activities of daily living in patients with spastic hemiplegic cerebral palsy. *Gait & Posture*, 38(1):148–152, 2012.

[KMMS01] A R Karduna, P W McClure, L A Michener, and B Sennett. Dynamic measurements of three-dimensional scapular kinematics: a validation study. *J Biomech Eng*, 123(2):184–190, 2001.

[KSMMT03] M Kang, H Sadri, L Moccozet, and N Magnenat-Thalmann. Hip joint modeling for the control of the joint center and the range of motions. In *IFAC Symposium on modelling and control in biomedical systems*, pages 23–27. Elsevier, aug 2003.

[LBC+99] A Leardini, M G Benedetti, F Catani, L Simoncini, and S Giannini. An anatomically based protocol for the description of foot segment kinematics during gait. *Clin Biomech*, 14(8):528–536, 1999.

[LBN+17] A Leardini, C Belvedere, F Nardini, N Sancisi, M Conconi, and V Parenti-Castelli. Kinematic models of lower limb joints for musculo-skeletal modelling and optimization in gait analysis. *J Biomech*, 62:77–86, 2017.

[LC18] A Lädermann and C Charbonnier. Effect of Critical Shoulder Angle, Glenoid Lateralization and Humeral Inclination on Range of Motion in Shoulder Reverse Arthroplasty. *J Arthroplasty*, Submitted, 2018.

[LCC+99] A Leardini, A Cappozzo, F Catani, S Toksvig-Larsen, A Petitto, and V Sforza. Validation of a functional method for the estimation of the hip joint centre location. *J Biomech*, 32(1):99–103, 1999.

[LCCC98] L Lucchetti, A Cappozzo, A Cappello, and U Della Croce. Skin movement artefact assessment and compensation in the estimation of knee joint kinematics. *J Biomech*, 31(11):977–984, 1998.

[LCCC05] A Leardini, L Chiari, U Della Croce, and A Cappozzo. Human movement analysis using stereophotogrammetry Part 3: Soft tissue artifact assessment and compensation. *Gait & Posture*, 21:212–225, 2005.

[LCKC16] A Lädermann, S Chagué, F C Kolo, and C Charbonnier. Kinematics of the Shoulder Joint in Tennis Players. *J Sci Med Sport*, 19(1):56–63, 2016.

[LCP+18] A Lädermann, S Chagué, D Preissmann, F C Kolo, O Rime, B Kevelham, and C Charbonnier. Is Acromioplasty Planification Useful? A Prospective Randomized Trial. *J Shoulder Elbow Surg*, Submitted, 2018.

[LCS+94] M A Lafortune, P R Cavanagh, H J Sommer, H J Ill, and A Kalenak. Foot inversion-eversion and knee kinematics during walking. *J Orthop Res*, 12:412–420, 1994.

[LDT+16] A Lädermann, P J Denard, J Tirefort, F C Kolo, S Chagué, G Cunningham, and C Charbonnier. Does surgery for instability of the shoulder truly stabilize the glenohumeral joint?: A prospective comparative cohort study. *Medicine*, 95(31):e4369–e4369, 2016.

[LLL+16] CC Lin, TW Lu, HL Lu, MY Kuo, and HC Hsu. Effects of soft tissue artifacts on differentiating kinematic differences between natural and replaced knee joints during functional activity. *Gait & Posture*, 26:154–160, 2016.

[LNL+08] P Lundgren, C Nester, A Liu, A Arndt, R Jones, A Stacoff, P Wolf, and A Lundberg. Invasive in vivo measurement of rear-, mid- and forefoot motion during walking. *Gait & Posture*, 28:93–100, 2008.

[LO99] T W Lu and J J O'Connor. Bone position estimation from skin marker co-ordinates using global optimisation with joint constraints. *J Biomech*, 32:129–134, 1999.

[LT01] C T Lawrence and A L Tits. A Computationally Efficient Feasible Sequential Quadratic Programming Algorithm. *SIAM J Optim*, 11(4):1092–1118, 2001.

[LTK+08] T W Lu, T Y Tsai, M Y Kuo, H C Hsu, and H L Chen. In vivo three-dimensional kinematics of the normal knee during active extension under unloaded and loaded conditions using single-plane fluoroscopy. *Med Eng & Phys*, 30(8):1004–1012, 2008.

[MAB+99] K Meister, J R Andrews, J Batts, K Wilk, and T Baumgarten. Symptomatic thrower's exostosis. Arthroscopic evaluation and treatment. *Am J Sport Med*, 27(2):133–136, 1999.

[MBP+12] D F Massimini, P J Boyer, R Papannagari, T J Gill, J P Warner, and G Li. In-vivo glenohumeral translation and ligament elongation during abduction and abduction with internal and external rotation. *J Orthop Surg Res*, 7:29–38, 2012.

[MBR+13] B K Moor, S Bouaicha, D A Rothenfluh, A Sukthankar, and C Gerber. Is there an association between the individual anatomy of the scapula and the development of rotator cuff tears or osteoarthritis of the glenohumeral joint? A radiological study of the critical shoulder angle. *Bone Joint J*, 95 B(7):935–941, 2013.

[MDA01] J Montagnat, H Delingette, and N Ayache. A review of deformable surfaces: topology, geometry and deformation. *Image Vis Comput*, 19(14):1023–1040, 2001.

[MFP+12] A Maurer, S F Fucentese, C W A Pfirrmann, S H Wirth, A Djahangiri, B Jost, and C Gerber. Assessment of glenoid inclination on routine clinical radiographs and computed tomography examinations of the shoulder. *J Shoulder Elbow Surg*, 21(8):1096–1103, 2012.

[MHHR07] M Mueller, B Heidelberger, M Hennix, and J Ratcliff. Position based dynamics. *J Vis Comun Image Represent*, 18(2):109–118, 2007.

[MMD07] A Malik, A Maheshwari, and L D Dorr. Impingement with Total Hip Replacement. *J Bone Joint Surg Am*, 89:1832–1842, 2007.

[MMR+02] K Manal, I McClay, J Richards, B Galinat, and S Stanhope. Knee moment profiles during walking: errors due to soft tissue movement of the shank and the influence of the reference coordinate system. *Gait & Posture*, 15:10–17, 2002.

[MMS+00] K Manal, I McClay, S Stanhope, J Richards, and B Galinat. Comparison of surface mounted markers and attachment methods in estimating tibial rotations during walking: an in vivo study. *Gait & Posture*, 11:38–45, 2000.

[MMY+12] K Matsuki, K O Matsuki, S Yamaguchi, N Ochiai, T Sasho, H Sugaya, T Toyone, Y Wada, K Takahashi, and S A Banks. Dynamic In Vivo Glenohumeral Kinematics During Scapular Plane Abduction in Healthy Shoulders. *J Orthop Sports Phys Ther*, 42(2):96–104, 2012.

[MRS06] M De Maeseneer, P Van Roy, and M Shahabpour. Normal MR Imaging Anatomy of the Rotator Cuff Tendons, Glenoid Fossa, Labrum, and Ligaments of the Shoulder. *Radiol Clin N Am*, 44:479–487, 2006.

[MTCS08] N Magnenat-Thalmann, C Charbonnier, and J Schmid. Multimedia Application to the Simulation of Human Musculoskeletal System: A Visual Lower Limb Model from Multimodal Captured Data. In *Proc of the IEEE International Workshop on Multimedia Signal Processing*, pages 520–525, Cairns, Australia, 2008. IEEE Publisher.

[Nee72] C S Neer. Anterior acromioplasty for chronic impingement syndrome in the shoulder: a preliminary report. *J Bone Joint Surg Am*, 54:41–50, 1972.

[NJL+07] C Nester, R K Jones, A Liu, D Howard, A Lundberg, A Arndt, P Lundgren, A Stacoff, and P Wolf. Foot kinematics during walking measured using bone and surface mounted markers. *J Biomech*, 40:3412–3423, 2007.

[NTM+08] N Nishinaka, H Tsutsui, K Mihara, K Suzuki, D Makiuchi, Yoshiaki Kon, TW Wright, MW Moser, K Gamada, H Sugimoto, and SA Banks. Determination of in vivo glenohumeral translation using fluoroscopy and shape-matching techniques. *J Shoulder Elbow Surg*, 17(2):319–322, 2008.

[NWS+06] R W Nyffeler, C M Werner, A Sukthankar, M R Schmid, and C Gerber. Association of a large lateral extension of the acromion with rotator cuff tears. *J Bone Joint Surg Am*, 88(4):800–805, 2006.

[OHM+07] T Moro Oka, S Hamai, H Miura, T Shimoto, H Higaki, B J Fregly, Y Iwamoto, and S A Banks. Can Magnetic Resonance ImagingDerived Bone Models Be Used for Accurate Motion Measurement with Single-Plane Three-Dimensional Shape Registration. *J Orthop Res*, 25:867–872, 2007.

[PHR+04] V V Patel, K Hall, M Ries, J Lotz, E Ozhinsky, C Lindsey, Y Lu, and S Majumdar. A three-dimensional MRI analysis of knee kinematics. *J Orthop Res*, 22:283–292, 2004.

[PLCS+14] J Pierrart, M.-M. Lefeèvre-Colau, W Skalli, V Vuillemin, E H Masmejean, C A Cuenod, and T M Gregory. New Dynamic Three-Dimensional MRI Technique for Shoulder Kinematic Analysis. *J Magn Reson Imaging*, 39(3):729–734, 2014.

[PLSH11] R Peter, A Lubbeke, R Stern, and P Hoffmeyer. Cup size and risk of dislocation after primary total hip arthroplasty. *J Arthroplasty*, 26(8):1305–1309, 2011.

[PMD+06] C W A Pfirrmann, B Mengiardi, C Dora, F Kalberer, M Zanetti, and J Hodler. Cam and Pincer Femoroacetabular Impingement: Characteristic MR Arthrographic Findings in 50 Patients. *Radiology*, 240(3):778–785, 2006.

[RCD17] V Richard, A Cappozzo, and R Dumas. Comparative assessment of knee joint models used in multi-body kinematics optimisation for soft tissue artefact compensation. *J Biomech*, 62:95–101, 2017.

[RLK99] D Reynolds, J Lucas, and K Klaue. Retroversion of the acetabulum. A cause of hip pain. *J Bone Joint Surg Am*, 81(2):281–288, 1999.

[RLL+16] V Richard, G Lamberto, T W Lu, A Cappozzo, and R Dumas. Knee Kinematics Estimation Using Multi-Body Optimisation Embedding a Knee Joint Stiffness Matrix: A Feasibility Study. *PLOS ONE*, 11(6):e0157010–e0157010, 2016.

[RSGP06] ME Russell, KH Shivanna, NM Grosland, and DR Pedersen. Cartilage contact pressure elevations in dysplastic hips: a chronic overload model. *J Orthop Surg Res*, 1:6, 2006.

[RTTS05] N A Ramaniraka, A Terrier, N Theumann, and O Siegrist. Effects of the posterior cruciate ligament reconstruction on the biomechanics of the knee joint: a finite element analysis. *Clin Biomech*, 20:434–442, 2005.

[RvdBL+97] C Reinschmidt, A J van den Bogert, A Lundberg, B M Nigg, and N Murphy. Effect of skin movement on the analysis of skeletal knee joint motion during running. *J Biomech*, 30(7):729–732, 1997.

[SAL+13] Y Sagawa, S Armand, A Lubbeke, P Hoffmeyer, D Fritschy, D Suva, and K Turcot. Associations between gait and clinical parameters in patients with severe knee osteoarthritis: A multiple correspondence analysis. *Clin Biomech*, 28(3):299–305, 2013.

[SC04] F G Shellock and J V Crues. MR procedures: Biologic effects, safety, and patient care. *Radiology*, 232:635–652, 2004.

[SCC+15] J Schmid, C Chênes, S Chagué, P Hoffmeyer, P Christofilopoulos, M Bernardoni, and C Charbonnier. MyHip: supporting planning and surgical guidance for a better total hip arthroplasty: A pilot study. *Int J CARS*, 10(10):1547–1556, 2015.

[Sch11] J Schmid. *Knowledge-based Deformable Models for Medical Image Analysis*. PhD thesis, Univesité de Genève, 2011.

[SdQD+07] A Stacoff, I Kramers de Quervain, M Dettwyler, P Wolf, R List, T Ukelo, and E Stuessi. Biomechanical effects of foot orthoses during walking. *The Foot*, 17:143–153, 2007.

[SE03] P J Schneider and D H Eberly. *Geometric Tools for Computer Graphics*. The Morgan Kaufmann Series in Computer Graphics and Geometric Modeling, 2003.

[SFC09] R Stagni, S Fantozzi, and A Cappello. Double calibration vs. global optimisation: Performance and effectiveness for clinical application. *Gait & Posture*, 29(1):119–122, 2009.

[SFCL05] R Stagni, S Fantozzi, A Cappello, and A Leardini. Quantification of soft tissue artifact in motion analysis by combining 3D fluoroscopy and stereophotogrammetry: a study on two subjects. *Clin Biomech*, 20:320–329, 2005.

[SKMT11] J Schmid, J Kim, and N Magnenat-Thalmann. Robust Statistical Shape Models for MRI Bone Segmentation in Presence of Small Field of View. *Med Image Anal*, 15(1):155–168, 2011.

[SMBT05] S Sarni, A Maciel, R Boulic, and D Thalmann. Spreadsheet Framework for Visual Exploration of Biomedical Datasets. In *IEEE CBMS 2005*, pages 159–164. IEEE Publisher, 2005.

[SMC+06] M Sangeux, F Marin, F Charleux, L Duerselen, and M C Ho Ba Tho. Quantification of the 3D relative movement of external marker sets vs. bones based on magnetic resonance imaging. *Clin Biomech*, 21:984–991, 2006.

[SPP+91] S J Snyder, A F Pachelli, W Del Pizzo, M J Friedman, R D Ferkel, and G Pattee. Partial thickness rotator cuff tears: results of arthroscopic treatment. *Arthroscopy*, 7(1):1–7, 1991.

[SW93] I Söderkvist and P A Wedin. Determining the movements of the skeleton using well-configured markers. *J Biomech*, 12:1473–1477, 1993.

[TLAB+13] MK Timmons, AD Lopes-Albers, L Borgsmiller, C Zirker, J Ericksen, and LA Michener. Differences in scapular orientation, subacromial space and shoulder pain between the full can and empty can tests. *Clin Biomech*, 28(4):395–401, 2013.

[TLC+10] T Y Tsai, T W Lu, C M Chen, M Y Kuo, and H C Hsu. A volumetric model-based 2D to 3D registration method for measuring kinematics of natural knees with single-plane fluoroscopy. *Med Phys*, 37(3):1273–1284, 2010.

[TLKL11] TY Tsai, TW Lu, MY Kuo, and CC Lin. Effects of soft tissue artifacts on the calculated kinematics and kinetics of the knee during stair-ascent. *J Biomech*, 44(6):1182–1188, 2011.

[WBD14] JD Webb, SS Blemker, and SL Delp. 3D finite element models of shoulder muscles for computing lines of actions and moment arms. *Comput Meth Biomech Biomed Eng*, 17(8):829–37, 2014.

[WBI+05] S Waldt, A Burkart, A B Imhoff, M Bruegel, E J Rummeny, and K Woertler. Anterior shoulder instability: accuracy of MR arthrography in the classification of anteroinferior labroligamentous injuries. *Radiology*, 237(2):578–583, 2005.

[WBND92] G Walch, P Boileau, E Noel, and S T Donell. Impingement of the deep surface of the supraspinatus tendon on the posterior glenoid rim: an arthroscopic study. *J Shoulder Elbow Surg*, 1:238–245, 1992.

[WLJ+08] P Wolf, A Liu, R Jones, A Arndt, A Lundberg, and A Stacoff. Rearfoot kinematics: invasive quantification of the skin movement artifact. *J Biomech*, 41(1):S164–S164, 2008.

[WSA+02] G Wu, S Siegler, P Allard, C Kirtley, A Leardini, D Rosenbaum, M Whittle, D Dima, L Cristofolini, H Witte, O Schmid, and I Strokes. ISB recommendation on definitions of joint coordinate system of various joints for the reporting of human joint motion - part I: Ankle, hip and spine. *J Biomech*, 35(4):543–548, 2002.

[WvdHV+05] G Wu, F C T van der Helm, H E J Veegerc, M Makhsouse, P Van Royf, C Angling, J Nagelsh, A R Kardunai, K McQuadej, X Wangk, F W Wernerl, and B Buchholzm. ISB recommendation on definitions of joint coordinate systems of various joints for the reporting of human joint motion - part II: shoulder, elbow, wrist and hand. *J Biomech*, 38:981–992, 2005.

[YCGMMT04] L Yahia-Cherif, B Gilles, T Molet, and N Magnenat-Thalmann. Motion capture and visualization of the hip joint with dynamic MRI and optical systems. *Computer Animation and Virtual Worlds*, 15,(3-4):377–385, jul 2004.

[YCMT06] L Yahia-Cherif and N Magnenat-Thalmann. Quantification of Skin Movements Artefacts using MRI. In *Proc of the 9th International Symposium on 3D Analysis of Human Movement*, Valenciennes, France, jun 2006.

[YHC+00] H J Yack, J Houck, T Cudderford, M Pierrynowski, and K Ball. Measuring 3D knee motion with surface markers, it can be done. *Gait & Posture*, 11(2):148–149, 2000.

[YOES08] G Yavuzer, O Oken, A Elhan, and H J Stam. Repeatability of lower limb three-dimensional kinematics in patients with stroke. *Gait & Posture*, 27:31–35, 2008.

[ZGS+06] M S Zihlmann, H Gerber, A Stacoff, K Burckhardt, G Szekeli, and W Stuessi. Three-dimensional kinematics and kinetics of total knee arthroplasty during level walking using single plane fluoroscopy and force plates: A pilot study. *Gait & Posture*, 208:475–481, 2006.

[ZMW+12] Z Zhu, D F Massimini, G Wang, J J P Warner, and G Li. The accuracy and repeatability of an automatic 2D-3D fluoroscopic image-model registration technique for determining shoulder joint kinematics. *Medical Engineering & Physics*, 34(9):1303–1309, 2012.